Title
Microtubule binding by the formin Cappuccino and its implications for Drosophila oogenesis

Author
Roth-Johnson, Elizabeth Anne

Publication Date
2014

Peer reviewed|Thesis/dissertation

UNIVERSITY OF CALIFORNIA

Los Angeles

Microtubule binding by the formin Cappuccino and its implications for *Drosophila* oogenesis

A dissertation submitted in partial satisfaction

of the requirements for the degree

Doctor of Philosophy in Molecular Biology

by

Elizabeth Anne Roth-Johnson

2014

ABSTRACT OF THE DISSERTATION

Microtubule binding by the formin Cappuccino and its implications for *Drosophila* oogenesis

by

Elizabeth Anne Roth-Johnson

Doctor of Philosophy in Molecular Biology

University of California, Los Angeles, 2014

Professor Margot E. Quinlan, Chair

Coordination of actin and microtubule cytoskeletal networks is required for a number of fundamental cellular processes. Formin family actin nucleators are emerging coordinators of the actin and microtubule cytoskeletons, as they can both nucleate actin filaments and bind microtubules *in vitro*. To gain a more detailed mechanistic understanding of formin-microtubule interactions and formin-mediated actin-microtubule crosstalk, we studied microtubule binding by Cappuccino (Capu), a formin involved in regulating actin and microtubule organization during *Drosophila* oogenesis. We report that two distinct domains within Capu, FH2 and tail, work together to promote high-affinity microtubule binding. Microtubules potently inhibit Capu's actin nucleation activity but have little effect on Capu once bound to the barbed end of an elongating actin filament, supporting a model in which Capu does not simultaneously bind microtubules and assemble actin *in vivo*. After characterizing Capu-microtubule binding *in vitro*, we examined the localization of Capu and microtubules in S2 cells. We did not observe any obvious colocalization and conclude that S2 cells are not an ideal system for visualizing *in vivo* formin-microtubule interactions. To better understand Capu's mechanisms of action during oogenesis, we then systematically characterized several classical *capu* alleles. While all of these *capu* mutants exhibit severe developmental defects, they variably affect Capu's actin assembly activity *in vitro*. Together with our microtubule binding data, this indicates that Capu's physiological role extends beyond its ability to nucleate actin filaments. We therefore performed tandem affinity purification experiments to

identify novel Capu binding partners and gain additional insight into Capu's role during oogenesis. We report several candidate binding partners involved in such diverse cellular processes as mitochondrial fission, endocytosis, and nuclear import. Though preliminary, these results suggest that Capu has additional uncharacterized functions in development; further investigation may help us uncover the physiological role of Capu-microtubule binding. Ultimately, our findings expand our understanding of Capu's role in *Drosophila* oogenesis and provide mechanistic insight into formins as coordinators of the actin and microtubule cytoskeletons.

The dissertation of Elizabeth Anne Roth-Johnson is approved.

Kent L. Hill

Frank A. Laski

Jorge Torres

Margot E. Quinlan, Committee Chair

University of California, Los Angeles

2014

Dedicated to my husband, Perry.

Table of Contents

List of Figures . . . . . **ix**

List of Tables . . . . . **xi**

Abbreviations . . . . . **xii**

1 Introduction **1**

1.1 The formin family of actin nucleators 1

1.2 Formins as potential coordinators of actin and microtubules 3

1.3 Capu's role in *Drosophila* oogenesis 6

1.4 Overview of the dissertation 9

2 *In vitro* analysis of Capu-microtubule binding **12**

2.1 Microtubule binding by Capu 15

2.2 Effect of microtubules on actin nucleation 16

2.3 Barbed end association in the presence of microtubules 19

2.4 Characterization of the tail-microtubule interaction 21

2.5 FH2 domain contribution toward microtubule binding 22

2.6 Discussion 25

3 Characterization of Capu localization in S2 cells **31**

3.1 Localization of Capu and microtubules in S2 cells 32

3.2 Capu localization in S2 cells treated with Cytochalasin D 34

3.3 Localization of Capu to the mitotic spindle 37

3.4 Discussion 37

4 Structure-function study of Capu mutants 40

4.1 Identification of causative lesions in *capu* alleles 40

4.2 *In vivo* characterization of classical *capu* alleles 43

4.3 Structural analysis of identified missense mutations 45

4.4 *In vitro* characterization of classical *capu* alleles 47

4.5 Identification and characterization of Capu's "loop" domain 49

4.6 Discussion 50

5 Tandem affinity purification of Capu binding partners 53

5.1 TAP-Capu expression and pulldown 55

5.2 Mass spectrometry results 55

5.3 Discussion 58

6 Conclusion 61

6.1 Emerging mechanisms of formin-microtubule binding 61

6.2 Implications for Capu-microtubule binding in oogenesis 64

6.3 Concluding remarks 66

7 Experimental procedures 69

7.1 Protein purification 69

7.2 Microtubule preparation 70

7.3 Microtubule-binding assays 70

7.4 Pyrene-actin polymerization assays 72

7.5 Actin elongation TIRF microscopy assays 72

7.6 Fluorescence imaging of S2 cells 73

7.7 Identification and confirmation of *capu* lesions 74

7.8 *Drosophila* oocyte imaging and analysis 74

7.9 Tandem affinity purification 75

A Full list of mass spectrometry results 77

References 86

List of Figures

1.1 Characteristics of formin family actin nucleators 2

1.2 Role of Capu and Spir in *Drosophila* oogenesis 7

1.3 Cytoskeletal organization during *Drosophila* oogenesis 9

2.1 High-affinity microtubule binding requires FH2 and tail 14

2.2 Microtubules potently inhibit Capu's nucleation activity 17

2.3 Microtubules do not disrupt Capu association with the barbed end of actin . 20

2.4 Tail binds microtubules through nonspecific charge-based interactions 21

2.5 Tail mutations affect both microtubule binding and actin nucleation 23

2.6 FH2 domain residues contribute to microtubule binding 24

2.7 Model of Capu-microtubule binding 26

3.1 Capu does not clearly colocalize with microtubules in S2 cells 33

3.2 Capu is not enriched in CytoD-induced projections 35

3.3 Capu localizes diffusely throughout the cytoplasm of S2 cells. 36

3.4 Capu is not enriched at the mitotic spindle in metaphase cells 38

4.1 Capu mutations identified across all sequenced fly lines 41

4.2 Capu gene structure and reported isoforms 43

4.3 Classical *capu* alleles lack actin mesh and exhibit premature streaming . . . 44

4.4 All identified mutations are located within Capu's FH2 domain 46

4.5 Mutants variably affect actin assembly and microtubule binding 48

4.6 Removing the "loop" domain increases Capu's actin polymerization activity 49

5.1 Experimental set-up for tandem affinity purification 54

5.2 Tandem affinity purification preliminary results 56

6.1 Potentially conserved mechanisms of formin-microtubule binding 62

List of Tables

2.1 Fit parameters for all microtubule binding curves 15

4.1 Identified *capu* lesions 42

4.2 Fit parameters for all microtubule binding curves 48

5.1 Selected mass spectrometry results 56

5.2 Predicted Capu phosphorylation sites 58

A.1 NCBInr 20131226 database search results 78

A.2 Drosophila_melanog 020314 database search results 82

Abbreviations

APC	Adenomatous polyposis coli
bic	*bicoid*
Capu	Cappuccino
Cdlc	Cytoplasmic dynein light chain
Chic	Chickadee
CID	Capu inhibitory domain
CLIP-170	Cytoplasmic linker protein 170
CytoD	Cytochalasin D
DAAM	Disheveled-associated activator of morphogenesis
Dia	Diaphanous
Drp1	Dynamin related protein 1
EB1	End binding protein 1
FH	Formin homology
FHOD	FH2-domain containing
FMN	Formin
FMNL	Formin-like
GAP	GTPase-activating protein
grk	*gurken*
GST	Glutathione S-transferase

INF	Inverted formin
KIND	Kinase inactive domain
LatA	Latrunculin A
LatB	Latrunculin B
nos	*nanos*
osk	*oskar*
PP2A	Protein phosphatase 2A
RACK1	Receptor of activated protein kinase C 1
Shot	Short stop
Spir	Spire
TAP	Tandem affinity purification
TIRF	Total internal reflection fluorescence

Acknowledgments

First and foremost, I thank my advisor, Margot Quinlan, for making this whole crazy project possible. Thanks to her guidance, I have grown so much as both a researcher and a communicator. Margot encouraged me to think deeply and creatively about my project; she pushed me through the low points when data were confusing and nothing seemed to be working; she generously sent me to Woods Hole to expand my horizons as a scientist; and through her own inspiring example, she showed me that every research project is a story and that a good research talk can be truly captivating. Even as my priorities and career plans evolved, Margot supported and embraced my ambitions. For this, and for everything, I cannot thank her enough.

I would also like to acknowledge the rest of my committee: Drs. Emil Reisler, Jorge Torres, Frank Laski, and Kent Hill. Though my committee meetings were few and far between, their insight and feedback was extremely helpful in shaping my research. A special thank you to Dr. Reisler and his lab for sharing their weekly journal club and training me to think like a true biochemist.

A huge thank you goes to the entire Quinlan Lab—my lab mates, colleagues, and friends. I will always remember our Indian buffet lunches, our epic foosball games, and our general lab shenanigans (I think the truck is still missing). I thank Justin Bois and Christina Vizcarra for being such wonderful mentors: I admire you both immensely as scientists and am so honored to have worked with you. Thank you also to Batbileg Bor and Amy Rasson, my partners in crime, for sharing all of the ups and downs of graduate school and making the lab feel like home. I thank Andrey Shur for being generally awesome and keeping the lab running like clockwork. And last but not least, many thanks to Haneul Yoo for her spectacular work. It was an absolute pleasure to mentor such a bright, talented, and diligent student; Chapter 4 would not exist without her dedication and hard work.

I would like to acknowledge my past advisors and colleagues at the Buck Institute and at UC Berkeley. I especially thank David Madden, who sparked my interest in research, showed me how much fun it could be to work in a lab, and taught me that the best way to

make PCR work is to think "happy thoughts"—thank you for being such a great mentor and friend through the years. I also thank Professor Randy Schekman for taking a chance on me (twice!) and giving me the privilege of working in his lab. Thanks to Siraprapha "Yui" Sanchatjate for introducing me to tandem affinity purification. And a special thank you to Robyn Barfield, who made science fun, gave me the freedom to work on my own project as an undergraduate student, and gave me the confidence I needed to grow as a scientist.

I also thank all of my mentors and colleagues who have challenged me to see biology in a new way. Thank you to Bill Klug for showing me the beauty and power of using math to describe biological systems. And a huge thank you to the amazing faculty, TAs, and students of the 2011 Physiology Course: Carolina Tropini for being an amazing lab partner and friend; Marija Zanic, Melissa Gardner, and Joe Howard for being wonderful mentors and co-authors; KC Huang, Enrique Rojas, and Tristan Ursell for teaching me to stop worrying and love the bash. All of you have forever changed my perception of scientific research and opened my eyes to new and wonderful ways of thinking about cell biology.

I thank my friends and family for being an unwavering network of love and support throughout the past five years. I thank my husband for agreeing to go on this crazy adventure, for being my rock, and for sharing all the highs and lows of graduate school—I truly could not have done it without you! Thank you also to my parents for always pushing me to succeed yet giving me room to explore my own interests. Thank you both for teaching me the value of a good education and sharing your wisdom along the way: to my Mom for nurturing my writing and critical thinking skills, and to my Dad for teaching me to be a self-reliant problem solver. I thank my brother, Tim, for being a great friend and confidante—you are such a smart, caring, and funny person, and it has been a treat to share so many high school, college, and now graduate school experiences with you. Thanks also to my new family for welcoming me, supporting me, and giving me a home away from home in Southern California. And thank you to everyone who helped me stay motivated and find my way toward a career outside of the lab: Amy Rowat and the wonderful people involved with Science & Food; the amazing Versatile PhD community; and all the friends and family who helped me network and get to where I am today.

Additionally, I would like to acknowledge my co-authors and collaborators on the work presented in this dissertation: Dr. Christina Vizcarra for performing the TIRF microscopy in Chapter 2; Dr. Justin Bois for creating the computational tools used for binding analysis in Chapter 2 and particle image velocimetry in Chapter 4; Dr. William Silkworth for his help with the tandem affinity purification experiments in Chapter 5; Joe Capri and Dr. Julian Whitelegge for performing the mass spectrometry analysis presented in Chapter 5; Haneul Yoo for her stellar work purifying classical *capu* point mutants and assisting with their characterization in Chapter 4; and Andrey Shur for his technical assistance purifying proteins and preparing reagents.

The research in Chapter 2 was originally published in the Journal of Biological Chemistry: Roth-Johnson EA, Vizcarra CL, Bois JS, and Quinlan ME. Interaction between microtubules and the *Drosophila* formin Cappuccino and its effect on actin assembly. *J Biol Chem.* 2014; 289:4395–4404. © The American Society for Biochemistry and Molecular Biology.

Finally, I acknowledge the generous support I received to complete this dissertation: an NIH Ruth L. Kirschstein National Research Service Award GM007185 from the UCLA Cell & Molecular Biology Traning Program and a Whitcome Fellowship awarded by the UCLA Molecular Biology Institute. This work was also made possible by a an NIH-NIGMS Grant R01 GM096133, a Burroughs Wellcome Fund Career Award in the Biomedical Sciences, and a March of Dimes Foundation Grant (#5-FY10-81) awarded to Margot E. Quinlan.

Vita

2005	Summer Intern, Buck Institute for Research on Aging, Novato, CA
2006	Undergraduate Researcher, Molecular & Cell Biology, UC Berkeley
2009	B.A., Molecular & Cell Biology, Music, UC Berkeley
2009	Departmental Citation in Music, UC Berkeley
2009	Honors in Molecular & Cell Biology, UC Berkeley
2009	Whitcome Fellow, Molecular Biology Institute, UCLA
2010	Honorable Mention, Graduate Research Fellowship, NSF
2010	NIH Cell & Molecular Biology Trainee, UCLA
2011	Graduate Student Member, American Society for Cell Biology
2011	Founder, Building Engineers & Mentors, UCLA | beam.ucla.edu
2011	Physiology Student, Marine Biological Laboratory, Woods Hole, MA
2012	Teaching Assistant, Physical Biochemistry, UCLA
2013	Student Member, National Association of Science Writers
2013	Blog Editor, Science & Food, UCLA | www.scienceandfood.org
2014	AAAS Mass Media Fellow, KQED Science, San Francisco, CA

Publications and Presentations

Roth-Johnson EA, Vizcarra CL, Bois JS, and Quinlan ME. Interaction between microtubules and the *Drosophila* formin Cappuccino and its effect on actin assembly. *J Biol Chem* 2014, 289:4395–4404.

Yoo H, Roth-Johnson E, and Quinlan ME. *In vivo* and *in vitro* characterization of *Drosophila* formin Cappuccino mutants. *Mol Biol Cell* 2013, 24(24):3775(suppl). Abstract #309.

Jakobsen MK, Cheng Z, Lam SK, Roth-Johnson E, Barfield RM, and Schekman R. Phosphorylation of Chs2p regulates interaction with COPII. *J Cell Sci* 2013, 126:2151–2156.

Roth-Johnson E and Quinlan M. Interactions between microtubules and the *Drosophila* formin Cappuccino. *Mol Biol Cell* 2012, 23(24):4663(suppl). Abstract #1796.

Tropini C[†], Roth EA[†], Zanic M, Gardner MK, and Howard J. Islands containing slowly hydrolyzable GTP analogs promote microtubule rescues. *PLoS ONE* 2012, 7(1):e30103. [†]Authors contributed equally to this work.

CHAPTER 1

Introduction

1.1 The formin family of actin nucleators

Cytoskeletal networks formed by actin filaments are essential for a wide range of cellular processes from cell motility to morphogenesis. In order to carefully control the spatiotemporal organization and molecular architecture of these actin networks, cells have developed a host of actin regulatory proteins. One such family of regulatory proteins, the formin actin nucleators, initiates assembly of new actin filaments from cellular pools of monomeric actin. These nucleators build linear, unbranched actin filaments to assemble such cellular structures as filopodia [1, 2], contractile rings [3, 4], and actin stress fibers [5, 6, 7]. The metazoan formins are organized into seven distinct groups based on phylogenetic analysis (Fig. 1.1A) [8]. Here, we will focus on the *Drosophila* formin Cappuccino (Capu), which belongs to the FMN group of formins and is one of six formins encoded by the *Drosophila melanogaster* genome [8, 9].

Formins are broadly characterized by their C-terminal formin homology 1 and 2 domains (FH1 and FH2; Fig. 1.1B) [8, 10]. These domains form the core actin nucleating machinery of formin proteins (Fig. 1.1C). The flexible, proline-rich FH1 domain binds profilin-actin to facilitate delivery of actin monomers to the FH2 domain [11]. The FH2 domain forms a flexibly tethered, antiparallel dimer that is thought to stabilize a dimer or trimer of actin monomers to promote filament nucleation [12, 13]. Once a filament has formed, the FH2 domain remains processively associated with the actin barbed end as it elongates [14, 15, 13]. Association with the barbed end protects the filament from capping protein [16, 17] and increases the rate of filament elongation in the presence of profilin-actin [18, 19, 11, 20].

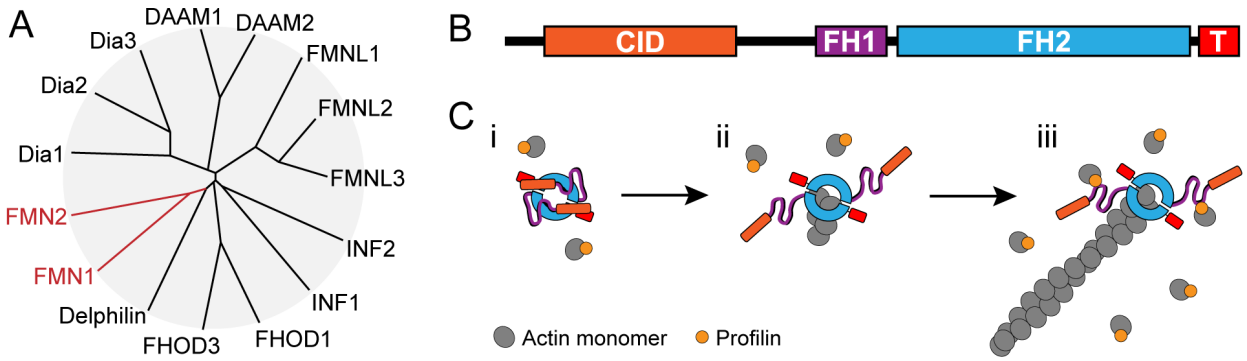

Figure 1.1 – Characteristics of formin family actin nucleators. (A) Fifteen mammalian formin isoforms represent the seven metazoan formin groups: Dia, Diaphanous; DAAM, disheveled-associated activator of morphogenesis; FMNL, formin-like; INF, inverted formin; FHOD, FH2-domain containing; FMN, formin; Delphilin. The *Drosophila* formin Capu belongs to the FMN group highlighted in red. The phylogenetic tree is adapted from Breitsprecher & Goode [9]. (B) Domain organization of Capu as a representative formin: CID, Capu inhibitory domain; FH1, formin homology 1; FH2, formin homology 2; T, tail. (C) General mechanism of formin-mediated actin assembly: (i) formins exist in an inactive, autoinhibited state; (ii) when autoinhibition is relieved, formins nucleate new actin filaments and (iii) remain processively attached to the growing actin barbed end.

Although the N-terminal half of formins is more variable than the highly conserved formin homology domains, it appears to play a common role in regulating formin activity. In diaphanous-related formins (Dia, DAAM, FMNL, and FHOD), an intramolecular interaction between an N-terminal diaphanous autoregulatory domain and a C-terminal diaphanous inhibitory domain potently inhibits actin assembly [21, 22, 23, 24] and can also control cellular localization of some formins [25, 26]. Although Capu and other members of the FMN group do not contain these canonical autoregulatory domains, it was recently shown that Capu is indeed autoinhibited through an interaction between its N-terminal Cappuccino inhibitory domain (Fig. 1.1, B and C) and its short C-terminal tail domain [20].

Perhaps the most curious feature of formins is the variable C-terminal tail domain (Fig. 1.1B). Except for the short autoregulatory domains contained within this region, the tail domain lacks clear sequence conservation among the formin groups and varies widely in both size and charge. For example, Capu's tail is extremely short (31 residues) and highly charged with a theoretical pI of 11.7 [27], while human INF2 has a much longer tail (309 residues) with a theoretical pI of only 4.8 [28]. Previous studies demonstrated that the

tail domain is important for robust actin nucleation activity of Capu, Dia1, and FMNL3 [29, 30, 31]. Capu and its mammalian homologues interact synergistically with the WH2 nucleator Spire (Spir) through the C-terminal tail domain [30, 32]. INF2, and to a lesser extent FMNL3, can also sever actin filaments via their C-terminal tails [33, 31]. Such variation likely contributes to formin diversity by fine tuning actin assembly activity and conferring additional specialized functions based on the distinct physiological roles of each formin.

1.2 Formins as potential coordinators of actin and microtubules

Over the past fifteen years, formins have emerged as coordinators of the actin and microtubule cytoskeletons. Before the mechanistic role of formins as actin nucleators had been discovered, genetic studies in yeast implicated formins as regulators of both actin and microtubules [34, 35, 36]. Lee *et al.* demonstrated early on that the formin Bni1p is required for mitotic spindle positioning in budding yeast, possibly mediating interactions between cytoplasmic microtubules and the cell cortex [35]. A complementary study in fission yeast showed that Cdc12p travels along microtubules to establish the contractile actomyosin ring required for cytokinesis [36]. Shortly thereafter, the mammalian formins mDia1 and Fmn2 were shown, respectively, to colocalize with the mitotic spindle in HeLa cells [37] and to play a role in asymmetric spindle positioning in mouse oocytes [38, 39], establishing a conserved role for formins in coordinating cytoskeletal organization during cell division.

Early studies of mammalian formins also revealed striking, formin-mediated rearrangements of actin and microtubules during interphase [5, 40, 6]. Ishizaki *et al.* were the first to demonstrate that a constitutively active form of mDia1 can induce cell elongation, actin stress fiber formation, and actin-microtubule alignment in cultured HeLa cells [5]. Mutating three conserved lysine residues within the FH2 domain abolishes these phenotypes [5], and intact FH1 and FH2 domains are required to induce cell elongation and actin-microtubule alignment [6]. In addition to these cytoskeletal rearrangements, Palazzo *et al.* showed that mDia2 can induce stable populations of posttranslationally detyrosinated microtubules [40]. This was the first of many studies demonstrating a role for formins in mediating the stability

and posttranslational state of microtubules [41, 42, 43, 44, 45, 46].

Once the biochemical activity of formins as actin nucleating proteins was established [14], it became more apparent how formins could induce such striking changes in actin network architecture. It remained unclear, however, how formins could regulate microtubule organization and stability. Palazzo *et al.* were the first to show that, in addition to colocalizing with microtubules *in vivo*, mDia2 directly binds microtubules *in vitro* [40]. This was later shown for several other formins, including mDia1, hINF2, Fmn2, and Capu [47, 28]. In fact, all formins tested to date can directly bind microtubules *in vitro* [28, 10]. Some formins, including Capu and hINF2, can bundle microtubules and crosslink microtubules to actin filaments [48, 47, 28]. mDia2 and hINF2 can also stabilize microtubules against cold-induced depolymerization *in vitro* [43, 28].

In addition to directly associating with microtubules, several formins interact with regulatory proteins that target microtubule plus ends. Diaphanous formins can bind directly to cytoplasmic linker protein 170 (CLIP-170) and end binding protein 1 (EB1), which bind and stabilize the growing plus ends of microtubules [49, 41, 50]. EB1 also acts as a molecular scaffold for other microtubule associated proteins including the mDia1 nucleation-promoting factor adenomatous polyposis coli (APC) [50, 51, 52]. Wen *et al.* demonstrated that EB1 stabilizes microtubules downstream of mDia and colocalizes with mDia and APC at the ends of stable, detyrosinated microtubules in TC-7 kidney cells [41]. Similar studies also found that Diaphanous formins participate in microtubule stabilization signaling pathways upstream of glycogen synthase kinase 3, which regulates APC recruitment to microtubule plus ends [42, 53].

Such a variety of binding partners and regulatory effects on microtubules likely reflects the range of physiological roles formins play in coordinating actin and microtubules. Already, formins have been implicated as cytoskeletal coordinators in such diverse cellular processes as focal adhesion turnover [54], centrosome reorientation [55, 45, 56, 57], acentric meiotic spindle positioning [38, 39], cell spreading [58], and cortical capture of microtubule plus ends [53, 59]. However, our mechanistic understanding of these formin-mediated processes is still extremely limited. The field currently lacks formin mutations that can be used as tools to selectively

disrupt microtubule interactions *in vivo*. As a result, important biological questions have yet to be answered. For example, it is still unknown whether particular physiological processes require direct formin-microtubule binding versus indirect interactions through microtubule associated proteins. And although it seems reasonable to assume that formins would use their actin assembly activity to regulate microtubules, it is still unclear whether formins directly coordinate actin and microtubules or instead regulate these cytoskeletal networks independently.

A few key biochemical studies have begun to shed light on formin-microtubule interactions. The first study to measure formin-microtubule binding affinity showed that an FH1/FH2 construct of mDia2 (residues 521-1040) binds the sides of microtubules with 6 μM affinity [43]. They also found that mDia2 actin nucleation activity and FH2 dimerization are not required for *in vitro* microtubule binding or *in vivo* microtubule stabilization. Subsequent studies have corroborated this finding, showing that actin nucleation activity is not required for mDia3 to mediate microtubule attachment to kinetochores [60] or for mDia1 to mediate cortical microtubule capture [59]. Most recently, Gaillard *et al.* conducted an in-depth, side-by-side analysis of three formins (mDia1, mDia2, and hINF2) and found striking differences among their interactions with microtubules [28]. All three formins can bind microtubules through their core FH1/FH2 domains, but their C-terminal tail domains have variable effects: the tail is required for robust mDia2-microtubule binding but is dispensable for binding by either mDia1 or hINF2. Of the three formins, only hINF2 can readily bundle microtubules, and only mDia2 is potently inhibited by microtubules in bulk actin assembly assays.

Given the diversity of formin function *in vivo*, it is not surprising that microtubule binding would vary mechanistically across formins. In addition to the differences observed by Gaillard *et al.*, unique microtubule binding sites have been identified in the C-terminus of INF1 [44] and a unique N-terminal exon of Fmn2 isoform Ib [61]. These sites are sufficient to bind microtubules *in vitro* and to colocalize with microtubules *in vivo*, yet similar regions do not appear to exist in other formins. Together, these findings suggest that formins may have unique modes of microtubule binding; however, given the limited number of biochem-

ical studies and focus on only a handful of formins, it is still too early to draw any clear conclusions about the molecular mechanisms of formin-microtubule binding. Therefore, to further improve our biochemical understanding of formin-microtubule interactions, we set out to characterize microtubule binding by the *Drosophila* FMN group formin, Capu.

1.3 Capu's role in *Drosophila* oogenesis

Capu was first discovered in screens for maternal effect genes important for oocyte polarity in *Drosophila* [62, 63]. During development, Capu is required for establishing both the anteroposterior and dorsoventral axes of the oocyte. This is accomplished through localization of polarity determinants such as *bicoid* (*bic*), *gurken* (*grk*) and *oskar* (*osk*) mRNAs (for review see Kugler & Lasko [64]). Localization of *osk* to the oocyte posterior is lost in *capu* mutants [65], which disrupts anteroposterior patterning and assembly of the pole plasm, a specialized cytoplasm containing maternal mRNAs and proteins essential for germline development [66, 67]. *capu* mutants also partially disrupt *grk* localization to the anterior margin, which is required for proper dorsoventral patterning [68]. As a result of *osk* and *grk* mislocalization, loss of Capu leads to severe polarity defects and female sterility [62].

Once Capu's molecular role as an actin nucleator was established, investigators began identifying Capu-dependent actin structures in the oocyte. Two such structures have been characterized to date: a cytoplasmic mesh (Fig. 1.2B) [69] and a collection of posterior actin projections (Fig. 1.2C) [70].

The first Capu-dependent actin structure discovered in the *Drosophila* oocyte is a cytoplasmic actin mesh present throughout mid-oogenesis (Fig. 1.3A). Capu works together with Spir to build this mesh [69, 32]. The kinase inactive domain (KIND) of Spir binds directly to the tail domain of Capu [32, 30] and can inhibit Capu's actin nucleation activity *in vitro* [47]. However, a larger Spir construct comprising both the KIND and WH2 actin nucleation domains can interact with Capu to form a functional nucleation complex [30]. Recent experiments in the *Drosophila* oocyte have revealed that construction of the cytoplasmic actin mesh requires both the Capu-Spir interaction and Capu's own actin nucleation

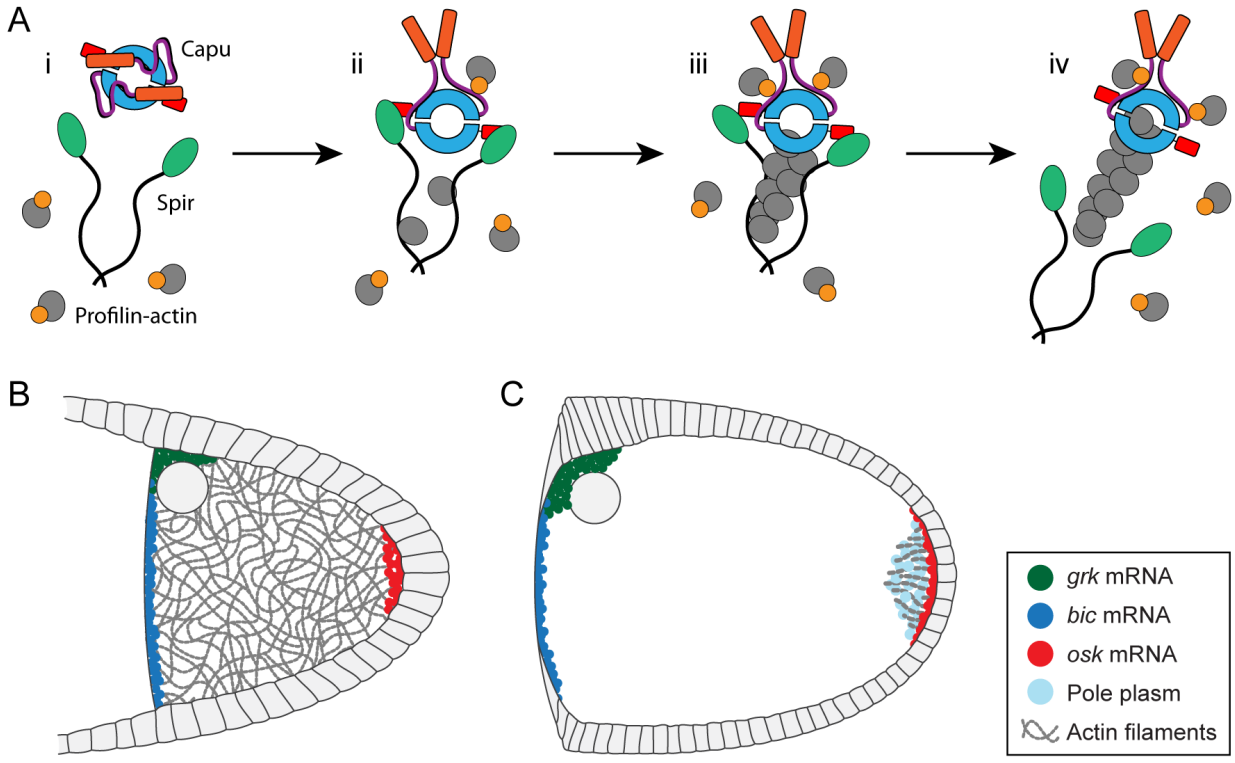

Figure 1.2 – Role of Capu and Spir in *Drosophila* oogenesis. (A) Model of synergistic actin assembly by Capu and Spir. (i) On its own, Capu is expected to be autoinhibited. Spir may be a monomer or a dimer. (ii) Spir and Capu interact to form a functional nucleation complex. Spir-KIND binding to Capu's tail domain relieves autoinhibition. (iii) Spir binds actin monomers to form a "pre-nucleation" complex. With Spir bound, Capu cannot nucleate or elongate actin filaments. (iv) Capu dissociates from Spir and processes along the growing barbed end of the new actin filament. Spir may or may not remain bound to the pointed end of the filament. (B) Capu and Spir build a cytoplasmic actin mesh during mid-oogenesis. The mesh is thought to prevent cytoplasmic streaming to facilitate localization of polarity factors such as *bic*, *grk*, and *osk* mRNA. (C) Starting around stage 10, Capu and Spir build posterior actin projections in response to *osk* localization. These projections are thought to play a role in pole plasm assembly and anchoring.

activity. From these genetic observations and biochemical data, it has been proposed that Capu and Spir form a synergistic nucleation complex that must also separate to function properly *in vivo* [32]. In this model (Fig. 1.2A), Spir and Capu bind actin to form a transient pre-nucleation complex; Spir is then released from the complex, while Capu remains processively attached to the barbed end where it can act as an elongation factor, accelerating the growth of the filament [20] and protecting it from being capped [30].

In wildtype oocytes, the cytoplasmic actin mesh disappears around stage 10b of development [69]. Disappearance of the mesh coincides with dramatic changes in microtubule organization and cytoplasmic fluid dynamics (Fig. 1.3, A and B). Throughout mid-oogenesis when the actin mesh is present, microtubules form a biased random network [71] and the cytoplasm exhibits slow, uncoordinated movements often referred to as "slow streaming" or "seething" [72]. After stage 10b when the actin mesh has disappeared, microtubules form more ordered cortical arrays and fast, coordinated movement of the cytoplasm begins [72, 69]. This "cytoplasmic streaming" is driven by kinesin movement along microtubules and is approximately ten times faster than the slow streaming observed throughout mid-oogenesis [73, 74]. In *capu* and *spir* loss-of-function mutants, the actin mesh is not detected and cytoplasmic streaming occurs prematurely [69]. Because *osk* mRNA does not localize properly in *capu* mutants [65], it is thought that premature cytoplasmic streaming disrupts *osk* transport during mid-oogenesis. Our current model proposes that Capu and Spir build the cytoplasmic mesh to regulate the timing of streaming and ensure the proper localization of polarity factors.

The second Capu-dependent actin structure discovered in the *Drosophila* oocyte is a collection of long (2.5 μm) posterior actin projections that form in response to *osk* localization (Fig. 1.2C) [75, 70]. Beginning around stage 10 of oogenesis, these actin projections appear to emanate from the posterior cortex and are rarely observed along the lateral cortex [75]. Anterior misexpression of *osk* induces ectopic actin projections at the anterior cortex [76]. Formation of the actin projections requires both Capu and Spir [70], suggesting that they may be assembled through a similar molecular mechanism as the cytoplasmic actin mesh.

Although the precise physiological role of these actin projections is still unclear, they have

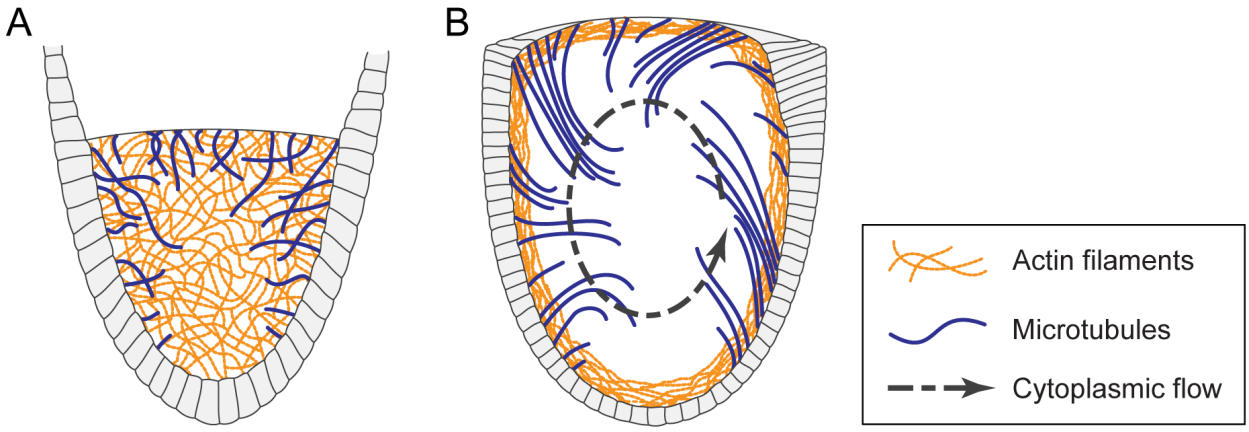

Figure 1.3 – Cytoskeletal organization during *Drosophila* oogenesis. (A) During mid-oogenesis (stages 7–10a), a cytoplasmic actin mesh traverses the oocyte and microtubules form a biased random network. (B) From stage 10b onward, the cytoplasmic actin mesh is absent, while cortical actin remains present and microtubules form loose cortical arrays. These dramatic cytoskeletal rearrangements coincide with the onset of the fast, coordinated movement of the cytoplasm known as cytoplasmic streaming. Figure adapted from Serbus *et al.* [74].

been proposed to play a role in anchoring *osk* mRNA and other pole plasm components to the posterior cortex [75, 77]. Intriguingly, both pole plasm assembly and formation of the actin projections are closely tied to endocytosis, which is locally upregulated at the oocyte posterior in response to *osk* localization [75]. Loss of Rabenosyn-5, which functions in early endosome transport, disrupts pole plasm assembly and causes the posterior actin projections to aggregate and diffuse away from the cortex [76]. Once the pole plasm is established, its maintenance and anchoring require Mon2, which is thought to regulate vesicular trafficking between the Golgi and endosomes [70, 78]. Mon2 is also required for the formation of the posterior actin projections and co-immunoprecipitates with Capu and Spir from S2 cell lysates [70]. Based on these observations, it has been hypothesized that specialized endocytic vesicles instruct Mon2 to regulate Capu and Spir activity to assemble the actin projections, which in turn play a role in anchoring the pole plasm to the posterior cortex [70].

1.4 Overview of the dissertation

This dissertation focuses on characterizing the interaction between Capu and microtubules in order to gain a more complete understanding of formin-microtubule binding and of

Capu's role in *Drosophila* oogenesis. By studying the molecular mechanisms of the Capu-microtubule interaction, we aim to identify mutations that selectively disrupt microtubule binding. Such mutations would be important tools for studying Capu's function in the oocyte and would elucidate the broader role of formins as coordinators of the actin and microtubule cytoskeletons. By studying classical *capu* mutations and identifying novel Capu binding partners, we aim to refine our understanding of how Capu assembles the cytoplasmic actin mesh and posterior actin projections during oogenesis. Moreover, Manseau *et al.* showed that strong *capu* alleles exhibit cytokinesis defects early in development, suggesting there are additional uncharacterized roles for Capu in the oocyte [65]. Our multifaceted approach should provide much needed insight into Capu's role in development as well as broader mechanisms of formin function.

In Chapter 2, we study *in vitro* microtubule binding by Capu with the aim of gaining a more detailed mechanistic understanding of formin-microtubule interactions and formin-mediated actin-microtubule crosstalk. We report that two distinct domains within Capu, FH2 and tail, work together to promote high-affinity microtubule binding. The tail domain appears to bind microtubules through non-specific charge-based interactions. In contrast, distinct residues within the FH2 domain are important for microtubule binding. Here we also report the first visualization of a formin polymerizing actin filaments in the presence of microtubules. Interestingly, microtubules are potent inhibitors of Capu's actin nucleation activity but appear to have little effect on Capu once it is bound to the barbed end of an elongating filament. This finding fits well with other studies suggesting that actin assembly and microtubule binding are mutually exclusive activities of formins [43, 79, 60, 59].

In Chapter 3, we examine the localization of Capu and microtubules in S2 cells. Although Capu does not appear to colocalize with microtubules in the *Drosophila* oocyte, clear formin-microtubule colocalization has been observed in mammalian tissue culture experiments [44, 61]. We report that Capu does not colocalize with microtubules in S2 cells during interphase or during cell division. Treating cells with an actin depolymerizing drug does not promote Capu-microtubule colocalization. Even mDia2, which associates with and stabilizes microtubules in mammalian cells [43, 79], does not colocalize with microtubules

in S2 cells. We therefore conclude that S2 cells are not an ideal system for examining formin-microtubule colocalization.

In Chapter 4, we present a systematic *in vivo* and *in vitro* characterization of seven classical *capu* alleles. Although many genetic *capu* mutants have been reported in the literature, their biochemical activities have not been studied extensively. We report that all identified missense mutations appear within Capu's FH2 domain. These mutations result in premature cytoplasmic streaming and a compromised cytoplasmic actin mesh, but variably affect actin nucleation activity *in vitro*. Surprisingly, several of the mutations alter microtubule binding density but do not substantially decrease microtubule binding affinity. Further characterization of these mutants will be necessary to fully explain these results. However, our findings suggest that the Capu mutants, despite falling within the FH2 domain, affect Capu through different mechanisms and that the *in vitro* nucleation activity of Capu does not correspond directly to its *in vivo* activity. Finally, we report the first characterization of a novel "loop" insert within the lasso region of Capu's FH2 domain. This insert is unique to Capu and does not appear to be important for actin assembly or microtubule binding. Future work in the *Drosophila* oocyte will determine the physiological relevance of this newly identified region.

In Chapter 5, we perform a tandem affinity purification experiment to elucidate Capu's roles and regulation during development. We identify several candidate Capu binding partners involved in such diverse cellular processes as mitochondrial fission, endocytosis, and nuclear import. Though preliminary, these results suggest that Capu plays additional roles in oogenesis beyond building the cytoplasmic actin mesh and posterior actin projections. We also report putative phosphorylation sites and regulatory kinases. Future work confirming and characterizing these findings will provide valuable insight into Capu's role during development and may shed light on the physiological relevance of Capu-microtubule binding.

CHAPTER 2

In vitro analysis of Capu-microtubule binding

Coordination of actin and microtubule cytoskeletal networks is required for a diverse set of cellular processes, from cell motility and morphogenesis to intracellular transport and nuclear migration [80, 81]. Recently, formin family actin nucleators have emerged as coordinators of the actin and microtubule cytoskeletons. In addition to nucleating actin filaments, all formins tested to date directly bind microtubules *in vitro* [10, 28].

Although actin polymerization by formins has been well characterized, how formins coordinate actin and microtubule networks remains an open question. In fact, only three formins (mDia1, mDia2, hINF2) representing just two of the fifteen metazoan formin groups have been characterized in any biochemical detail [28], and experimental data for formin-microtubule binding varies widely across the few formins studied. Several *in vitro* experiments suggest that actin and microtubules directly compete for formin binding: for example, microtubules potently inhibit actin polymerization by mDia2, while actin monomers compete with microtubules for binding to hINF2 [28]. In contrast, other findings support a role for formins in the coordination of actin and microtubule networks: overexpression of mDia1 or FHOD1 aligns actin and microtubule networks in cells [5, 6], and hINF2 and Capu can crosslink actin and microtubules *in vitro* [28, 48]. While this variety likely reflects the specialized cellular roles of distinct formins, it is unclear if conserved microtubule binding mechanisms exist or if this functional diversity stems from fundamental differences in formin-microtubule interactions. Addressing this question will require careful biochemical analysis of microtubule binding by a variety of formins representing the many formin groups.

To further improve our mechanistic understanding of formin-microtubule interactions and formin-mediated actin-microtubule crosstalk, we studied microtubule binding by the

Drosophila formin Capu. Capu belongs to the FMN group of formin nucleators and has two conserved mammalian homologs, Fmn1 and Fmn2 [8]. All three proteins are involved in cytoskeletal regulation during key stages of development. Capu is required for establishing the major body axes of the developing *Drosophila* oocyte, and loss of Capu leads to severe polarity defects and female sterility [62]. Similarly, Fmn1 and Fmn2 have been implicated in a variety of developmental processes including limb patterning and oocyte spindle positioning [82, 83, 84]. Although these proteins all bind microtubules *in vitro* [47, 61], little else is known about how FMN group formins interact with microtubules and coordinate the actin and microtubule cytoskeletons. The absence of comprehensive mechanistic data for these and other formins has made it difficult to study the physiological relevance of such formin-microtubule interactions.

In this study, we have characterized Capu-microtubule binding in detail and examined the relationship between Capu's microtubule binding and actin assembly activities. We report that Capu binds microtubules with high affinity, suggesting that this is a physiologically relevant interaction. Binding requires distinct residues within the FH2 domain as well as non-specific charge-based interactions with Capu's C-terminal tail domain. Additionally, we found that Capu does not bind microtubules and assemble new actin filaments simultaneously. Specifically, microtubules are potent inhibitors of Capu's actin nucleation activity both in the absence and presence of profilin, but cannot effectively compete for binding to Capu that is already bound to the barbed end of an elongating actin filament. This study provides new mechanistic information about formin-microtubule binding and represents the first detailed biochemical study of microtubule binding by a FMN group formin. Together with biochemical studies of other formins, our findings offer insight into the physiological relevance of the formin-microtubule interaction and will help create necessary tools for future *in vivo* work.

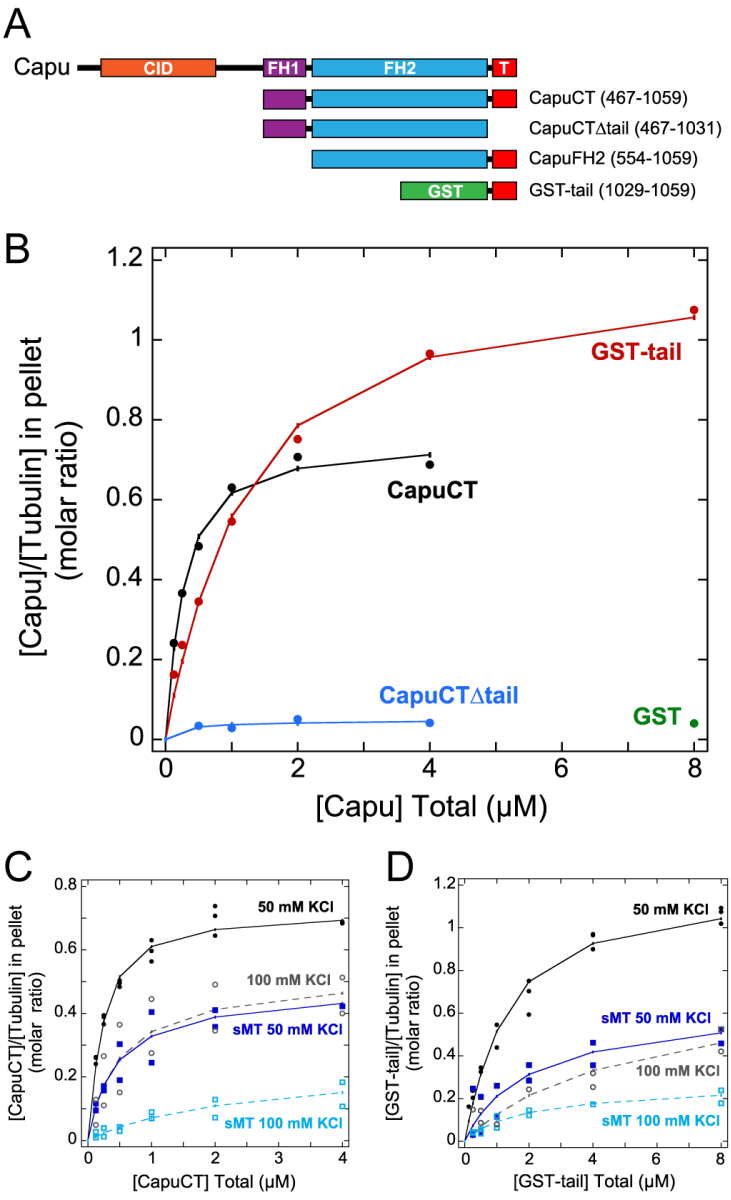

Figure 2.1 – High-affinity microtubule binding requires FH2 and tail. (A) Schematics of Capu (1059 aa) and the constructs used in this study. CID, Capu inhibitory domain (orange); FH1, formin homology 1 (purple); FH2, formin homology 2 (blue); T, tail (red); GST, glutathione-S-transferase (green). (B) Binding of CapuCT, CapuCTΔtail, GST-tail, and GST control to taxol-stabilized microtubules at 50 mM KCl. Total tubulin concentration is 0.5 μM in all binding assays. CapuCT (C) and GST-tail (D) binding to intact microtubules at 50 mM KCl (solid circles, solid line) or 100 mM KCl (open cirlces, dashed line) and to subtilisin-treated microtubules (sMT) at 50 mM KCl (solid squares, solid line) or 100 mM KCl (open squares, dashed line).

Table 2.1 – Fit parameters for all microtubule binding curves. The free energy of binding ($\Delta_r G$) is expressed with units kJ/mol and the binding site size (n) is expressed as the number of α/β-tubulin dimers per binding site. Error bars for $\Delta_r G$ and n represent one standard deviation. The most probable dissociation constant (K_d) values are reported in units of μM and calculated from $\Delta_r G$ at 25°C (see Section 7.3 for additional information). Experiments performed with high salt conditions (100 mM KCl) and/or subtilisin-treated microtubules (sMT) are indicated; all other binding curves were measured at 50 mM KCl with untreated microtubules.

Binding Experiment	$\boldsymbol{\Delta_r G}$ **(kJ/mol)**	$\boldsymbol{K_d}$ **(μM)**	$\boldsymbol{n}$ **(α/β dimers)**
CapuCT	5.21 ± 0.16	0.12	1.44 ± 0.01
CapuCT + 100 mM KCl	0.55 ± 0.20	0.80	1.67 ± 0.04
CapuCT + sMT	1.47 ± 0.46	0.55	1.89 ± 0.09
CapuCT + sMT + 100 mM KCl	−5.67 ± 0.33	9.8	2.30 ± 0.31
GST-tail	−0.26 ± 0.14	1.1	0.83 ± 0.01
GST-tail + 100 mM KCl	−5.37 ± 0.15	8.7	1.40 ± 0.07
GST-tail + sMT	−3.55 ± 0.40	4.2	1.43 ± 0.11
GST-tail + sMT + 100 mM KCl	−4.58 ± 0.29	6.4	2.94 ± 0.16
CapuCT-Scr	6.31 ± 0.58	0.08	1.40 ± 0.04
CapuCT-L1048A	5.56 ± 0.10	0.11	1.35 ± 0.01
CapuCT-I706A	4.71 ± 0.25	0.15	1.41 ± 0.02
CapuCT-D854N	5.66 ± 0.29	0.10	1.44 ± 0.02
CapuCT-K858A	4.01 ± 0.17	0.20	1.20 ± 0.01
CapuCT-K856A	3.33 ± 0.11	0.26	0.83 ± 0.01

2.1 Microtubule binding by Capu

We used high-speed taxol-microtubule pelleting assays to measure microtubule binding by the C-terminal half of Capu, CapuCT, comprising Capu's FH1, FH2, and short C-terminal tail domains (see Fig. 2.1A for diagrams of core constructs used in this study). We fit our data to a non-cooperative, polar, one-dimensional lattice binding model [85] to determine the dissociation constant (K_d) and the number of α/β-tubulin dimers (n) in each binding site. At 50 mM KCl, CapuCT binds microtubules with affinity on the order of 100 nM and occupies a binding site of approximately 1.4 tubulin dimers (Fig. 2.1B, Table 2.1).

A previous study showed that the C-terminal tails of different formins have varying effects on microtubule binding [28]. We therefore measured microtubule binding of CapuCTΔtail, a construct lacking Capu's 30 amino acid tail domain, and found that the tail is required for microtubule binding (Fig. 2.1B). To test tail-microtubule binding directly, we created a glutathione S-transferase (GST)-fusion protein of Capu's tail domain, since the orientation

of the GST-tail dimer is thought to mimic the antiparallel orientation of the formin dimer [28]. Although GST-tail could indeed bind microtubules, it bound with lower affinity (on the order of 1 μM) and higher binding density than CapuCT (approximately 0.8 tubulin dimers per binding site; Fig. 2.1B and Table 2.1). GST binding to microtubules was negligible even at the highest protein concentration used in these assays (Fig. 2.1B).

To further characterize the nature of Capu-microtubule binding, we assessed the contribution of ionic contacts in the microtubule pelleting assays. We first repeated the assay at a higher ionic strength. At 100 mM KCl, CapuCT and GST-tail both exhibit reduced microtubule binding density and binding affinity (Fig. 2.1, C and D, Table 2.1). Because the Capu-microtubule interaction is sensitive to salt, we next asked whether the glutamate-rich C-terminal tails of α- and β-tubulin are involved in Capu binding. We treated microtubules with the protease subtilisin to selectively remove the acidic tubulin tails. Similar to what we observed at higher ionic strengths, both CapuCT and GST-tail exhibited reduced binding density and binding affinity to subtilisin-treated microtubules at 50 mM KCl compared to untreated microtubules (Fig. 2.1, C and D, Table 2.1). Binding to subtilisin-treated microtubules was further reduced at 100 mM KCl (Fig. 2.1, C and D, Table 2.1), suggesting that the tubulin tails are not the only sources of ionic interaction.

2.2 Effect of microtubules on actin nucleation

Because Capu is a potent actin nucleator, we next asked whether microtubule binding affects Capu's ability to assemble actin filaments. We first performed bulk pyrene-actin polymerization assays. In these assays, Capu was pre-incubated with microtubules before being added to actin. Microtubules inhibited actin assembly by CapuCT in a dose-dependent manner (Fig. 2.2A). This effect is specific to microtubules since CapuCT was only minimally inhibited by a 40-fold molar excess of unassembled tubulin dimers (Fig. 2.2D). Microtubules failed to inhibit CapuCTΔtail, showing that inhibition requires high affinity microtubule binding (Fig. 2.2E). We used higher concentrations of CapuCTΔtail in this assay because this construct exhibits reduced polymerization activity as previously reported [30].

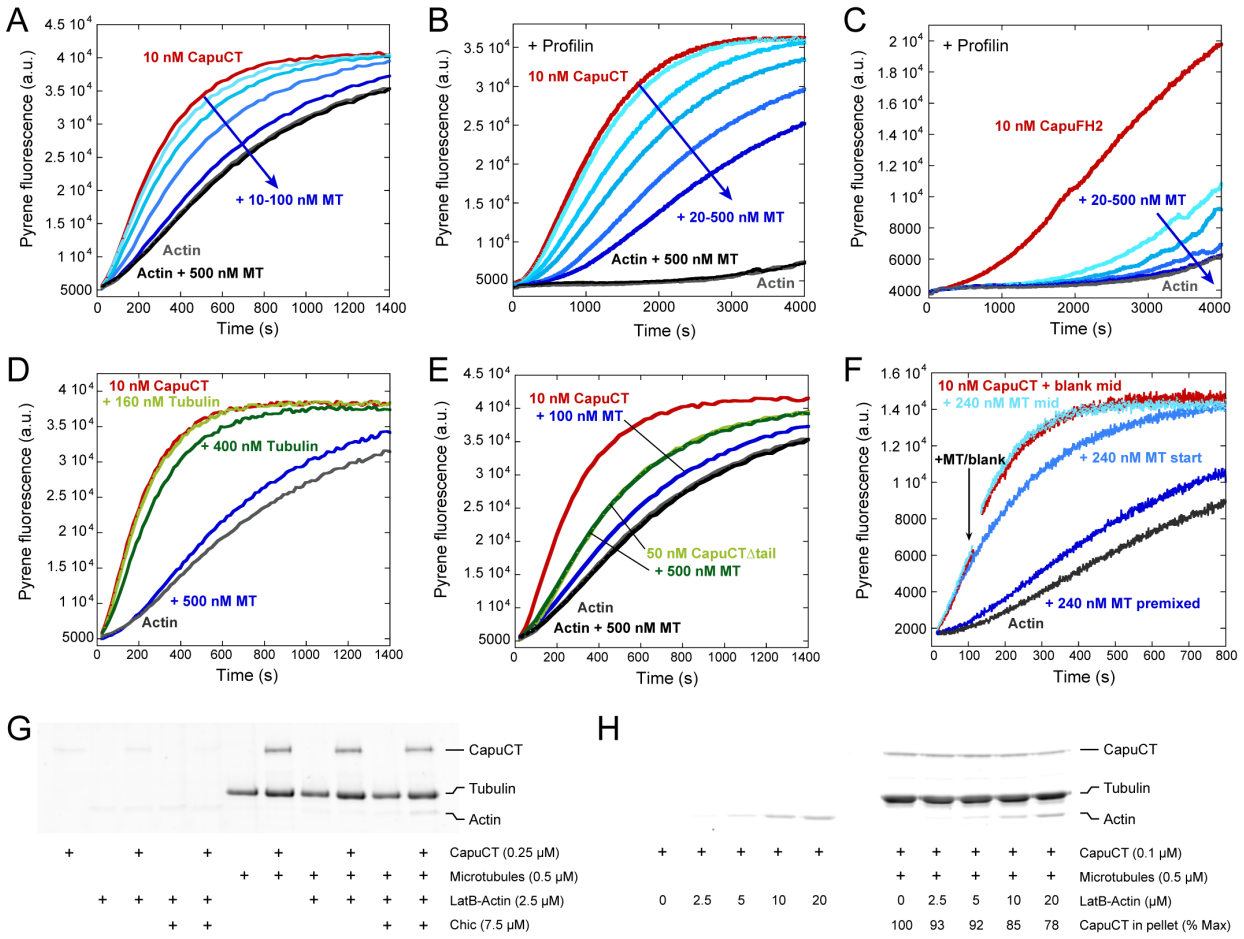

Figure 2.2 – Microtubules potently inhibit Capu's nucleation activity. (A) Dose-dependent inhibition of 10 nM CapuCT by 10, 20, 50, and 100 nM microtubules (MT) in bulk pyrene-actin polymerization assays. Microtubules do not affect baseline actin polymerization rates. (B–C) Microtubules inhibit nucleation from profilin-actin by 10 nM CapuCT (B; 20, 50, 100, 200, 500 nM MT) and 10 nM CapuFH2 lacking the FH1 domain (C; 20, 50, 100, 500 nM MT). (D) Unassembled tubulin dimers have a negligible effect on CapuCT actin polymerization activity compared to taxol-stabilized microtubules. (E) Microtubules do not inhibit actin polymerization by CapuCTtail. At a 10:1 molar ratio, microtubules potently inhibit actin polymerization by CapuCT but not CapuCTtail. (F) Inhibition is sensitive to the time at which microtubules are added to the assay. Microtubules were added to CapuCT before adding actin (premixed), immediately after adding actin (start), or approximately 120 seconds into the assay (mid, arrow indicates beginning of mixing). (G–H) Latrunclin B-stabilized actin monomers (LatB-Actin; twofold molar excess of LatB) weakly compete with microtubules to bind CapuCT in high-speed pelleting assays. Pellet fractions are shown and concentrations are given. (G) No noticeable competition was observed with 2.5 μM LatB-Actin in the absence or presence of Chic (*Drosophila* profilin). (H) Some competition between microtubules and LatB-Actin can be observed at very low CapuCT and very high LatB-Actin concentrations, similar to those used in bulk pyrene-actin nucleation assays. CapuCT bound to microtubules is reported as a percentage of the maximum CapuCT bound at 0 μM LatB-Actin.

We next tested whether this inhibitory effect persisted when high levels of profilin were added to the assay. We used *S. pombe* profilin in these assays because, unlike other profilins, it exhibits minimal bias against binding actin labeled at Cys-374 (data not shown). Even in the presence of excess profilin (2:1 molar ratio with actin), microtubules inhibited CapuCT in a dose-dependent manner (Fig. 2.2B). Profilin not only suppresses formin nucleation activity, but also works together with the FH1 domain to accelerate elongation of formin-bound filaments (23, 24). We therefore used a Capu construct lacking the FH1 domain (CapuFH2; Fig. 2.1A) to specifically test nucleation inhibition by microtubules in the presence of excess profilin. Although nucleation by CapuFH2 was very slow in the presence of profilin, microtubules further inhibited nucleation in a dose-dependent manner (Fig. 2.2C).

To test whether microtubules were hindering the elongation of Capu-associated filaments, we measured the effect of microtubules added at different timepoints throughout the polymerization assay. When we added microtubules immediately after mixing CapuCT with actin, as opposed to before actin was added, inhibition was dramatically reduced (Fig. 2.2F). Microtubules added midway through the assay, when nucleation is negligible, had no noticeable inhibitory effect (Fig. 2.2F). These results show that microtubules specifically inhibit Capu's nucleation activity and do not noticeably slow or inhibit the elongation of Capu-associated actin filaments.

To gain a better mechanistic understanding of how microtubules inhibit Capu's nucleation activity, we tested whether microtubules and actin monomers directly compete for CapuCT binding. We first tried the same high-speed pelleting assay conditions used by Gaillard *et al.* to test actin monomer competition with mDia1 and hINF2 [28]. Under these assay conditions, a 10-fold molar excess of actin monomers, we did not observe a change in CapuCT binding to microtubules in the presence or absence of *Drosophila* profilin, Chickadee (Chic; Fig. 2.2G). However, our bulk pyrene-actin polymerization assays contain a much higher (400-fold) molar excess of actin monomers compared to CapuCT. To better simulate the conditions of our polymerization assay, we tried high-speed pelleting assays with much lower and higher CapuCT and actin concentrations, respectively. At a 200-fold molar excess of actin monomers, approximately 20% of the bound CapuCT was successfully competed

away from the microtubules (Fig. 2.2H). Together with our bulk polymerization data, these findings suggest that microtubules inhibit actin nucleation at least in part by preventing actin monomers from associating with CapuCT.

2.3 Barbed end association in the presence of microtubules

To better understand the interplay between actin polymerization and microtubule binding, we turned to single filament analysis. Using total internal reflection fluorescence (TIRF) microscopy, we directly observed elongating actin filaments in a field of immobilized, taxol-stabilized microtubules. To help limit the total number of actin filaments in these assays, filaments were grown from preassembled actin seeds stabilized with AlexaFluor488-labeled phalloidin, and CapuCT was added at very low concentrations. We included Chic to differentiate filaments with Capu bound at the barbed end from filaments free of Capu [20]: in the presence of Chic, Capu-associated filaments appear dimmer and elongate much faster than bright Capu-free filaments.

In this experiment, elongating actin filaments that encountered a microtubule were observed to either cross over the microtubule and continue growing (Fig. 2.3A, panel i); grow along the microtubule (Fig. 2.3A, panel ii); or turn away from the microtubule and continue growing (Fig. 2.3A, panel iii). Consistent with our bulk polymerization assays (Fig. 2.2D), CapuCT associated filaments never stopped upon encountering a microtubule. The frequencies of the three observed behaviors were similar for both CapuCT-bound (dim) and CapuCT-free (bright) filaments (Fig. 2.3B); we therefore believe that these behaviors, though intriguing, reflect our experimental set-up. The illumination field is deep enough (110 nm) to visualize filaments crossing without physically encountering each other. At the surface of the coverslip, microtubules could act as physical barriers and cause actin filaments to turn or elongate along the microtubule. Interactions between fluorescent labels could also promote alignment of microtubule and actin filaments.

Although CapuCT occasionally dissociated from the barbed end of an actin filament upon encountering a microtubule (Fig. 2.3A, panel iv), CapuCT remained bound to the

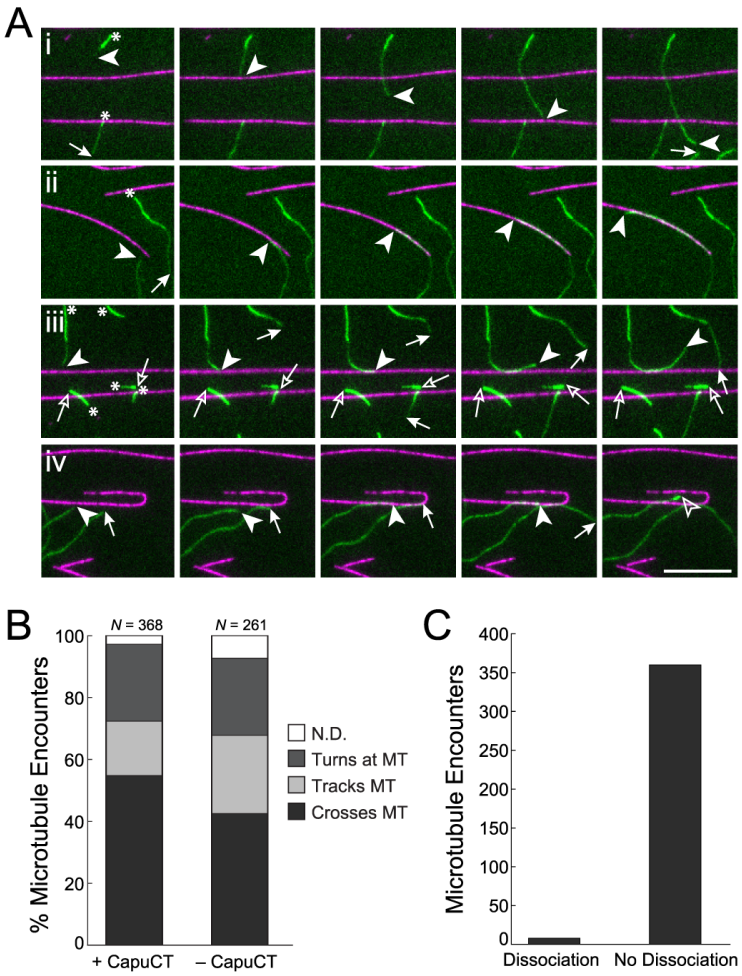

Figure 2.3 – Microtubules do not disrupt Capu association with the barbed end of actin. (A) Upon encountering a microtubule (magenta), elongating actin filaments (green) either (i) crossed the microtubule, (ii) tracked the microtubule, or (iii) turned at the microtubule; (iv) occasionally CapuCT dissociated from the barbed end upon encountering a microtubule. Arrowheads denote the barbed ends of interest, while arrows denote all other barbed ends; free and CapuCT-associated barbed ends are represented by open and filled symbols, respectively. Asterisks (*) in the first panel denote bright, AlexaFluor488-phalloidin-labeled actin seeds that were not nucleated by CapuCT. Images are shown at 60 second intervals. Scale bar is 10 μm. (B) Quantification of actin behavior upon encountering microtubules in the presence or absence of CapuCT. Events that could not be classified into one of these three categories are reported as not determined (N.D.). (C) Quantification of microtubule encounters that resulted in CapuCT dissociation from the barbed end of an elongating actin filament (N = 368; same data set as +CapuCT in B).

barbed end in 98% of all the microtubule encounters we observed (Fig. 2.3C). These data show directly that microtubules are unable to effectively compete CapuCT away from the barbed ends of actin filaments.

2.4 Characterization of the tail-microtubule interaction

We attempted to map a more specific microtubule binding region within the tail domain. In addition to microtubule binding, Capu's tail domain is involved in actin polymerization, protein-protein interactions, and autoinhibition [30, 20]. A single point mutation, L1048A, is sufficient to disrupt Capu binding to the actin nucleator Spir *in vitro* [30] but does not decrease autoinhibition [20]. This mutation had no effect on microtubule binding (Fig. 2.4C, Table 2.1), suggesting that the different functions of Capu's tail domain may be separable. We started by making a series of truncations and found that CapuCT-microtubule binding decreased monotonically as the tail was successively truncated (Fig. 2.4, A and B, Fig. 2.5A).

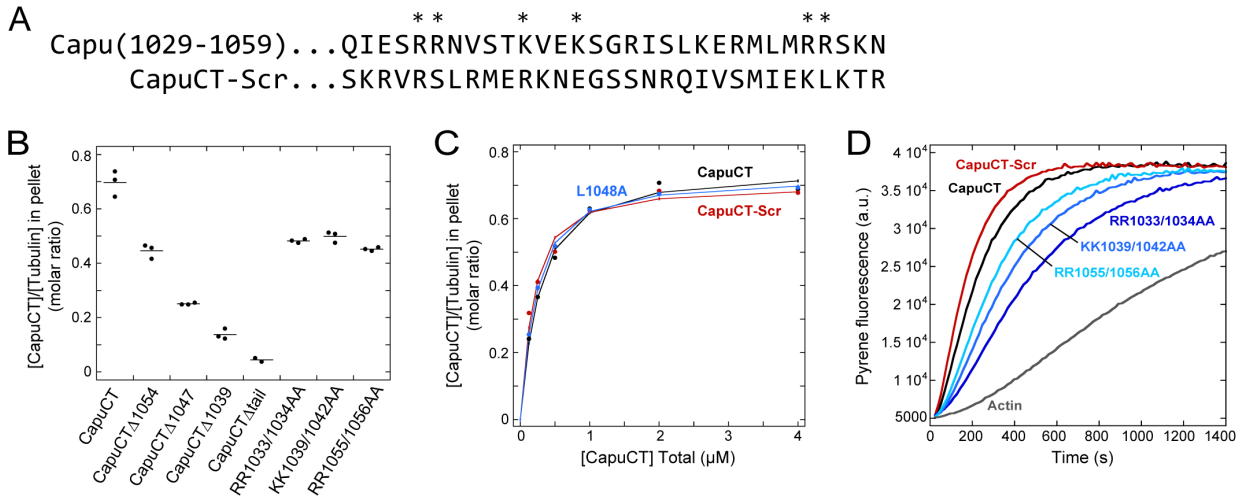

Figure 2.4 – Tail binds microtubules through nonspecific charge-based interactions. (A) Sequences of wildtype and scrambled tail (residues 1029-1059). Residues mutated to alanine within wildtype are denoted by an asterisk (*). (B) Microtubule binding by CapuCT truncation and point mutation constructs. Experimental conditions are 0.5 μM tubulin and 2 μM of the designated CapuCT construct in 50 mM KCl buffer. Individual experiments are plotted as dots with a line showing the mean. (C) CapuCT with a scrambled tail (CapuCT-Scr) or a Spir-binding point mutation (CapuCT-L1048A) bind microtubules comparably to wildtype CapuCT. All binding assays are at 50 mM KCl with 0.5 μM tubulin. (D) Actin polymerization activity of 10 nM each CapuCT tail point mutant and CapuCT-Scr compared to wildtype.

Truncating the tail domain also decreased actin assembly activity (Fig. 2.5C) From this, we conclude that the microtubule-binding region cannot be readily narrowed down to a small patch of neighboring residues within the tail domain.

Our earlier experiments showed that microtubule binding by Capu is sensitive to ionic strength and is therefore likely mediated by charge-based interactions. Consistent with this hypothesis, Capu's tail domain is basic, with a theoretical pI of 11.7 [27] and a fairly even distribution of positively charged residues. To test more directly whether positively charged residues within the tail domain are important for microtubule binding, we created several arginine/lysine-to-alanine double point mutations (Fig. 2.4A). Despite being spread throughout Capu's tail domain, each set of mutations had a measurable and approximately equal effect on microtubule binding (Fig. 2.4B). These mutations also decreased Capu's actin nucleation activity (Fig. 2.4D and Fig. 2.5D), suggesting that Capu-tail contributions to microtubule binding and actin assembly are not readily separable. Even after testing many point mutations within the tail domain, we were unable to identify distinct residues important for microtubule binding (Fig. 2.5B)

Together with our truncation results, this point mutation data suggested that Capu's tail domain binds microtubules through nonspecific charge-based interactions. To investigate this further, we generated a CapuCT mutant in which the tail residues were randomly scrambled to give a new sequence with the same total charge and theoretical pI as the original (CapuCT-Scr; Fig. 2.4A). CapuCT-Scr bound microtubules with comparable affinity and binding density to wildtype CapuCT (Fig. 2.4C, Table 2.1), further supporting our model that Capu's tail binds microtubules nonspecifically. Interestingly, scrambling the tail sequence of CapuCT did not diminish CapuCT-Scr's actin nucleation activity (Fig. 2.4D).

2.5 FH2 domain contribution toward microtubule binding

Although Capu's tail domain is required for microtubule binding, the differences in affinity and binding density between CapuCT and GST-tail indicated that the FH2 domain also contributes to microtubule binding. Because microtubules inhibit Capu's actin polymeriza-

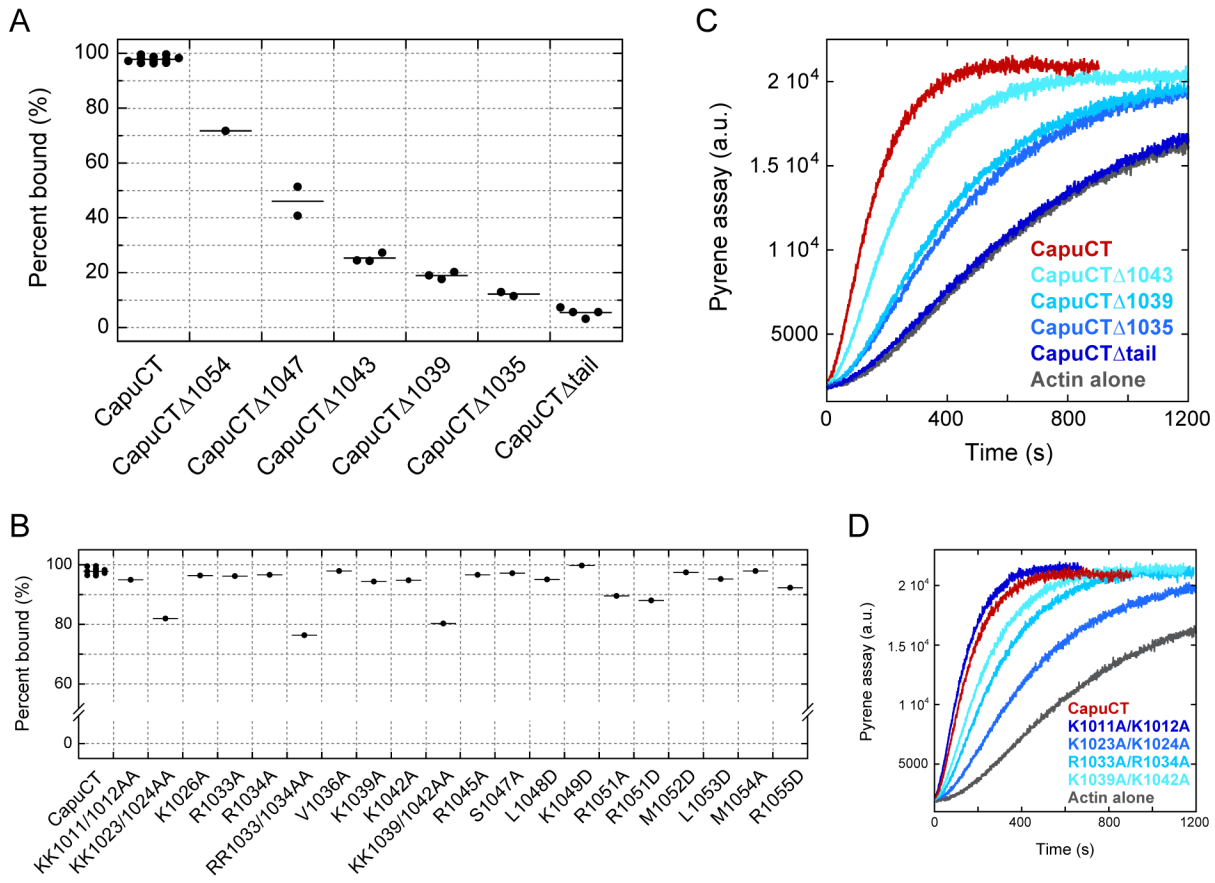

Figure 2.5 – Tail mutations affect both microtubule binding and actin nucleation. (A–B) Microtubule binding by CapuCT truncation (A) and tail point mutation (B) constructs. Experimental conditions are 2 μM tubulin and 0.5 μM of the designated CapuCT construct in 50 mM KCl buffer. Individual experiments are plotted as dots with a line showing the mean. In several cases, only one experiment was performed. Percent bound was calculated by comparing the intensity of each construct in the supernatant sample versus the load sample. (C–D) Actin polymerization activity of 10 nM each CapuCT truncation (C) and selected tail double point mutation (D) constructs compared to wildtype.

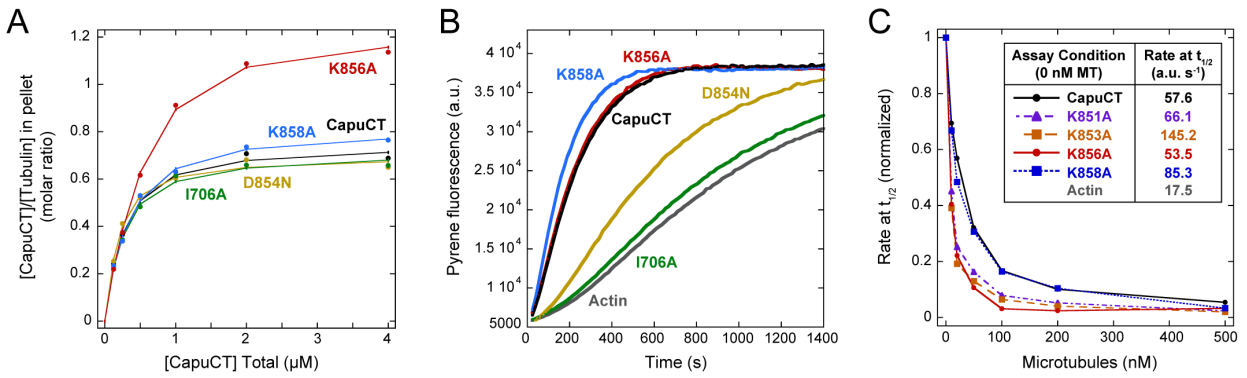

Figure 2.6 – FH2 domain residues contribute to microtubule binding. (A) Microtubule binding by CapuCT-I706A, -D854N, -K858A, -K856A, and wildtype at 50mM KCl with 0.5 μM tubulin. (B) Actin polymerization activity of 10 nM each CapuCT FH2 mutant. (C) CapuCT-K856A, but not CapuCT-K858A, is more sensitive to microtubule inhibition than wildtype CapuCT. Two additional FH2 mutants, CapuCT-K851A and CapuCT-K853A, also exhibited increased sensitivity to microtubule inhibition. For each construct, 10 nM was used and rates at the time until half-maximal polymerization ($t_{1/2}$) were normalized to the maximum polymerization rate (0 nM MT) and the baseline polymerization rate (actin) reported in the table inset.

tion activity, we first mutated two conserved actin binding residues in Capu's FH2 domain (I706A and K856A; Fig. 2.7B) that are known to abolish actin assembly activity in the yeast formin Bni1p [12]. The I706A mutation dramatically reduced Capu's actin nucleation activity but had little effect on microtubule binding (Fig. 2.6, A and B, Table 2.1). Unexpectedly, the K856A mutation had a negligible effect on actin nucleation activity but caused a noticeable increase in microtubule binding density. The binding density of CapuCT-K856A was intriguingly similar to that of GST-tail, with an approximate binding site size of 0.8 tubulin dimers versus 1.4 for wildtype CapuCT (Fig. 2.6, A and B, Table 2.1). Consistent with this, CapuCT-K856A is more sensitive to microtubule inhibition than wildtype CapuCT in pyrene-actin polymerization assays (Fig. 2.6C).

We next investigated whether other residues around Lys-856 are important for actin nucleation or microtubule binding. First, we examined a point mutation (D854N; Fig. 2.7B) that we identified by sequencing an EMS-generated *capu* mutant from an earlier screen [86]. Similar to I706A, this D854N mutation had little effect on microtubule binding, but markedly decreased Capu's actin nucleation activity (Fig. 2.6, A and B, Table 2.1). In contrast to both D854N and K856A, mutating a poorly conserved lysine residue (K858A;

Fig. 2.7B) had little effect on either actin nucleation activity or microtubule binding (Fig. 2.6, A and B, Table 2.1). Two additional mutants we tested, K851A and K853A, were unstable in pelleting assays but had robust actin nucleation activity. We indirectly tested microtubule binding by these mutants by measuring sensitivity to microtubule inhibition in bulk pyrene-actin polymerization assays. Both mutants exhibited an increased sensitivity to microtubule inhibition similar to CapuCT-K856A (Fig. 2.6C). As a control, we also measured microtubule inhibition of CapuCT-K858A and saw very little difference compared to wildtype (Fig. 2.6C). From this we conclude that microtubule binding is mediated by specific residues within the FH2 domain and, unlike binding by the tail domain, is not dependent on random charged-based interactions. Therefore, while the tail domain is required for high affinity binding, FH2 domain interactions are likely necessary to properly orient Capu on the microtubule lattice.

2.6 Discussion

Based on structural information and our experimental findings, we propose a simple model to describe the mechanism of Capu-microtubule binding (Fig. 2.7C). A homology model of Capu based on the crystal structure of hDAAM1 [87] reveals that residues within the FH2 domain that affect microtubule binding (Lys-851, Lys-853, Lys-856) are clustered into a positively charged patch near the base of Capu's tail domain, suggesting that these regions form a continuous binding surface (Fig. 2.7A). Negatively charged residues in the patch (Asp-854) or positively charged residues located away from the patch (Lys-858) have little or no effect on microtubule binding. Capu binds microtubules through a seemingly synergistic interaction involving both its tail and FH2 domains. The FH2 domain alone is insufficient to measurably bind microtubules *in vitro*, but the highly charged tail domain could act as an electrostatic tether that promotes FH2 binding by increasing the local FH2 concentration at the microtubule surface.

We further propose that the differences in microtubule binding density we observed reflect the size of the FH2 binding footprint along the microtubule lattice: loss (GST-tail) or

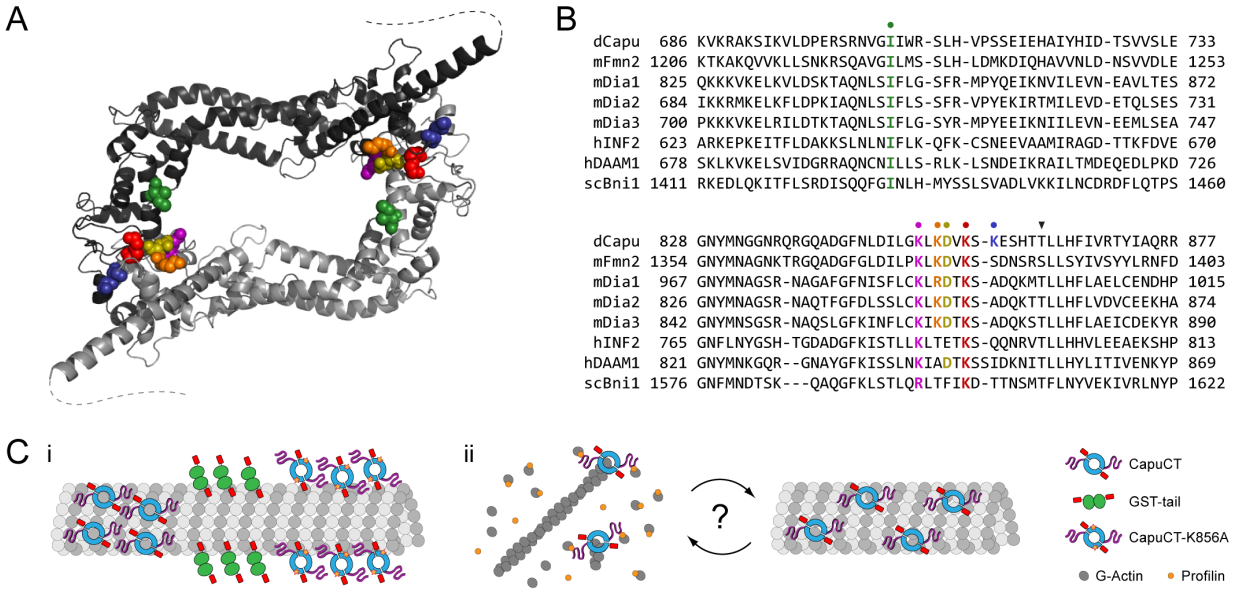

Figure 2.7 – Model of Capu-microtubule binding. (A) Expected locations of Capu FH2 mutations based on a Capu homology model. Residues are colored as in (B), and dashed lines represent the disordered C-terminal tail domains (residues 1037–1059). Homology model was generated from generated from the hDAAM1 crystal structure (PDB # 2J1D; [87]) using SWISS-MODEL [88]. (B) Sequence alignments of several formins in the regions surrounding Ile-706 (green), Lys-851 (purple), Lys-853 (orange), Asp-854 (gold), Lys-856 (red), and Lys-858 (blue). Sequences were acquired from the NCBI Protein Database (*Drosophila* Capu, NP_476966; mouse Fmn2, NP_062318; mouse Dia1, NP_031884; mouse Dia2, NP_062644; mouse Dia3, NP_766081; human INF2, NP_071934; human DAAM1, NP_055807; *S. cerevisiae* Bni1p, NP_014128) and aligned using ClustalW (43). The arrowhead denotes an mDia3 threonine residue previously shown to be phosphorylated by Aurora B kinase [60]. (C) Cartoon model for Capu-microtubule binding and actin-microtubule coordination. (i) CapuCT binds microtubules through both its FH2 and tail domains; changes in binding density reflect the level of contact between the FH2 domain and the microtubule lattice. (ii) Actin barbed ends and microtubules compete for Capu binding; regulatory factors such as binding partners or posttranslational modifications could control the degree of actin versus microtubule binding *in vivo*.

reduction (K856A mutation) of FH2 domain binding results in a smaller binding footprint and a corresponding increase in binding density (Fig. 2.7C, panel i). This model could also explain the different microtubule binding densities seen among different formins. An emerging trend shows that formins whose tails can bind microtubules (Capu and mDia2) have higher binding densities than formins whose tails do not bind microtubules (mDia1 and hINF2) [28]. In the absence of tail binding, formins may rely on more extensive FH2 contacts with the microtubule lattice and thus have a larger binding footprint.

Our data also support a model in which Capu does not simultaneously assemble actin filaments and bind microtubules (Fig. 2.7C, panel ii). We found that microtubules could potently inhibit Capu's actin nucleation activity in bulk assays but had little effect on Capu once it was bound to the end of an elongating actin filament. The location of residues Lys-851, Lys-853, and Lys-856 on our homology model suggests that the FH2 domain binds both microtubules and the actin barbed end through similar or overlapping surfaces, further supporting our model that microtubules and actin barbed ends directly compete for Capu binding. When Capu binds microtubules, its tail domain becomes unavailable for actin monomer binding [30, 29] and the inner FH2 domain becomes sterically occluded and inaccessible to newly formed actin barbed ends. Conversely, the microtubule binding surface in the FH2 domain is inaccessible when Capu is associated with an actin barbed end, allowing Capu to elongate actin filaments in the presence of microtubules.

Our TIRF microscopy assays provide additional insight into important questions surrounding formin-mediated actin-microtubule crosstalk. Microtubules did not anchor elongating actin filaments nor act as scaffolds for actin nucleation. Although we did observe actin filaments tracking along microtubules, this behavior was essentially the same in the presence or absence of CapuCT, suggesting that low concentrations of Capu do not actively align or bundle microtubules and actin filaments. It was previously shown that Capu can crosslink actin filaments and microtubules [48], mostly likely through side binding of both microtubules and actin filaments. However, at the very low CapuCT concentrations used in our TIRF assays, we expect much of the CapuCT to be bound to the barbed end of elongating filaments and unavailable for binding the sides of actin filaments. Because of this,

we were specifically testing the relationship between microtubule and barbed end binding rather than filament side binding.

There is strong evidence that Capu helps build a cytoplasmic actin mesh in the mid-stage *Drosophila* oocyte [69, 32]. Here we consider Capu's role as both a microtubule binding protein and actin assembly factor in the ooctye and how these functions might be regulated. Our observation that actin barbed ends and microtubules compete for Capu binding suggests that Capu does not simultaneously bind microtubules and assemble actin filaments within the oocyte. Acting as a microtubule binding protein, Capu could directly regulate the microtubule cytoskeleton without invoking its actin assembly activity. It could crosslink microtubules to each other and/or to pre-existing actin filaments. Conversely, when assembling actin filaments and not binding microtubules, Capu could still indirectly influence microtubule organization through the actin cytoskeleton. Spatial and/or temporal regulation of Capu could control when Capu is associated with microtubules versus actin filaments and could be achieved through additional binding partners, posttranslational modification, or some combination thereof. For instance, Capu binds the actin nucleator Spir through its tail domain [30]. Spir competes directly with microtubules for Capu binding [47] and forms a functional nucleation unit when bound to Capu [47, 30]. This Spir-Capu nucleation unit may be much more efficient at nucleating actin in the microtubule-rich oocyte than Capu would be alone. Additional unidentified binding partners may also play a role in regulating Capu association with microtubules. Several mammalian Diaphanous group formins bind and/or colocalize with microtubule-associated proteins such as EB1, APC, and CLIP-170 [60, 49, 41]. Future work will determine whether Capu has similar binding partners within the *Drosophila* oocyte.

Posttranslational modifications, especially phosphorylation, are commonly used to regulate microtubule binding by a variety of microtubule-associated proteins [89, 50]. With respect to formins, mDia3 association with microtubules has been shown to be mediated by phosphorylation by the Aurora B kinase [60]. Notably, one mDia3 phosphorylation site is conserved across many formins and is within 10 amino acids of Capu's conserved Lys-856 residue (Fig. 2.7B). Moreover, lysine-to-alanine mutations in this region of mDia1 have

been shown to disrupt actin-microtubule coordination in HeLa cells [5], suggesting that this region within the FH2 domain could be a hotspot for microtubule binding among formins. Additionally, we anticipate that posttranslational modification within Capu's tail will be important for regulating Capu function in the *Drosophila* oocyte. Though only approximately 30 amino acids long, the tail domain is involved in Spir binding, microtubule binding, actin nucleation, and Capu autoinhibition [30, 20]. Such a promiscuous domain will likely require careful regulation *in vivo*.

Finally, it is possible that microtubules themselves are a means of regulating Capu activity in the oocyte. Throughout mid- and late-oogenesis, microtubules are nucleated from all regions of the oocyte cortex except the posterior pole [71], and it was recently shown that Capu-dependent actin projections emanate specifically from the posterior cortex of the oocyte [70]. Could microtubule organization restrict the location of these Capu-dependent actin projections to the oocyte posterior? Similarly, microtubules could tune the processivity of Capu as it elongates actin filaments within the oocyte. Our TIRF experiments show that microtubules do not effectively compete Capu away from the barbed end of actin filaments, causing barbed end dissociation in only 2% of all microtubule encounters. However, this relatively low probability of dissociation could have a much more substantial effect over the span of the entire oocyte where a single barbed end may encounter hundreds of microtubules. Together with Capu's own autoinhibitory activity [20], microtubules could also prevent Capu from nucleating new actin filaments after falling off the end of an elongating filament.

In conclusion, our results provide mechanistic details of Capu-microtubule binding and the interplay of microtubule binding and actin assembly *in vitro*. Beyond providing valuable insight into Capu's role as a cytoskeletal regulator in the *Drosophila* oocyte, these findings may help advance our understanding of Capu's mammalian homologs, Fmn1 and Fmn2. Capu FH2 residues 851–856 are perfectly conserved in Fmn1 and Fmn2, and both formins contain well conserved, short, basic C-terminal tail domains, suggesting a conserved mechanism for microtubule binding [47]. These formins have been implicated in a number of processes in a wide variety of cell types, including intercellular adhesion and cell spreading, as well as spindle positioning and cytokinesis during mammalian oogenesis

[82, 83, 90, 39, 58, 91]. How our findings relate to the broader class of formin proteins remains to be seen. Although the microtubule binding FH2 residues we identified are well conserved across several formin groups, the C-terminal tail domains are more variable. Gaillard *et al.* [28] recently showed that INF2, mDia1, and mDia2 have distinct microtubule interaction properties. Notably, mDia2 has the most basic tail of the three formins and behaves the most like Capu *in vitro*. Future work will reveal whether our model for Capu-microtubule binding can be generalized to other formins such as mDia2.

CHAPTER 3

Characterization of Capu localization in S2 cells

After establishing that Capu binds microtubules with sub-micromolar affinity *in vitro*, we were curious whether Capu could be seen localizing to microtubules *in vivo*. In *Drosophila* egg chambers, Capu is enriched at the cortex of nurse cells and is diffuse in both nurse cells and oocytes [32]; to our knowledge, Capu has never been shown to localize to microtubules or other filamentous structures during *Drosophila* oogenesis [32, 47, 48]. The Capu-microtubule interaction may be too sparse or transient in the oocyte to be clearly observed by standard fluorescent methods.

Obvious formin-microtubule colocalization has been observed in mammalian cell culture experiments [44, 61]. In particular, Fmn1 isoform Ib clearly colocalizes with microtubules in NIH 3T3 cells [61]. Furthermore, some formins appear to preferentially localize to the microtubule organizing center [57, 79], yet mid-to-late stage *Drosophila* oocytes lack this specialized microtubule structure [92]. We therefore reasoned that although Capu does not clearly colocalize with microtubules in the *Drosophila* oocyte, we might be able to detect such colocalization in a different cell type.

Here we used cultured S2 cells to examine the localization of Capu. We looked for colocalization between Capu and microtubules under several different conditions and ultimately conclude that, just as in *Drosophila* egg chambers, Capu-microtubule colocalization cannot be readily observed in this cell type.

3.1 Localization of Capu and microtubules in S2 cells

To characterize Capu and microtubule localization, we co-expressed fluorescently labeled GFP-tubulin and tdTomato-Capu in cultured S2 cells. Neither full-length Capu (CapuFL) nor a constitutively active C-terminal construct (CapuCT; residues 467–1059) exhibited any obvious colocalization with microtubules or other filamentous structures (Fig. 3.1). Both constructs were distributed diffusely throughout the cell body, with CapuFL frequently appearing in large, unidentified foci (Fig. 3.1).

Whereas CapuFL was largely excluded from lamellar regions, CapuCT appeared to localize to microtubule-rich regions in the cell periphery (Fig. 3.1). To explore whether this peripheral overlap could be the result of specific Capu-microtubule interactions, we examined the localization of tdTomato alone. Apart from its nuclear localization, the tdTomato control was indistinguishable from tdTomato-CapuCT (Fig. 3.1). Both proteins were diffuse throughout the cell body and overlapped with microtubules toward the cell periphery. From this, we conclude that any peripheral Capu-microtubule overlap is most likely coincidental.

Mammalian tissue culture studies have shown global changes in microtubule organization upon formin over-expression. In particular, formins can actively align microtubules with actin stress fibers [6, 46] and promote cell elongation [5]. In contrast with these past studies, we did not observe any striking changes in microtubule structure or cell shape when expressing CapuFL or CapuCT in S2 cells (Fig. 3.1).

Finally, we examined the localization of a constitutively active mouse Dia2 construct (mDia2; residues 512–1060), which had been previously shown to overlap with stable populations of microtubules in NIH 3T3 cells [40]. This mDia2 construct differed from CapuCT and the tdTomato control in that it localized more to lamellar regions than the main cell body and seemed to induce more ruffling. However, no obvious colocalization was observed between mDia2 and microtubules (Fig. 3.1).

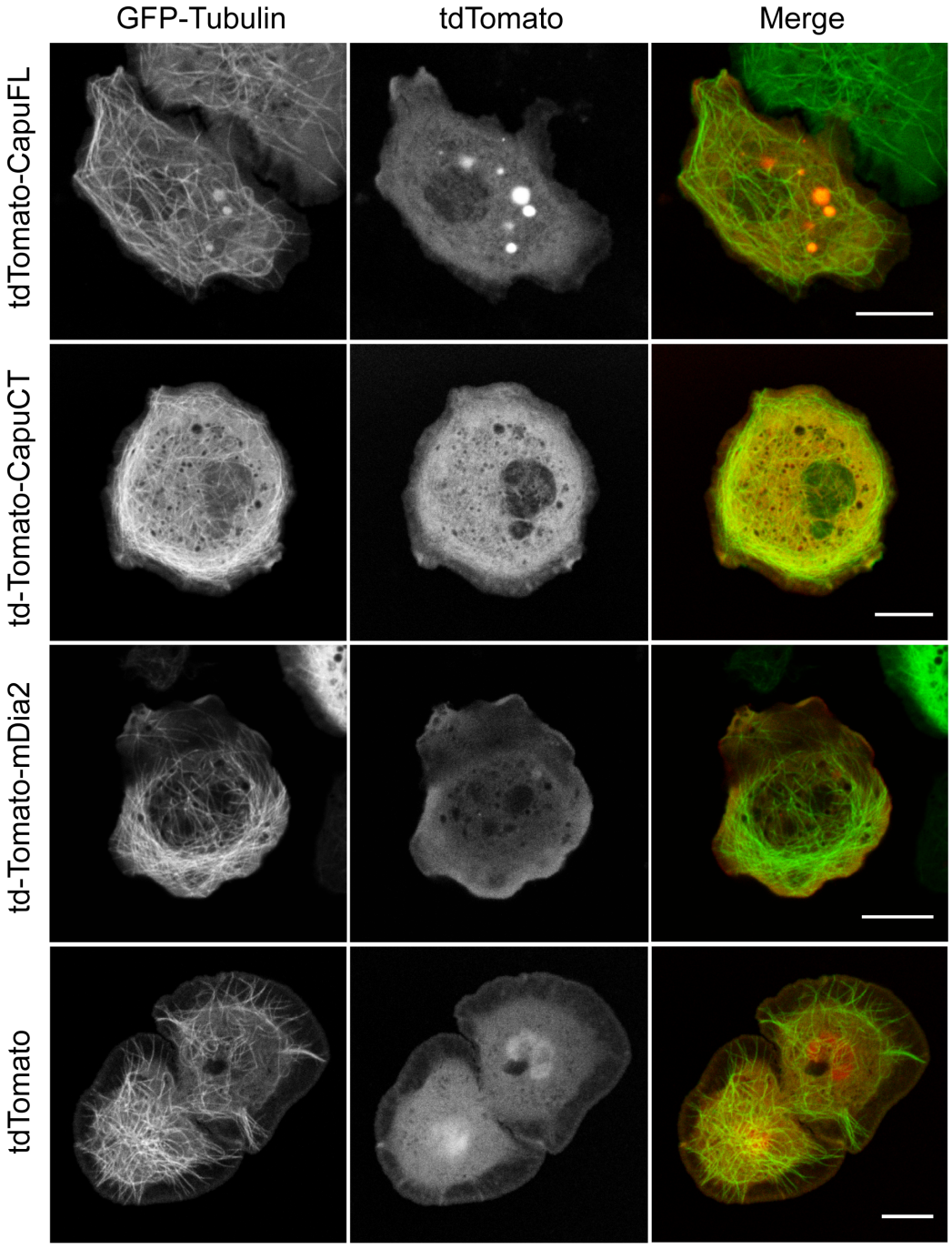

Figure 3.1 – Capu does not clearly colocalize with microtubules in S2 cells. The following constructs were transiently expressed in a stable S2 cell line expressing GFP-tubulin: tdTomato-CapuFL (Capu residues 1–1059), tdTomato-CapuCT (Capu residues 467–1059), tdTomato-mDia2 (mDia2 residues 512–1060), tdTomato control. A representative cell is shown for each experiment. Scale bars are 10 μm.

3.2 Capu localization in S2 cells treated with Cytochalasin D

It was previously shown that actin depolymerization by Latrunculin A (LatA) can promote mDia1 colocalization with microtubules [79]. We therefore tested whether depolymerizing actin filaments could force Capu onto microtubules by treating S2 cells with Cytochalasin D (CytoD). This drug caps the barbed ends of actin filaments, leading to the disappearance of long filaments and the appearance of thin, microtubule-rich projections that lack filamentous actin [93]. In cells treated with CytoD, both CapuCT and the tdTomato control were diffuse throughout the cell body and the microtubule-rich projections (Fig. 3.2). CapuFL was less enriched in cell projections and localized to large foci in the cell body just as in untreated cells. Interestingly, the localization of mDia2 changed noticeably in these cells, forming a punctate pattern throughout the cell body (Fig. 3.2). This could also be seen, albeit to a lesser extent, in cells expressing CapuCT (Fig. 3.2), suggesting that disruption of the actin cytoskeleton can cause global changes in the localization of these two constitutively active formin constructs.

While conducting these experiments, we noticed that our stable GFP-tubulin cell line behaved somewhat differently from our wildtype S2 cell line. Cells expressing GFP-tubulin not only grew more slowly than wildtype, but also had more trouble adhering to surfaces. When treated with CytoD, these GFP-tubulin cells also had fewer, fatter microtubule projections than observed in treated wildype cells (compare Fig. 3.2 and Fig. 3.3B). Because the labeled tubulin seemed to disrupt normal cellular processes, we wanted to control for the possibility that this labeled tubulin was globally disrupting Capu's association with microtubules. We therefore expressed and visualized labeled Capu constructs in wildtype S2 cells. No differences in Capu localization were observed in these cells whether untreated (Fig. 3.3A) or treated with CytoD (Fig. 3.3B).

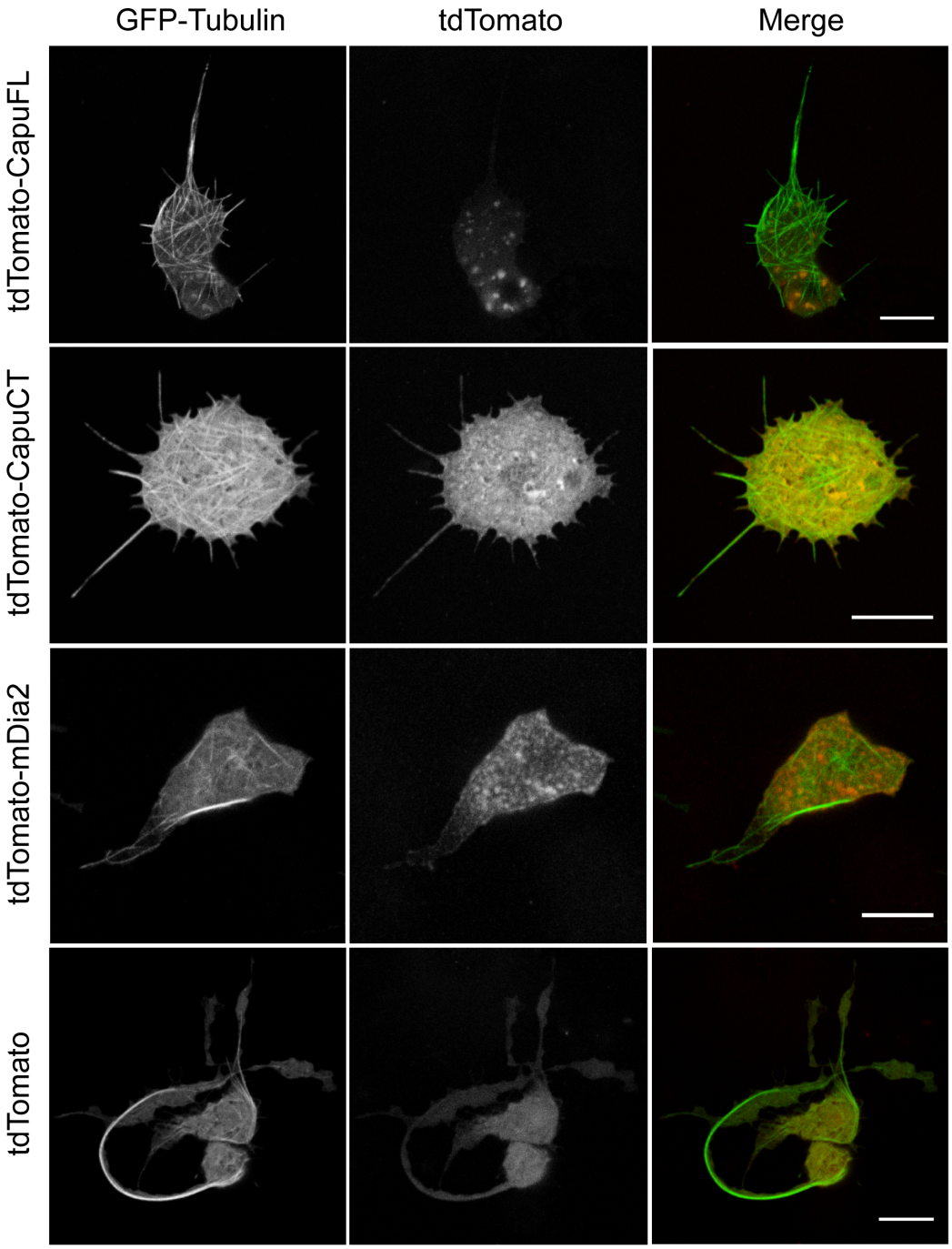

Figure 3.2 – Capu is not enriched in CytoD-induced projections. The following constructs were transiently expressed in a stable S2 cell line expressing GFP-tubulin: tdTomato-CapuFL (Capu residues 1–1059), tdTomato-CapuCT (Capu residues 467–1059), tdTomato-mDia2 (mDia2 residues 512–1060), tdTomato control. Cells were treated with 5 μM CytoD for 1 hour prior to imaging. A representative cell is shown for each experiment. Scale bars are 10 μm.

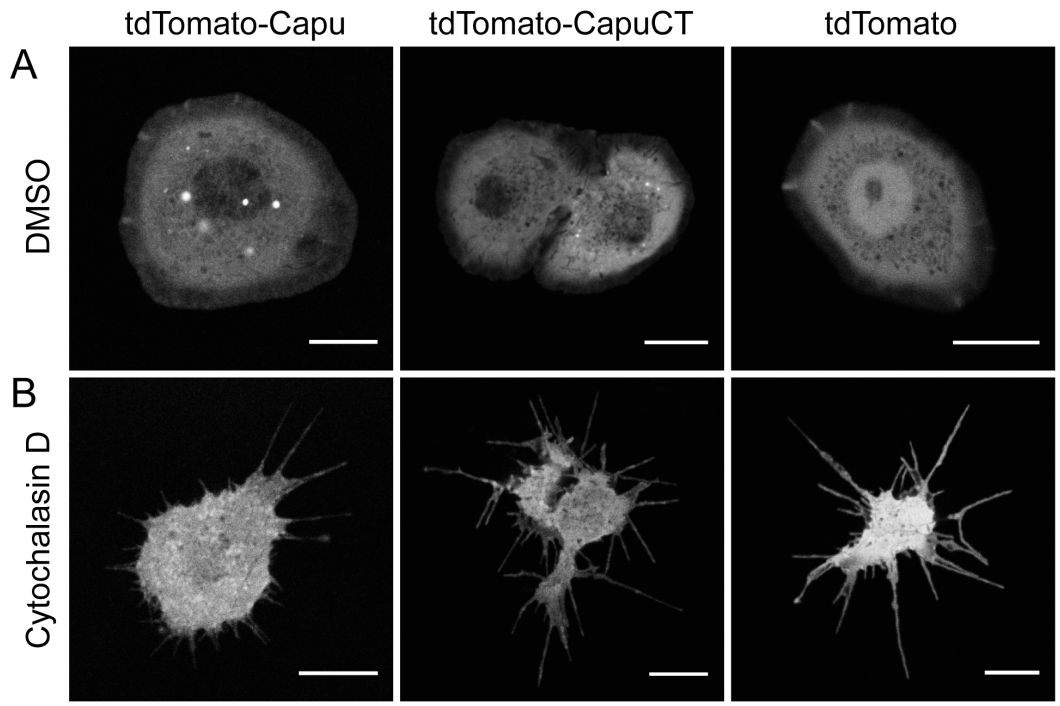

Figure 3.3 – Capu localizes diffusely throughout the cytoplasm of S2 cells. tdTomato-CapuFL (Capu residues 1–1059), tdTomato-CapuCT (Capu residues 467–1059), or a tdTomato control was transiently transfected in wildtype S2 cells treated with DMSO (A) or CytoD (B). A representative cell is shown for each experiment. Scale bars are 10 μm.

3.3 Localization of Capu to the mitotic spindle

Although we did not readily observe Capu-microtubule colocalization in interphase S2 cells, we wondered whether Capu might localize to microtubules at different points in the cell cycle. For example, mDia1 colocalizes with the mitotic spindle in HeLa cells [37], and mDia3 is important for chromosome congression to the metaphase plate [60]. We therefore examined Capu localization during cell division.

Because S2 cells have a very low mitosis rate and are notoriously difficult to synchronize in culture, we used the proteasome inhibitor MG132 to arrest cells in metaphase. Interestingly, we noticed a subtle enrichment of CapuFL and CapuCT at the spindle of metaphase cells (Fig. 3.4). However, we saw a similar enrichment with the tdTomato control (Fig. 3.4), suggesting that this spindle localization is not a result of direct Capu-microtubule binding. Instead, this enrichment could be caused by bleedthrough between the two fluorescent channels and/or tdTomato interacting with components of the mitotic spindle. Finally, we did not observe any spindle localization for mDia2, but could only find one metaphase cell expressing mDia2 (Fig. 3.4).

3.4 Discussion

Consistent with previous studies in the *Drosophila* oocyte, we did not observe clear colocalization between microtubules and Capu in cultured S2 cells. Even mDia2, which colocalizes with microtubules and promotes microtubule stabilization in mammalian cell types [43, 79], did not colocalize with microtubules in S2 cells. It is possible that these interactions are too transient or sparse to be readily detected by fluorescence microscopy. Formin-microtubule interactions could also be highly regulated in this particular cell type. Cheng *et al.* showed that mDia3 association with the mitotic spindle can be mediated by Aurora B phosphorylation [60]. Posttranslational modifications or other regulatory mechanisms in S2 cells could be effectively preventing Capu and mDia2 from interacting with microtubules. Furthermore, Bartolini *et al.* demonstrated that treating NIH 3T3 cells with LatA depolymerizes actin

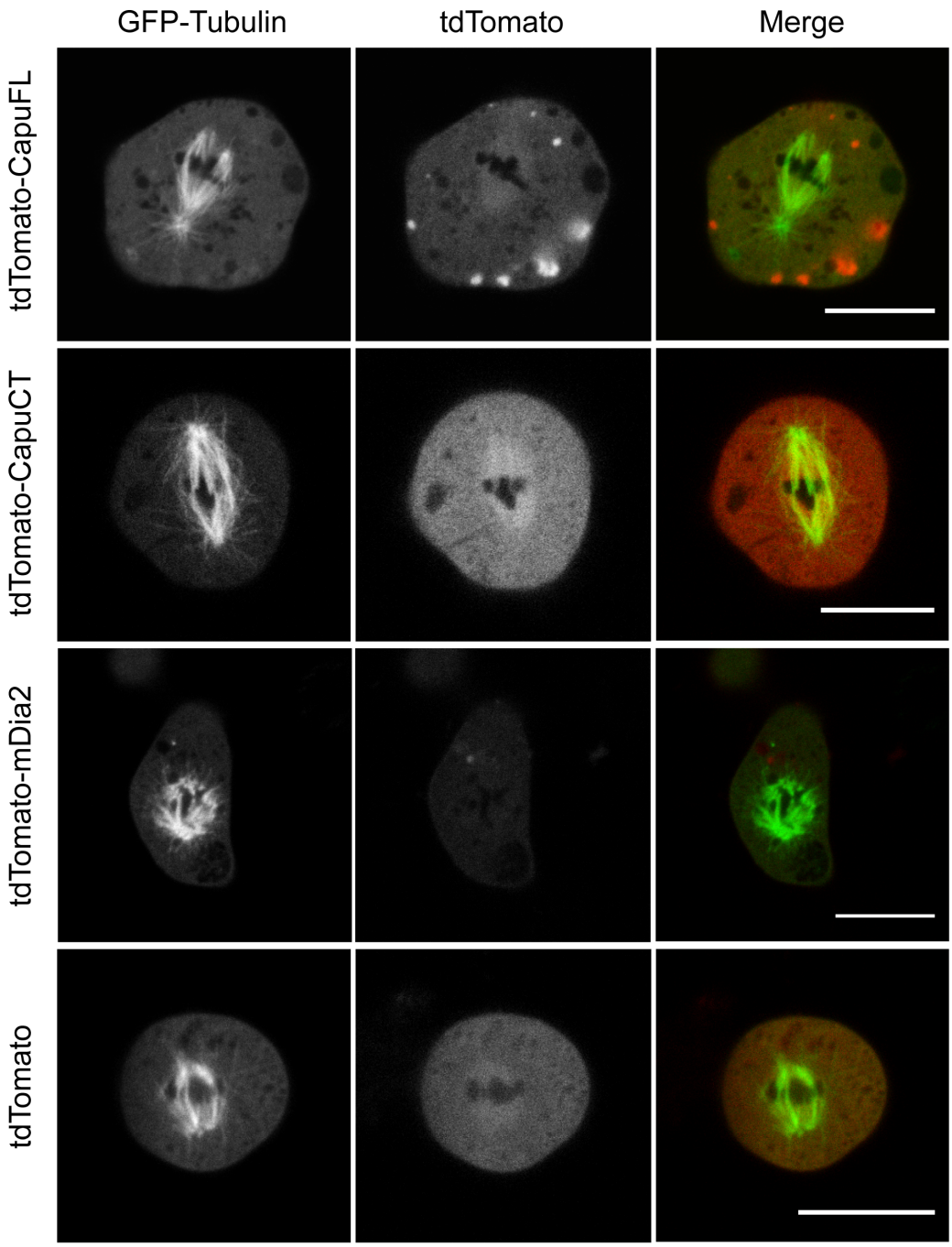

Figure 3.4 – Capu is not enriched at the mitotic spindle in metaphase cells. The following constructs were transiently expressed in a stable S2 cell line expressing GFP-tubulin: tdTomato-CapuFL (Capu residues 1–1059), tdTomato-CapuCT (Capu residues 467–1059), tdTomato-mDia2 (mDia2 residues 512–1060), tdTomato control. Cells were treated with 20 μM MG132 approximately 3 hours prior to imaging. Only one metaphase cell was observed in the mDia2-transfected cells. A representative cell is shown for all other experiments. Scale bars are 10 μm.

filaments and shifts mDia1 localization onto microtubules [79]. In our experiments, treating S2 cells with the actin depolymerizing drug CytoD changed Capu and mDia2 localization but did not result in colocalization with microtubules. Such discrepancies indicate that S2 cells are not an ideal system for studying formin-microtubule interactions.

Together with previous findings, our results suggest that formin-microtubule colocalization may only be readily observable with specific formins and/or particular microtubule structures. For example, Fmn1 isoform Ib exhibits beautiful microtubule colocalization that can be easily detected by fluorescence microscopy; a unique exon in this isoform is both necessary and sufficient for microtubule colocalization [61]. In stark contrast, Fmn1 isoform IV shows only transient microtubule colocalization as observed through electron microscopy of immuno-gold labeled cells [58]. Considering these data, it is possible that Capu may never clearly localize to microtubules in any cell type, let alone in S2 cells. It is also unclear whether formin-microtubule colocalization occurs through direct binding or through formin interactions with microtubule associated proteins. Detectable microtubule localization could require additional proteins that might preferentially bind different formins or be poorly expressed in S2 cells. For example, several Diaphanous formins bind and colocalize with microtubule plus end associated proteins such as APC and EB1 [41, 56]; Capu, however, has not yet been shown to interact with any such proteins.

Finally, it is possible that Capu binds specialized microtubule structures that are not present in S2 cells. Although we focus on Capu's role in mid-oogenesis, *capu* mRNA transcripts are detectable throughout development until late-embryogenesis [63]. Capu could associate with specialized developmental microtubule structures that have been overlooked in the oocyte or that occur later in development. In particular, Capu association with developmental meiotic and mitotic spindles warrants further investigation. Although Capu behaved just like our tdTomato control, it did seem to be slightly enriched at the mitotic spindle in S2 cells. We speculate that Capu association with spindles or other specialized microtubule structures may be easier to detect in a developmental context than in S2 cells.

CHAPTER 4

Structure-function study of Capu mutants

At the time of writing, approximately 30 unique *capu* alleles have been reported in FlyBase [94]. Many of these alleles were initially isolated in genetic screens and have been studied *in vivo*. However, very little work has been done to understand how these mutations affect Capu's biochemical activity, in part because Capu's role as an actin nucleator was still unknown when many of these mutations were first discovered. Previous work has demonstrated that two mutant alleles, $capu^{1}$ and $capu^{2F}$, have compromised actin nucleation and microtubule bundling activities *in vitro* [48]. This raises the intriguing possibility that classical *capu* mutations may not only affect actin nucleation, but also alter microtubule binding and/or disrupt other as-yet-unknown Capu functions.

Here we have begun characterizing the physiological and biochemical consequences of these mutations. Intriguingly, we found that these mutations have similar effects *in vivo* but exhibit a range of actin assembly defects *in vitro*. Ulitmately, our findings support our larger goal of elucidating Capu's mechanism of action and role during *Drosophila* oogenesis.

4.1 Identification of causative lesions in *capu* alleles

We first set out to identify unreported lesions and confirm reported missense mutations that could be readily studied *in vitro*. To identify new lesions, we generated and sequenced ovarian *capu* cDNA from the following fly lines: $capu^{2}$, $capu^{EE}$, $capu^{L201}$, $capu^{L219}$, $capu^{L250}$, and $capu^{L277}$. We discovered unique missense mutations in the coding region (CG3399-PA) of three of these alleles, as reported in Fig. 4.1 and Table 4.1. Surprisingly, $capu^{2}$, $capu^{EE}$, and $capu^{L250}$ did not appear to contain any unique causative lesions.

Figure 4.1 – Capu mutations identified across all sequenced fly lines. Sequencing cDNA transcripts revealed several mutations within the Capu coding region (CG3399-PA). Red mutations represent newly identified causative lesions. Black mutations are background variants previously reported by Emmons *et al.* [63], while blue mutations are background variants in fly lines generated by Luschnig *et al.* [86].

Table 4.1 – Identified *capu* lesions.

Allele name(s)	Lesion*	First Reported
$capu^{1}$, $capu^{RK}$, $capu^{RK12}$	L768H	Manseau & Schüpbach, 1989 [62]
$capu^{HK3}$	I751T	Manseau & Schüpbach, 1989 [62]
$capu^{38}$, $capu^{HK38}$	H977Y	Emmons *et al.*, 1995 [63]
$capu^{2F}$	**P597L**§	Emmons *et al.*, 1995 [63]
$capu^{L201}$, $capu^{2L-7-13}$	**D854N**	Luschnig *et al.*, 2004 [86]
$capu^{L219}$, $capu^{2L-91-5}$	**K586M**	Luschnig *et al.*, 2004 [86]
$capu^{L277}$, $capu^{2L-281-6}$	**W247stop**	Luschnig *et al.*, 2004 [86]
$capu^{A354}$	**D662N**†	Tanaka *et al.*, 2011 [70]

*Bold denotes new lesions identified in this study.

§Previously reported as P597T [63].

†Previously reported as D670N [70].

Although the Capu-A isoform is thought to be the primary ovarian transcript [63], several other Capu isoforms have been annotated in FlyBase [94]. These isoforms differ in the N-terminal half of the transcript, upstream of the conserved FH1 and FH2 domains (Fig. 4.2). Because we cannot rule out the possibility that different Capu isoforms are important during oogenesis, we checked for lesions in reported coding exons not included in Capu-A (exons 3, 4, and 6 as shown in Fig. 4.2). Sequencing genomic DNA from $capu^{2}$ and $capu^{EE}$ fly lines revealed no unique mutations in these upstream exons. Exon sequencing was not completed for $capu^{L250}$. We speculate that the causative lesions in these fly lines occur in regulatory elements that control expression level or in intronic regions that lead to splicing defects. Although we were able to amplify full Capu-A cDNA from these fly lines, more subtle splicing defects could disrupt proper protein expression levels. Interestingly, one sequenced $capu^{EE}$ cDNA transcript was missing exon 7 even though no reported isoforms contain exon 6 and lack exon 7 (Fig. 4.2). It is unclear whether this one cDNA represents a real splice variant or simply an artifact of the reverse transcription reaction.

After identifying new *capu* lesions, we confirmed all reported missense mutations by isolating and sequencing genomic DNA from each fly line (Table 4.1). Tanaka *et al.* originally reported the $capu^{A354}$ lesion as D670N [70], but Capu-A (CG3399-PA) does not contain an aspartate residue at this position. We identified nearby D662N as the causative mutation in our $capu^{A354}$ fly line. Similarly, $capu^{2F}$ was originally reported to contain P597T [63], but our

sequencing revealed a P597L mutation. This discrepancy could be due to a natural evolution in the fly line or an error in the original sequencing analysis. We chose to characterize the P597L mutation to be consistent with our current fly stock.

4.2 *In vivo* characterization of classical *capu* alleles

During development, Capu helps to build a cytoplasmic actin mesh that persists through mid-oogenesis [69, 32]. In *capu* loss-of-function mutants, this mesh is never detected and loss of the mesh corresponds to premature onset of cytoplasmic streaming [69]. To characterize the physiological ramifications of each classical *capu* allele, we therefore examined the cytoplasmic mesh and measured cytoplasmic streaming in pre-stage 10 oocytes. To avoid any potential phenotypic contribution from off-site mutations, we characterized all alleles over a chromosomal deficiency encompassing the entire *capu* gene locus.

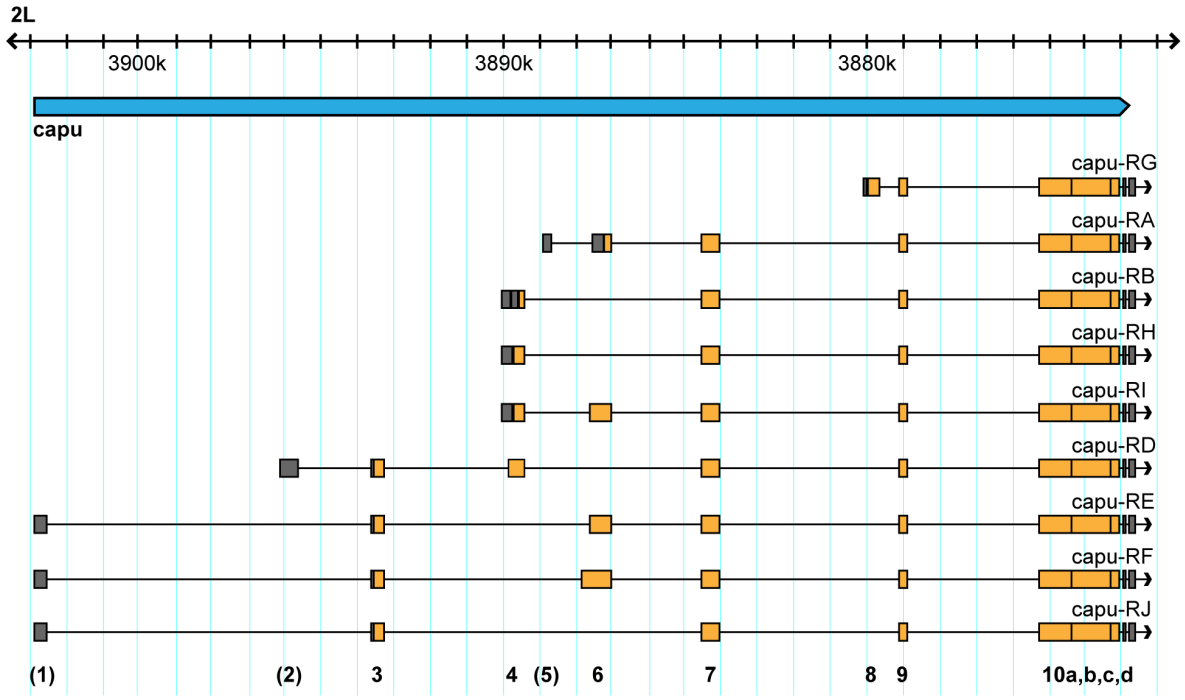

Figure 4.2 – Capu gene structure and reported isoforms. Capu has several reported isoforms, many of which contain coding exons upstream of the Capu-A isoform. Capu exons are numbered, with non-coding exons in parenthesis. Coding exon regions are shown in orange and non-coding exon regions are shown in gray. Figure adapted from FlyBase [94].

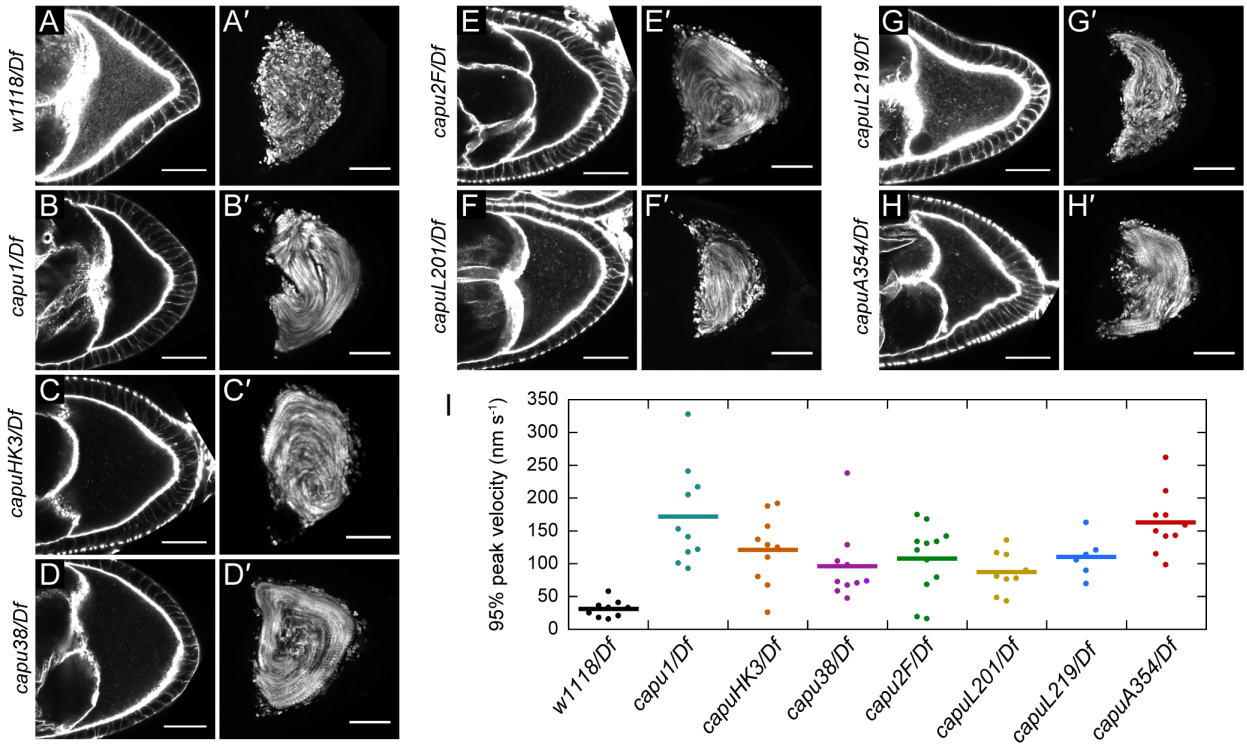

Figure 4.3 – Classical *capu* alleles lack actin mesh and exhibit premature streaming. (A–H) Pre-stage 10 egg chambers stained with AlexaFluor-phalloidin to visualize the actin mesh in *capu* mutant flies. (A′–H′) Standard deviation projections of autofluorescent yolk granules over 3 minutes for typical pre-stage 10 oocytes. All scale bars are 30 μm. (I) Quantification of streaming velocities for $n \geq 6$ oocytes from each fly line. Dots represent individual oocytes and bars represent the mean.

Before stage 10, the actin mesh was compromised in all mutants compared to wildtype, which exhibited a dense, uniform mesh spanning the oocyte cytoplasm (Fig. 4.3A–H). In $capu^{1}$ and $capu^{HK3}$ flies, the mesh was undetectable and only small spots of actin could be seen throughout the oocyte. $capu^{2F}$ and $capu^{38}$ oocytes were similar, but also exhibited a very faint fluorescent signal with no clearly defined structure. The remaining fly lines had a detectable, albeit severely compromised, cytoplasmic actin meshwork. Even in the best case, $capu^{L219}$, the mesh appeared sparse, lacked clear organization, and exhibited occasional actin aggregates.

Consistent with our observations of the actin mesh, premature cytoplasmic streaming was observed for all mutant alleles (Fig. 4.3A′–H′). We qualitatively observed some variability in the speed of streaming within each fly line, so we used particle image velocimetry to quantify the speed of streaming in these oocytes (Fig. 4.3I). On average, all of the mutants had substantially faster streaming than wildtype. Two mutants, $capu^{HK3}$ and $capu^{2F}$, had outliers with streaming velocities comparable to wildtype, suggesting that these may be slightly less penetrant than the other alleles. Because the *capu* alleles exhibited variable mesh phenotypes, we wondered whether the presence of a compromised mesh could still lead to slower streaming speeds. However, we did not observe any correlation between mesh signal and mean streaming speed (Fig. 4.3, A–H and I). We therefore conclude that the actin mesh is sufficiently compromised in all mutants to have no detectable inhibitory effect on cytoplasmic streaming.

4.3 Structural analysis of identified missense mutations

Identified missense mutations were mapped to a Capu homology model based on the crystal structure of hDAAM1 [87]. All of these mutations occur in the FH2 domain (Fig. 4.4A). Although these residues are not particularly well conserved at the sequence level, they all appear to be clustered in the structurally important lasso, knob, and post regions of the FH2 domain. We note that these mutations also reside within coding exons 10a–d of the *capu* gene locus, which are common to all putative Capu splice variants (Fig. 4.2).

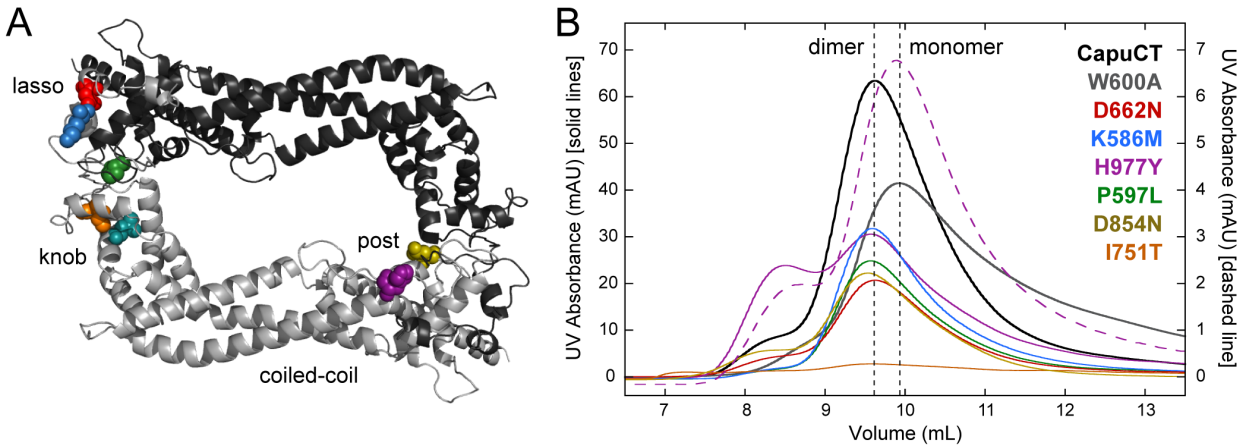

Figure 4.4 – All identified mutations are located within Capu's FH2 domain. (A) Location of mutated residues within the FH2 domain. Capu homology model is based on the crystal structure of hDAAM1 (PDB # 2J1D; [87, 88]). (B) Size exclusion chromotography of all mutants compared to wildtype CapuCT (dimer) and CapuCT-W600A (monomer).

To study the biochemical consequences of these mutations, point mutants were created in a C-terminal Capu construct (CapuCT; residues 467–1059). All CapuCT mutants were amenable to purification except CapuCT-L768H. Because of its predicted location inside the globular knob region of the FH2 domain, we suspect that mutating this buried hydrophobic residue disrupts the structure of CapuCT and/or causes misfolding. A neighboring knob mutation, CapuCT-I751T, was also difficult to purify and the yield was reduced approximately 10-fold compared to the wildtype construct.

The lasso/post interface, where many of the mutations are located, is important for formin dimerization [12]. We therefore tested whether any of these mutations dramatically alters the dimerization state of Capu. Purified mutant constructs were analyzed by size exclusion chromatography and compared to wildtype CapuCT as a dimer control and CapuCT-W600A as a monomer control [87, 30] (Fig. 4.4B). From this, we confirmed that CapuCT-D662N, -K586M, -D854N, and -P597L exist predominantly in a dimeric state. Interestingly, two mutant proteins, CapuCT-I751T and CapuCT-H977Y, eluted differently than the other mutants. Although a similar quantity of protein was run on the column, CapuCT-I751T did not form any clear elution peaks, further supporting our hypothesis that this buried hydrophobic mutation disrupts the structure and/or folding of CapuCT. CapuCT-H977Y eluted primarily as a dimer, but exhibited a broader shoulder and an unusually high peak in the void volume.

This void volume peak was reproducible when the dimer fraction was run a second time on the size exclusion column (Fig. 4.4B, dashed line), suggesting that CapuCT-H977Y is in equilibrium with a higher-order complex or aggregation product. Consistent with this being an unfavorable aggregation product, the higher-order fraction was less active in pyrene-actin assembly assays than the dimer fraction (data not shown).

4.4 *In vitro* characterization of classical *capu* alleles

All of the classical *capu* alleles that we tested *in vivo* compromised Capu's ability to build the cytoplasmic actin mesh during oogenesis (Fig. 4.3A–H). To test whether any of these deleterious point mutations affect Capu's ability to nucleate actin filaments, we measured the activity of each mutant in bulk pyrene-actin polymerization assays. Many of the mutants exhibited impaired activity in both the absence or presence of excess profilin (Fig. 4.5, A and B). However, the extent to which actin assembly activity was reduced varied widely across the different mutants. Most strikingly, CapuCT-D662N was indistinguishable from wildtype CapuCT in these assays.

We had previously shown that FH2 mutations can alter the interaction between CapuCT and microtubules *in vitro*. Because the classical *capu* mutations had variable effects on actin assembly activity, we wondered if any of them might play a role in microtubule binding. We therefore used high-speed pelleting assays to measure binding of each mutant to taxol-stabilized microtubules. CapuCT-I751T was omitted from this analysis because it could not be purified at high enough concentrations. Surprisingly, all of the other mutants except for CapuCT-D854N showed a substantial increase in microtubule binding density (Fig. 4.5C and Table 4.2). Without better structural information about CapuCT or the CapuCT-microtubule interface, it is difficult to explain this shift in binding density. For now, we hypothesize that the mutations alter the CapuCT's conformation in a way that reduces the binding footprint and allows more CapuCT to bind the microtubule lattice. Because the mutants still bind microutbules with sub-micromolar affinity, we speculate that this shift in microtubule density is not directly responsible for the phenotypes observed during oogenesis.

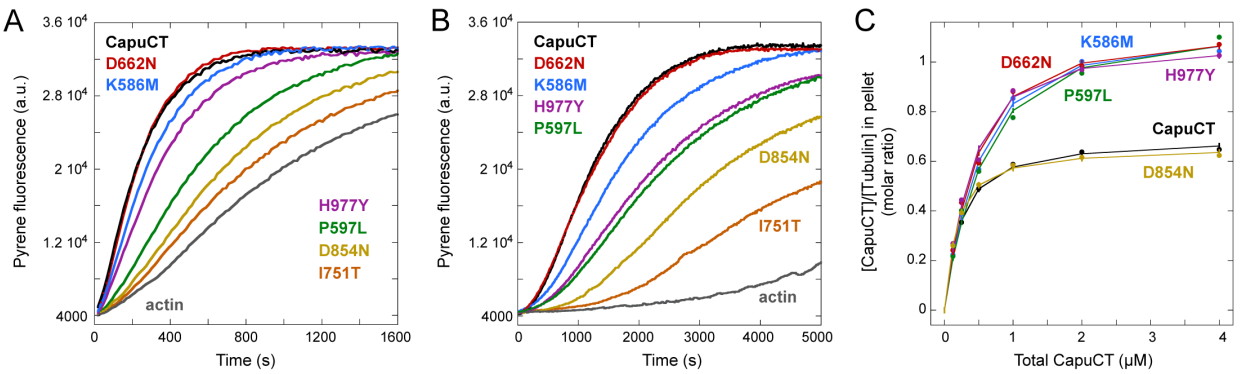

Figure 4.5 – Mutants variably affect actin assembly and microtubule binding. Actin assembly activity of 10 nM of each construct in the absence (A) or presence (B) of profilin. (C) Microtubule binding by all constructs at 50mM KCl with 0.5 μM tubulin.

Table 4.2 – Fit parameters for all microtubule binding curves. The free energy of binding ($\Delta_r G$) is expressed with units kJ/mol and the binding site size (n) is expressed as the number of α/β-tubulin dimers per binding site. Error bars for $\Delta_r G$ and n represent one standard deviation. The most probable dissociation constant (K_d) values are reported in units of μM and calculated from $\Delta_r G$ at 25°C (see Section 7.3 for additional information). All binding curves were measured at 50 mM KCl with untreated microtubules.

Binding Experiment	$\boldsymbol{\Delta_r G}$ **(kJ/mol)**	$\boldsymbol{K_d}$ **(μM)**	$\boldsymbol{n}$ **(α/β dimers)**
CapuCT	4.74 ± 0.11	0.15	1.42 ± 0.01
CapuCT-K586M	3.39 ± 0.14	0.25	0.88 ± 0.01
CapuCT-P597L	2.96 ± 0.22	0.30	0.88 ± 0.02
CapuCT-D662N	3.41 ± 0.17	0.25	0.87 ± 0.01
CapuCT-D854N	5.70 ± 0.13	0.10	1.48 ± 0.01
CapuCT-H977Y	4.27 ± 0.14	0.18	0.95 ± 0.01
CapuCTΔloop	4.39 ± 0.14	0.17	1.30 ± 0.01

4.5 Identification and characterization of Capu's "loop" domain

While studying these classical mutations, we noticed that the lasso region of Capu varies substantially from all other formins identified to date. Whereas most formins contain 10–20 residues between the two perfectly conserved tryptophan residues in the lasso, Capu contains 52 residues in this region (Fig. 4.6A). We expect this proline-rich lasso insertion to be fairly unstructured, and thus refer to it as the "loop" domain.

To begin characterizing this novel loop domain, we created and purified a construct lacking 38 of the loop residues (CapuCTΔloop, residues 467–610+649–1059). In size exclusion chromotagraphy experiments, CapuCTΔloop elutes between the dimer and monomer controls (Fig. 4.6B). There are two feasible explanations for this shift: First, CapuCTΔloop could exist in equilibrium as a monomer and dimer. Second, CapuCTΔloop could have a more compact shape compared to wildtype, causing it to elute as a smaller molecular species.

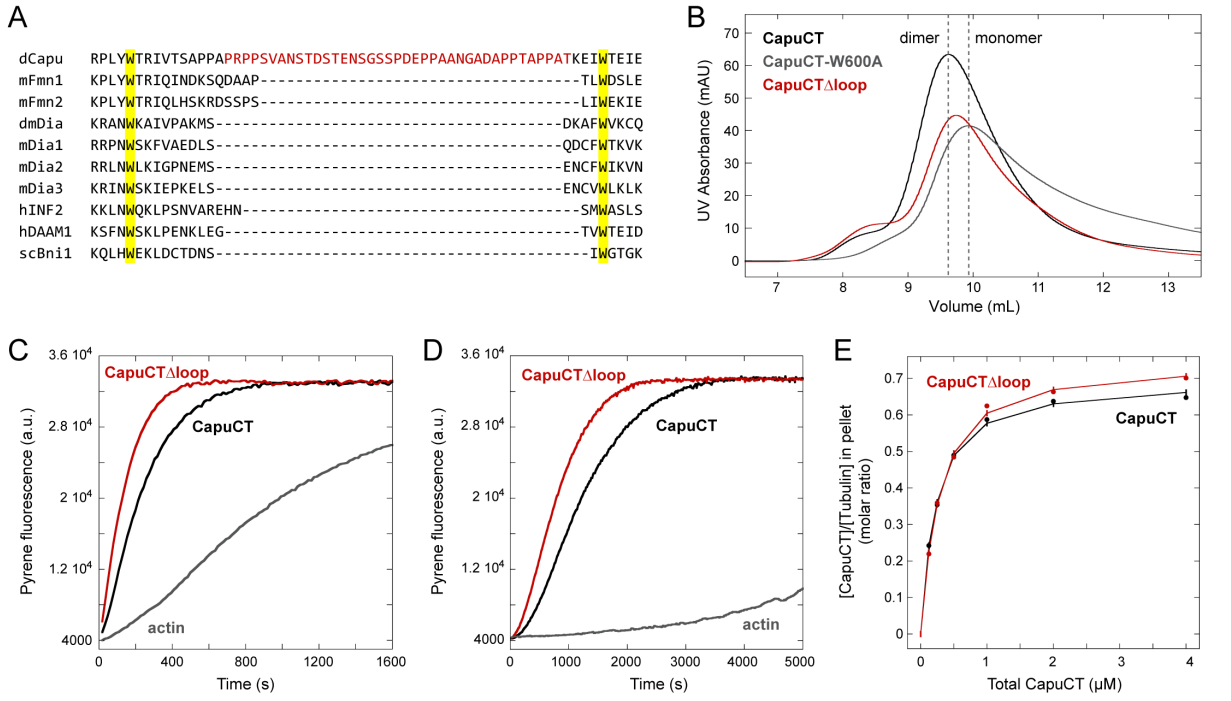

Figure 4.6 – Removing Capu's "loop" domain increases actin assembly activity. (A) Sequence alignment showing the location of Capu's extra "loop" domain between the highly conserved lasso Trp residues. (B) Size exclusion chromotography of CapuCTΔloop compared to wildtype CapuCT (dimer) and CapuCT-W600A (monomer). Actin assembly activity of 10 nM CapuCTΔloop in the absence (C) or presence (D) of profilin. (E) Microtubule binding by CapuCTΔloop compared to wildtype at 50mM KCl with 0.5 μM tubulin.

In bulk pyrene-actin polymerization assays, CapuCTΔloop was a faster actin nucleator than wildtype, both in the presence and absence of profilin (Fig. 4.6, C and D). Because monomeric CapuCT loses its actin assembly activity (data not shown), this supports our hypothesis that removing the loop domain changes the overall shape of the CapuCT dimer rather than impairing its ability to dimerize.

We next tested CapuCTΔloop binding to microtubules. Although microtubule binding was very similar to the wildtype control, CapuCTΔloop did exhibit a small increase in binding density (Fig. 4.6E and Table 4.2). Based on our size exclusion chromatography experiments, we speculate that removal of the loop domain results in a more compact CapuCT dimer; this CapuCTΔloop dimer could have a smaller binding footprint on the microtubule, which would lead to an increased binding density.

4.6 Discussion

Here we have identified and characterized several point mutations from classical *capu* alleles. While we had hoped to identify mutations within uncharacterized regions of Capu, the fact that all mutations appear in the FH2 domain underscores this domain's functional importance *in vivo*. Based on our Capu homology model, all mutations reside in three key regions of the FH2 domain: the lasso, post, and knob.

The two mutations in the knob (I751T and L768H) appear to be buried hydrophobic residues. This observation fits well with our *in vitro* analysis: CapuCT-I751T was difficult to purify and exhibited severely reduced nucleation activity while CapuCT-L768H could not be purified at all. Moreover, these mutations displayed the most severe reduction in actin mesh of all the alleles tested. From this we conclude that the I751T and L768H mutations globally disrupt the structural stability of Capu, leading to the deleterious phenotypes observed *in vivo*.

The remaining mutations are clustered around the lasso and post regions of the FH2 domain, but do not impair Capu's ability to dimerize *in vitro*. These mutants varied widely in their actin assembly activity. The D854N and P597L mutations severely compromised

actin assembly to levels at least 2-fold slower than wildtype. We believe that this reduction in actin assembly is sufficient to explain the *in vivo* phenotypes observed for these two alleles. The H977Y mutation had a more moderate effect on Capu's actin nucleation activity, but behaved poorly in size exclusion chromatography experiments. In addition to forming a dimer, this mutant appeared to be in equilibrium with an inactive, higher order complex or aggregate. This finding suggests that the H977Y mutation may structurally destabilize Capu just enough to be relatively active *in vitro* but deleterious in a cellular environment.

The remaining two mutations, K586M and D662N, are difficult to explain with our current data, as both have *in vitro* actin assembly activities comparable to wildtype. In the oocyte, the K586M mutant had the most intact cytoplasmic actin mesh of all the alleles tested; however, this mesh was still insufficient to prevent premature cytoplasmic streaming, suggesting that Capu-K586M may be able to create actin filaments but cannot properly assemble the actin mesh. Capu-D662N is the most intriguing mutation in that it leads to a severely reduced actin mesh but retains full actin assembly activity *in vitro*. Instead of abolishing actin assembly, this mutation could disrupt a critical interaction between Capu and one of its binding partners in the oocyte. We will follow up on this hypothesis by testing this mutant's ability to bind Spir's KIND domain, Capu's own N-terminal autoregulatory domain, and the sides of actin filaments [30, 20, 47]. We will also examine actin assembly in greater detail by using TIRF microscopy to measure the elongation rates and processivity of all mutants. These experiments will further our understanding of the classical *capu* mutations and the role of Capu's FH2 domain in oogenesis.

A major motivation of this study was to identify mutations that selectively disrupt microtubule binding by Capu. We were surprised to find that almost all of our mutations affected microtubule binding, exhibiting a clear shift in microtubule binding density. This shift in binding density is nearly identical to the shift we observed for several FH2 mutations in Chapter 2. Unfortunately, we currently lack sufficient structural information about CapuCT and the Capu-microtubule binding interface to readily explain the shift in binding density. As such, it is unclear whether the shift observed with the classical *capu* mutations is mechanistically similar to the shift we observed in Chapter 2. Furthermore, it is diffi-

cult to assess whether this shift holds any physiological relevance for Capu's function in the oocyte. It was previously reported that a P597T mutation compromises Capu's ability to crosslink microtubules and actin filaments *in vitro* [48]. There is currently no known role for this crosslinking activity in the oocyte, but it is possible that these mutations not only affect microtubule binding density, but also actin/microtubule crosslinking. If this is true, the D662N mutation could be a powerful tool for understanding the potential role for Capu-mediated microtubule bundling during development. Otherwise, we are skeptical that any of these mutations will be useful for studying Capu-microtubule interactions *in vivo*. All of the mutants still bind microtubules with sub-micromolar affinity, and many have a negative effect on actin assembly activity.

Finally, we report here the first identification and characterization of a unique "loop" region within Capu's FH2 domain lasso. Although we have not yet studied it *in vivo*, we discovered that removing the loop does not compromise actin nucleation or microtubule binding by Capu. In fact, CapuCTΔloop was a faster actin nucleator than wildtype. Could this region be important for regulating Capu by being posttranslationally modified or by binding novel interacting partners? As with the other mutations, our future work will explore the loop's role in mediating known interactions with Spir, Capu's N-terminus, and actin filaments. Additional *in vivo* analysis of a CapuΔloop construct will also provide important insight into the physiological relevance of this unique region.

CHAPTER 5

Tandem affinity purification of Capu binding partners

Through our work in the preceding chapters, we have gained useful mechanistic insight into Capu's interaction with microtubules. While we can use this information to speculate about the role of Capu-microtubule binding in *Drosophila* oogenesis, it remains unclear how exactly this interaction contributes to development and whether it is important for Capu's ability to build the cytoplasmic actin mesh.

Our *in vitro* studies in Chapter 2 support a model in which Capu does not simultaneously assemble actin filaments and bind microtubules. If these activities are in fact mutually exclusive, it follows that they are spatially and/or temporally regulated within the oocyte. To date, all known Capu binding partners interact through its short C-terminal tail domain and compete with one another for Capu binding [47, 30, 20]. This competition for Capu binding could be sufficient to regulate Capu *in vivo*. For example, Spir and microtubules directly compete for Capu binding and have opposite effects on Capu's nucleation activity: microtubules potently inhibit Capu's nucleation activity while Spir and Capu form a functional nucleation complex [47, 30]. On the other hand, additional regulatory mechanisms may still be required to further mediate Capu's function *in vivo*. Posttranslational modifications have been shown to regulate autoinhibition and microtubule binding by other formins [60, 7, 95], and we hypothesize that similar regulatory mechanisms exist for Capu in the oocyte.

Additionally, it is unclear whether Capu's ability to bind microtubules contributes to the creation of the cytoplasmic mesh or if microtubule binding is instead important for an entirely different function during oogenesis. Our biochemical characterization of classical *capu* alleles in Chapter 4 suggests that while actin assembly is important for Capu's function *in vivo*, there may be other interactions necessary for building a coherent cytoplasmic mesh.

In particular, the *capu*^{A354} allele had compromised mesh *in vivo* but was indistinguishable from wildtype in all of our *in vitro* actin assembly assays. Our CapuCTΔloop construct also behaved like wildtype CapuCT *in vitro*, suggesting that this loop region may be important for regulating Capu *in vivo*. Furthermore, it is possible that Capu has other functions in the oocyte beyond building the cytoplasmic actin mesh. It has already been shown, for example, that Capu assembles actin projections that emanate from the posterior pole of the oocyte in response to Osk localization [70]. This supports a role for Capu in additional pathways in oogenesis beyond building the cytoplasmic actin mesh.

Here we used tandem affinity purification to retrieve Capu interacting proteins from *Drosophila* ovary lysates. By identifying novel Capu binding partners, we will gain further insight into Capu's function and regulation *in vivo*.

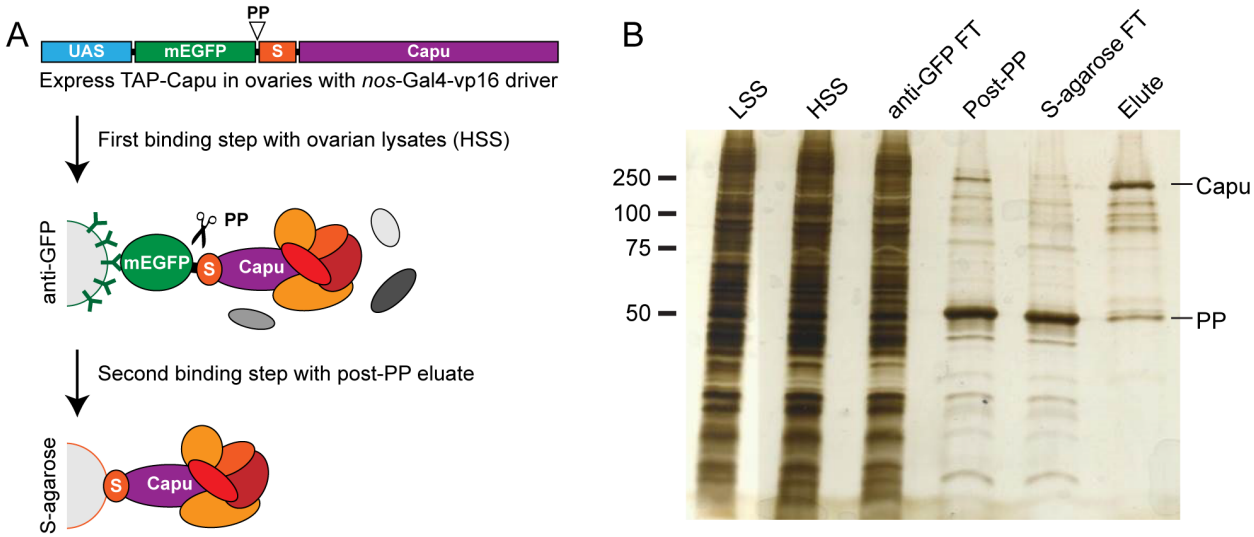

Figure 5.1 – Experimental set-up for tandem affinity purification. (A) Schematic of the tandem affinity purification process. The TAP-Capu construct comprises monomeric EGFP (mEGFP), a PreScission Protease cleavage site (PP), S-peptide, and Capu residues 1–1059 all under control of an upstream activating sequence (UAS) promoter. This construct was expressed in fly ovaries under the control of a germline-specific *nanos* driver (*nos*-Gal4-vp16). TAP-Capu and its interacting partners were pulled down from ovarian lysates using anti-GFP beads. TAP-Capu was then cleaved from the anti-GFP beads using PreScission Protease (PP) and was further purified by binding to S-agarose. See Section 7.9 for additional experimental details. (B) Silver stained gel showing fractions from key steps in the tandem affinity purification process: low-speed supernatant (LSS), high-speed supernatant (HSS), anti-GFP flowthrough (FT), supernatant after treatment with PreScission Protease (Post-PP), S-agarose flowthrough (FT), and the final elution fraction (Elute). The final elution fraction contains Capu, PreScission Protease contaminant (PP) and several bands indicating candidate interacting partners. Molecular weight is indicated in kDa.

5.1 TAP-Capu expression and pulldown

We created a transgenic fly line containing an N-terminally TAP-tagged Capu construct (TAP-Capu; Capu residues 1–1059) and expressed it in fly ovaries using a germline specific *nanos* driver (Fig. 5.1A). Capu and its binding partners were then isolated from ovary lysates in two consecutive binding steps as outlined in Fig. 5.1A (see Section 7.9 for experimental procedures). Using this approach, we were able to isolate Capu along with several binding partners that could be readily detected on a silver stained gel (Fig. 5.1B).

Once we established that our protocol could successfully isolate Capu and its binding partners, we repeated the pulldown in tandem with a negative control lysate prepared from ovaries expressing GFP instead of TAP-Capu (Fig. 5.2). In general, there was very little overlap between the bands detected for the TAP-Capu pulldown and the negative control. Several bands could be detected on the negative control gel, but these were very faint and appeared mainly in the 45–70 kDa range. Far more bands were detected on the TAP-Capu gel ranging from approximately 10 kDa (the lower limit of the gel) up to approximately 114 kDa (the size of the Capu monomer). To identify these binding partners, we scaled up our experiment and sent our final elution fraction to the laboratory of Dr. Julian Whitelegge. There it was digested with trypsin and analyzed by nano-liquid chromatography with tandem mass spectrometry (see Section 7.9 for additional experimental details).

5.2 Mass spectrometry results

Mass spectrometry analysis identified a number of potential Capu interacting partners. Peptide results were searched against two sequence databases: a database encompassing all *Drosophila* species (228,960 sequences) and a database specific to *D. melanogaster* (5,129 sequences). Searching these two databases revealed 68 and 88 different binding candidates, respectively, as shown in Tables A.1 and A.2. From these results, we then selected a smaller subset of protein hits that had particularly good peptide coverage or were of particular physiological interest (Table 5.1).

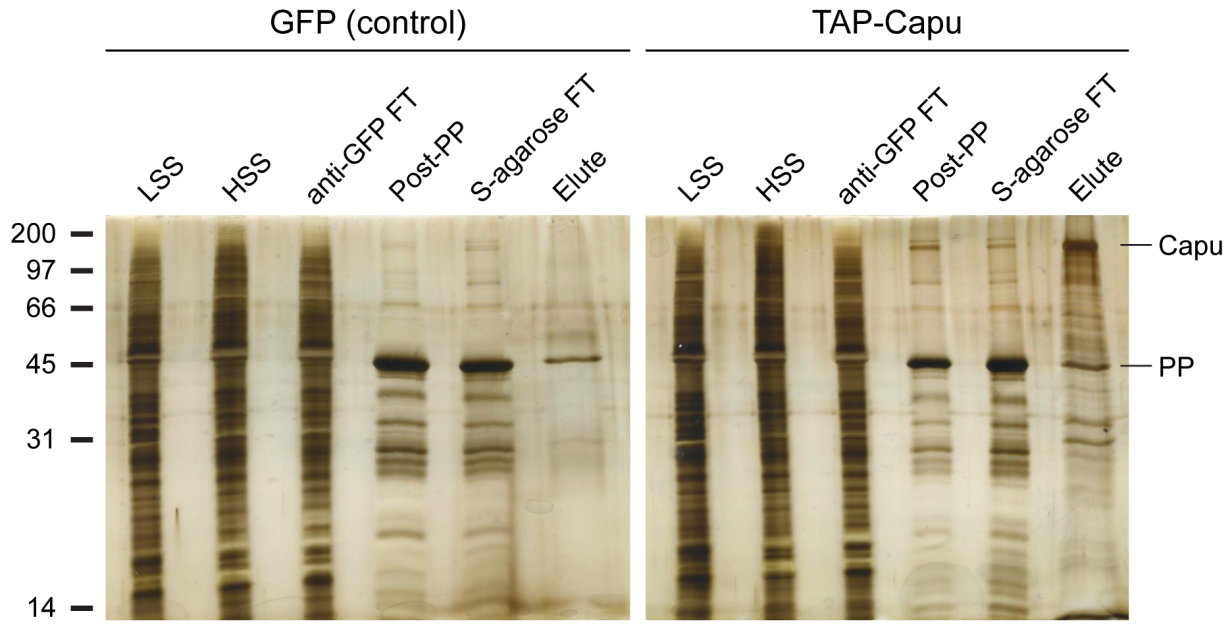

Figure 5.2 – **Tandem affinity purification preliminary results.** Silver stained gels from two separate pulldowns: GFP (negative control) and TAP-Capu. Each gel shows fractions from key steps in the tandem affinity purification process: low-speed supernatant (LSS), high-speed supernatant (HSS), anti-GFP flowthrough (FT), supernatant after treatment with PreScission Protease (Post-PP), S-agarose flowthrough (FT), and the final elution fraction (elute). Molecular weight is indicated in kDa.

Table 5.1 – **Selected mass spectrometry results.** For full results see Tables A.1 and A.2.

Gene	**Mass**	**Matches**[†]	**% Coverage**[§]
Cappuccino, isoform E	138486	1105 (923)	54.8
Cytoplasmic dynein light chain	10468	65 (56)	55.1
Receptor of activated protein kinase C 1	36109	21 (15)	62.2
Dynamin related protein 1	83085	22 (5)	23.5
Ketel (importin β)	99886	15 (5)	12.9
Pendulin (importin α2)	58071	23 (1)	24.5
Protein phosphatase 2A	72542	17 (4)	18.0
Polo (protein kinase)	67588	4 (2)	9.2
CG4552 (putative Rab GAP)	78449	32 (18)	32.7
Yolkless (vitellogenin receptor)	222297	12 (2)	6.2
Rab9	28848	6 (1)	7.8

[†]Total number of peptide matches. The number of significant ($p < 0.05$) matches is indicated in parentheses.
[§]Percentage of total protein sequence for which peptide matches were identified.

As expected, our top protein hit was Capu itself. However, several peptides matched Capu sequences N-terminal to the Capu-A isoform used to create our TAP-Capu construct. While this could simply reflect computer bias in matching peptide fragments, this opens the intriguing possibility that other Capu isoforms besides Capu-A do in fact exist in the *Drosophila* oocyte. Because we specifically pulled down Capu-A in our experiments, this also suggests that other Capu isoforms may be able to form heterodimers and/or higher-order complexes with Capu-A.

Other high scoring protein hits with particularly good peptide coverage included Cytoplasmic dynein light chain, Receptor of activated protein kinase C 1 (RACK1), and dynamin-related protein 1 (Drp1). The cytoplasmic dynein light chain hit could be Cytoplasmic dynein light chain 2 or Cut up, which differ by only one amino acid and cannot be differentiated by our peptide matches. The remaining hits in Table 5.1 were selected based on their known or putative physiological function: Ketel (importin β) and Pendulin (importin $\alpha 2$) are both involved in nuclear import; Polo (protein kinase) and Protein phosphatase 2A (PP2A) are posttranslational modifiers; and Yolkless (vitellogenin receptor), CG4552 (a putative Rab GAP), and Rab9 are known or likely to be important for endocytosis [96, 97, 98].

In addition to identifying potential interacting partners, we were able to search our mass spectrometry results for phosphorylated Capu peptides and identified several putative phosphorylation sites (Table 5.2). Two of these sites, Ser-160 and Ser-565, are already annotated in the Phosida posttranslational modification database [99]. We note that Ser-565 (FH1 domain), Ser-680 (FH2 domain linker region), and Ser-1047 (tail domain) all lie in fairly unstructured regions of Capu where they could be easily accessible to posttranslational modifiers. We also ran these putative phosphorylation sites through three different kinase prediction servers [100, 99, 101] and identified potential kinases for all but one of the phosphorylation sites (Table 5.2). We stress, however, that these putative phosphorylation sites and kinases have not been rigorously tested and are presented here purely as a starting point for further analysis.

Table 5.2 – Predicted Capu phosphorylation sites. Mass spectrometry results were submitted to an error tolerant search to identify potential posttranlsational modifications. Maximum peptide scores for each predicted phosphorylation site are shown. Scores are calculated as $-10log(P)$ where P is the probability that the observed match between the experimental data and the database sequence is a random event.

Residue	Score	Predicted Kinases
Ser-35	15	
Ser-160	47	PKC[1], PKD[2], CHK1[2]
Thr-318	60	CDK1[2,3], CDK2[2], ERK[2], NEK6[2], CKI[1], p38MAPK[1], GSK3[1], cdk5[1]
Ser-565	57	p38MAPK[1], cdk5[1]
Ser-680	8	PKC[1]
Ser-822	11	NEK6[2], cdc2[1]
Thr-925	5	PKA[1,2], cdc2[1]
Ser-1047	3	PKA[1,2], PKC[1], CKI[2], CK2[2], Aurora[2]

[1]NetPhosK 1.0 Server (http://www.cbs.dtu.dk/services/NetPhosK) [100]
[2]Phosida Motif Matcher (http://www.phosida.com) [99]
[3]Scansite 3 (http://scansite3.mit.edu) [101]

5.3 Discussion

Through our tandem affinity pulldown experiments, we hoped to address two major questions surrounding Capu's role in the oocyte: how is Capu regulated and how does microtubule binding relate to Capu's physiological function? Although the results presented in this chapter are still preliminary, they offer some interesting insights into these two questions.

As a first step toward exploring Capu regulation, we identified a handful of putative phosphorylation sites and pulled down two candidate binding partners, Polo and PP2A, that could potentially modify Capu's posttranslational state. Capu contains three polo-like kinase consensus sequences at Ser-772, Ser-793, and Ser-954 [102]; however, none of these putative polo phosphorylation sites correspond to the sites identified by mass spectrometry (Table 5.2). Further characterization will be needed to determine whether Polo acts directly on Capu and in what context Polo might regulate Capu's function. Polo-like kinases are important regulators of mitosis [103]. A recent study showed that Polo and PP2A collaborate to promote cell cycle progression in the syncytial blastoderm during *Drosophila* development [104]. Although germline cell division does not occur during mid-oogenesis, Capu could be important for cell division pathways in the germarium and/or the embryo. Because we used

whole ovary lysates for our pulldown experiments, it is quite likely that we are probing a wide range of developmental pathways.

In addition to potential regulatory proteins, our mass spectrometry analysis identified several different Capu isoforms and a second *Drosophila* formin, Diaphanous (Dia). Because peptide matches were scattered throughout the entire coding regions of these proteins, we do not believe that these hits are simply false positives resulting from conserved FH2 domain sequences. Daou *et al.* recently discovered that mDia1, mDia2, and mDia3 can form heterodimers in the cell [59]. Together with our findings, this supports an interesting new model for formin heterodimerization. Although the physiological relevance of formin heterodimerization is not yet clear, this could be yet another example of how formin function is specialized and regulated within the cell. Such a possibility warrants further investigation and should be a focus of future research.

With respect to our second question of how microtubule binding relates to Capu's physiological function, we were pleased to see several microtubule-related hits among our mass spectrometry results. We were surprised, however, by the lack of actin and actin-binding proteins considering Capu's known role as an actin nucleator. It is possible that the high-speed centrifugation step removed most, if not all, of the actin filaments from solution. Because our tandem affinity purification was performed on ice, microtubules likely depolymerized in the cold while actin remained intact. This could explain the presence of tubulin but not actin in our mass spectrometry results. To correct for this bias, experiments should be repeated in the presence of an actin depolymerizing drug such as LatA. We were also surprised that Spir was not among our mass spectrometry results. It is well established that Capu and Spir directly interact during oogenesis [30, 32], and a previous study demonstrated that Capu and Spir co-immunoprecipitate from ovary lysates [47]. We speculate that storing ovaries in the freezer could selectively break down Spir or that the Capu-Spir interaction may not be stable enough to survive the multiple purification steps and relatively high salt (300 mM KCl) conditions used in our tandem affinity purification procedure. In future work, a combination of tandem affinity purification, Western blot analysis, and direct comparison of frozen versus fresh ovary lysates should clear up this discrepancy.

Moving forward, we still need to rigorously test and confirm our newly identified Capu binding partners. In the meantime, these preliminary results suggest intriguing possibilities for Capu's role in oogenesis. Cytoplasmic dynein light chain is a particularly exciting hit given its clear connection with the microtubule cytoskeleton. Following up on this putative interaction could provide much needed insight into Capu's relationship with microtubules during oogenesis. RACK1 and Drp1 are also interesting hits as they both have emerging roles in *Drosophila* oogenesis but have not been thoroughly characterized in this context [105, 106]. Similarly, the importins we identified might play important developmental roles distinct from the canonical nuclear import pathway. Rather than localizing to the nucleus, Pendulin associates with the cortex, binds actin filaments, and is important for proper ring canal assembly during oogenesis [107]. Further characterization of these candidate binding partners will ultimately improve our understanding of oogenesis and the role of Capu during development.

CHAPTER 6

Conclusion

6.1 Emerging mechanisms of formin-microtubule binding

Here we have characterized the mechanism of Capu-microtubule binding as well as its effect on Capu-mediated actin assembly. To place our work in a broader context, we will discuss three emerging features of formin-microtubule interactions: (1) the mutually exclusive nature of actin assembly and microtubule binding, (2) the variable role of the formin tail in microtubule binding, and (3) a putative microtubule binding hot spot in the FH2 domain.

There is a developing trend in the formin field that microtubule binding and actin assembly activity may be mutually exclusive *in vivo* and represent two distinct aspects of formin function. Our *in vitro* data presented in Chapter 2 support a model in which Capu does not simultaneously assemble actin filaments and bind microtubules. Microtubules potently inhibit actin nucleation by Capu but have little effect on Capu once it is bound to the end of an elongating actin filament. Our model fits with previous studies demonstrating that formin actin nucleation activity is dispensable for microtubule stabilization [43], microtubule attachment to kinetochores [60], and cortical microtubule capture [59]. Furthermore, mDia1 exhibits a clear tradeoff between barbed end association and microtubule binding *in vivo*: treating cells with actin depolymerizing drugs or overexpressing actin capping protein liberates mDia1 from actin barbed ends and promotes mDia1-mediated microtubule stabilization [79]. Our analysis suggests that microtubule binding and actin barbed end association require overlapping surfaces on the FH2 domain, and Daou *et al.* recently demonstrated a similar functional overlap for mDia [59]. Future work will reveal whether this tradeoff between microtubule binding and actin assembly is a characteristic of all formins.

A

Tail	Size (aa)	pI	K_d (μM)
hINF2	309	4.8	> 20
mDia1	107	9.8	> 20
mDia2	164	10.3	0.7
Capu	31	11.7	1.1

B

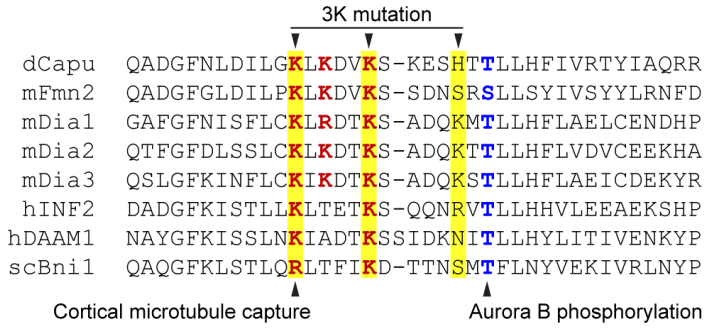

C

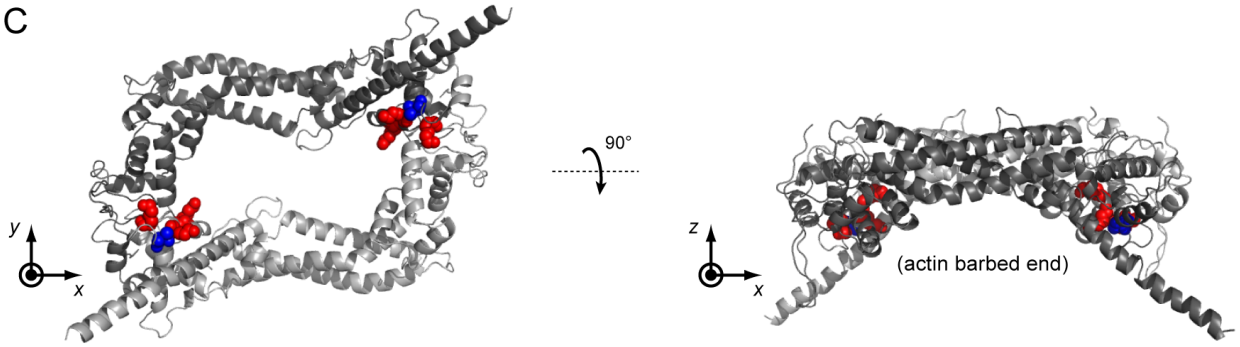

Figure 6.1 – Potentially conserved mechanisms of formin-microtubule binding. (A) Summary of microtubule binding data for several formin tail domains. Formin tails that bind microtubules with measurable affinity have a theoretical pI > 10. Data for hINF2, mDia1, and mDia2 are from Gaillard *et al.* [28]. (B) A putative microtubule binding hot spot in the FH2 domain. The original 3K mutation made by Ishizaki *et al.* is highlighted in yellow. Residues in and around this region are important for cortical microtubule capture [59] and regulation by Aurora B kinase [60]. Residues important for *in vitro* Capu-microtubule binding (Lys-851, Lys-853, and Lys-856) are shown in red. The residue important for mDia3 phosphorylation by Aurora B is shown in blue. (C) Structural location of the putative microtubule binding hot spot. Capu homology model is based on the crystal structure of hDAAM1 (PDB # 2J1D; [87, 88]). Lys-851, Lys-853, and Lys-856 are shown as red spheres, and Thr-863 is shown as blue spheres. These residues lie on the same FH2 surface that contacts the actin barbed end.

A second formin development is the variable role of the C-terminal tail domain in microtubule binding. Of the four formins carefully studied *in vitro*, Capu and mDia2 require their C-terminal tails for high affinity microtubule binding, while mDia1 and hINF2 do not [28]. We note that the Capu and mDia2 tail domains, which can also bind microtubules on their own, are much more basic than the mDia1 and hINF2 tail domains (Fig. 6.1A). We found in Chapter 2 that Capu's tail domain binds microtubules through nonspecific charge-based interactions. Perhaps any formin tail with sufficient charge can bind the microtubule lattice and contribute to microtubule binding in this way. Why tail binding may be important for some formins and not others remains unclear. It is possible that absence or presence of tail binding shifts the mode of microtubule binding to influence how different formins interact with microtubules. For instance, tail binding could alter the ability of formins to stabilize and/or bundle microtubules. Additional information about the formin-microtubule binding interface will allow us to begin dissecting the interaction and understand the precise role of the formin tail.

Finally, there appears to be a putative hot spot for microtubule binding within the FH2 domain of several formins. In an early formin study, Ishizaki *et al.* identified a three-lysine (3K) mutation in the FH2 domain that disrupts mDia1-mediated microtubule reorganization [5]. Based on sequence alignments, this 3K mutation corresponds to Capu residues Lys-851, Lys-856, and His-861 (Fig. 6.1B). Structural studies of the FH2 domain later revealed that the second 3K lysine (Capu Lys-856) directly contacts the actin barbed end and is essential for the actin nucleation activity of the yeast formin Bni1p [12, 13]. However, when we mutated this residue in Capu, we observed little effect on nucleation activity and measured a striking increase in microtubule binding density. Concurrent with our study, Daou *et al.* discovered that mutating the first 3K lysine (Capu Lys-851) disrupts mDia-mediated cortical microtubule capture [59]. Cheng *et al.* also demonstrated that phosphorylation by Aurora B near the 3K mutation region (Capu Thr-863) disrupts mDia3 association with microtubules *in vitro* and *in vivo* [60]. All of these residues are located within a small, well-conserved region of the FH2 domain. This region lies along the inner surface of the FH2 dimer, which directly contacts the actin barbed end (Fig. 6.1C). Although future work will be necessary to

better characterize this region across all formin groups, these findings point to a key region that may play a conserved role in formin-microtubule binding.

6.2 Implications for Capu-microtubule binding in oogenesis

During *Drosophila* oogenesis, Capu builds two important actin structures: a cytoplasmic actin mesh and a collection of posterior actin projections. Although we have characterized Capu's ability to bind microtubules *in vitro*, it is still unclear how this relates, if at all, to Capu's developmental role building either of these actin structures. Addressing this question will ultimately require better tools for selectively disrupting microtubule binding *in vivo*. However, the results of this dissertation should provide useful alternative avenues for exploring the role of Capu-microtubule binding during development. Here we discuss the implications of our findings with respect to Capu's role during oogenesis and suggest possible directions for future research.

Capu and Spir work together to form the cytoplasmic actin mesh during mid-oogenesis [69, 32]. However, Capu's own actin assembly activity is also required for this process [32], supporting a model in which Capu remains processively attached to growing actin filaments to build a coherent meshwork. Our *in vitro* experiments in Chapter 2 revealed that despite their potent inhibitory effect on Capu's actin nucleation activity, microtubules have little effect on Capu once it is bound to the barbed end of an elongating actin filament. Because Spir directly competes with microtubules for Capu binding [47], the Capu-Spir complex may be able to efficiently nucleate actin in the presence of microtubules. Once Capu is released from this complex, it is already attached to the barbed end of an actin filament and could therefore act as a processive elongation factor in the microtubule-rich oocyte. We suspect that Capu's role as an elongation factor is essential during oogenesis. This hypothesis is reinforced by our results in Chapter 4 demonstrating that some classical *capu* alleles fail to build a functional mesh but nucleate actin filaments *in vitro*. Future work will reveal whether these mutants are compromised in their ability to processively elongate actin filaments. Finally, we note the presence of cytoplasmic dynein light chain (Cdlc) in our tandem affinity

purification results presented in Chapter 5. While the exact mechanism is unknown, dynein is required to repress premature cytoplasmic streaming during mid-oogenesis [74]. Capu may therefore interact with dynein to build the cytoplasmic actin mesh and regulate the timing of streaming. Confirming and characterizing Capu's putative interaction with Cdlc could provide valuable insight into Capu-mediated coordination of the actin and microtubule cytoskeletons.

In addition to building the cytoplasmic actin mesh, Capu works with Spir to build a set of long actin projections at the oocyte posterior [75, 70]. These projections appear around stage 10 in response to *osk* mRNA localization [75]. At this point in development, microtubules are nucleated from all regions of the oocyte cortex except the posterior pole [71]. Given the antagonistic relationship between microtubule binding and actin assembly, microtubules could help regulate Capu function at this stage of oogenesis by restricting the location of the actin projections. In the current model for actin projection assembly, the regulatory protein Mon2 acts as a scaffold to link Capu and Spir to a special population of Osk-induced endocytic vesicles and to promote actin assembly [70]. Again, we point out our identification of Cdlc as a candidate Capu binding partner as dynein is involved in the retrograde transport of endosomes and other vesicles [108]. At the oocyte posterior, the endosomal compartment is restricted to within 1μm beneath the plasma membrane [109], whereas actin projections are on average 2.5 μm in length [75]. Perhaps dynein-mediated transport is needed to move specialized Capu/Spir/Mon2 vesicles farther into the oocyte to facilitate construction of such long actin projections. Intriguingly, another candidate binding partner, RACK1, has been shown to regulate recycling endosome distribution via the dynein/dynactin complex [110, 111]. Several other candidate binding partners are also involved in endocytosis including the putative Rab-GAP CG4552, the late endosome GTPase Rab9 [112], a handful of vitellogenins (yolk proteins), and the vitellogenin receptor Yolkless, which marks all endocytic structures except yolk granules [75]. Some or all of these proteins may form endosomal complexes with Mon2, Capu, and Spir to regulate the posterior actin projections and/or promote Cdlc-mediated vesicle association with microtubules.

Another intriguing possibility is that Capu helps mediate microtubule capture at the

oocyte posterior. In addition to inducing posterior actin projection formation, *osk*-upregulated endocytosis is required for the maintenance of microtubule polarity and proper localization of additional *osk* mRNAs to the posterior [76]. Sanghavi *et al.* recently demonstrated that microtubule plus ends decorated with CLIP-190 (*Drosophila* CLIP-170) and EB1 are enriched at the oocyte posterior [113]. In their study, disrupting the posterior enrichment of either protein led to reduced levels of posterior endocytosis, suggesting that this population of microtubules is somehow important for the *osk*-induced endocytic pathway. In mammalian cells, mDia mediates cortical microtubule capture during cell migration in a pathway that involves microtubule plus end associated proteins and the spectraplakin ACF7 [53, 59]. Perhaps not coincidentally, both Capu and the *Drosophila* spectraplakin, Short stop (Shot), were identified in a screen for novel *osk* mRNA localization and anchoring factors [77]. Because Shot is necessary for oocyte specification in the germarium [114], its role later in oogenesis has not yet been characterized; however, Shot is known to organize microtubules and colocalize with both EB1 and APC in larval tendon cells [115]. It will be interesting to see whether Capu, like mDia, can work with Shot and microtubule plus end associated proteins to capture microtubules at the oocyte posterior. Capu-mediated microtubule capture could help promote *osk* mRNA localization and pole plasm assembly and/or help guide incoming yolk granules onto microtubule tracks. More experimental evidence will be required to sort out the precise role, if any, of Capu in such processes.

6.3 Concluding remarks

In this study, we have characterized *in vitro* Capu-microtubule binding (Chapter 2), studied the biochemical effects of classical *capu* mutations (Chapter 4), and identified candidate Capu binding partners that may be important during development (Chapter 5). When we began this work, we had hoped to identify point mutations that could be used as tools to selectively disrupt formin-microtubule binding *in vivo*. Although we have yet to uncover such point mutations, our findings have improved our mechanistic understanding of formin-microtubule binding and provide intriguing directions for future investigation. In particu-

lar, we are optimistic that the emerging microtubule binding hot spot in the FH2 domain (Fig. 6.1, B and C) may play a conserved role in microtubule binding among many, if not all, formins. Continued characterization of formin-microtubule binding will be necessary to identify any conserved binding mechanisms and useful tools for disrupting microtubule binding *in vivo*. In particular, it will be helpful to characterize microtubule binding by formins from the remaining formin groups (FHOD, DAAM, FMNL, and Delphilin) to provide a more complete picture of formin-microtubule interactions. Electron microscopy studies of formin-microtubule complexes will be especially useful for characterizing the formin-microtubule binding interface. Elucidating the basic mechanisms of direct formin-microtubule binding will help us to understand how exactly formins regulate microtubule stability and organization in the cell. Furthermore, it will shed light on the variety of specialized formin roles within the cell. Why do some formins bundle microtubules but not others? Why are only some formin tails involved in microtubule binding? In the cell, do formins associate with microtubules directly, through secondary binding partners, or some combination thereof? Addressing these questions will advance the field by better characterizing the role of formin-microtubule binding across many different formins and cell types.

With respect to Capu's role in *Drosophila* development, our tandem affinity purification results in Chapter 5 suggest that Capu does more than build the cytoplasmic actin mesh and posterior actin projections. This is not particularly surprising considering that *capu* mRNA transcripts can be detected throughout oogenesis and into mid-embryogenesis [63]. In fact, not long after Capu was first cloned, Manseau *et al.* reported a cytokinesis defect in *capu* and *chic* mutant fly lines that resulted in egg chambers with multinucleate nurse cells [65]. Moreover, GFP-Capu appears enriched along nurse cell membranes [32], yet nothing is currently known about how Capu might function at this location. The candidate binding partners identified in Chapter 5 may point us toward uncovering these and other unknown developmental roles for Capu. For example, identification of the candidate binding partner Drp1 suggests that Capu may be important for mitochondrial fission during development. In mammalian cells, the ER-associated formin INF2 assembles actin at mitochondrial fission sites and actively recruits Drp1 [116]. Careful characterization of mitochondria in *capu*

alleles may reveal a similar role for Capu in the oocyte. Identification of the candidate binding partners Ketel (importin β) and Pendulin (importin $\alpha 2$) suggests that Capu may also play a novel role in nuclear import during development. Because Capu is not detected in the nuclei of live egg chambers [32], we are skeptical that Capu itself is imported into the nucleus. Instead, Capu could regulate the import of other proteins or interact with Ketel and Pendulin in roles distinct from nuclear import. Notably, Pendulin has been shown to bind actin, associate with the oocyte cortex, mediate assembly of ring canals during oogenesis, and play a role in mitosis [107, 117]. Capu's role as a cytoskeletal regulator makes it an interesting candidate for regulating such noncanonical importin functions.

There is clearly much more to learn about Capu's association with microtubules and its physiological role during *Drosophila* development. In this dissertation, we have provided useful mechanistic details of Capu-microtubule binding as well as intriguing avenues for future research. Ultimately, we hope that careful characterization of Capu and its role in oogenesis will elucidate broader mechanisms of formin function and advance our understanding of Capu's mammalian homologs, Fmn1 and Fmn2. In mouse oogenesis, movement of recycling endosomes is driven by cytoplasmic actin filaments nucleated by Spir and Fmn2 [118]. Based on previous *Drosophila* studies and our preliminary tandem affinity purification results, it seems likely that Capu may form a similar endosomal complex to build posterior actin projections. Recent mass spectrometry experiments in mammalian cells also identified novel mDia associated proteins in similar pathways as our Capu candidate binding partners. In particular, mDia1 associates with cytoplasmic dynein heavy chain and mDia2 associates with a number of nuclear proteins [59]. Further characterization of novel formin binding partners and formin-microtubule binding will help tease apart the molecular details of formin function and answer important questions about the physiological role of formins as coordinators of the actin and microtubule cytoskeletons.

CHAPTER 7

Experimental procedures

7.1 Protein purification

A. castellani actin, Chic (*Drosophila* profilin), and *S. pombe* profilin were purified according to published protocols [119, 20].

Wildtype (aa 467–1059), mutant, and truncated CapuCT constructs were sub-cloned into a modified version of pET15b with an N-terminal His_6 tag as previously described [30]. Capu tail (aa 1029–1059) was subcloned into the vector pGEX-6P-2 (GE Healthcare) as described [30]. Point mutations were introduced using QuikChange Site Directed Mutagenesis (Stratagene).

All His_6-tagged CapuCT and CapuFH2 proteins were expressed and purified as described [30] with the following modifications for CapuFH2: dialysis buffers were supplemented with 50 mM KCl and storage buffer contained 100 mM NaCl to improve protein solubility. The total concentration of protein was calculated by quantitative Sypro-Red (Invitrogen) staining using wildtype CapuCT as a standard.

GST and GST-tail were expressed as described [30]. Briefly, extracts were passed over glutathione-Sepharose (GE Healthcare), eluted using glutathione, dialyzed overnight against 10 mM Tris-HCl pH 8.0, 1 mM DTT, and further purified over a MonoQ anion exchange column (GE Healthcare).

To analyze purified proteins by size exclusion chromotagraphy, a Superdex 200 10/300 GL size exclusion column (GE Healthcare) was equilibrated with Column Buffer (50 mM HEPES, pH 7.0, 150 mM NaCl, 1 mM DTT). Approximately 4 nmol of each CapuCT construct was diluted in Column Buffer, centrifuged at 100,000 × g for 20 min at 4°C, and

loaded onto the equilibrated column.

7.2 Microtubule preparation

Frozen aliquots of tubulin in BRB buffer (80 mM K-PIPES, pH 6.8, 1 mM EGTA, 1 mM $MgCl_2$) supplemented with 1 mM GTP were prepared from lyophilized tubulin (Cat. # T240, Cytoskeleton, Inc.). Tubulin was thawed quickly at 37°C, incubated for 5 min on ice, and centrifuged at 100,000 × g for 10–20 min at 4°C. Tubulin concentration in the supernatant was determined by its absorbance at 280 nm (ϵ_{280} = 115,000 cm^{-1} M^{-1}) and subsequently polymerized in BRB buffer plus 2 mM GTP at 37°C by addition of 0.1, 1, and 20 μM taxol (paclitaxel, Sigma-Aldrich) at 10 min intervals from 100-fold concentrated DMSO stocks.

For experiments with subtilisin-treated microtubules, polymerized tubulin was incubated with 100 μg/mL subtilisin (Sigma-Aldrich) at 37°C for 1 hour. The reaction was quenched with 2 mM PMSF, and microtubules were spun over a 10% sucrose cushion at 70,000 × g for 10 min at 25°C to remove cleaved peptides. The pellet was washed and resuspended in microtubule-binding buffer (MTB; 10 mM Na-HEPES, pH 7.0, 1 mM EGTA, 1 mM $MgCl_2$, 1 mM DTT, 20 μM taxol, 0.5 mM thesit [nonaethylene glycol monodecyl ether, P-9641; Sigma-Aldrich] and 50 or 100 mM KCl as indicated).

7.3 Microtubule-binding assays

Microtubule-binding assays were performed essentially as described [47] with modifications. Briefly, CapuCT proteins, GST, or GST-tail were cleared at 100,000 × g for 20 min at 4°C. For actin monomer competition experiments, actin was pre-incubated on ice with a 2-fold molar excess of Latrunculin B (LatB; EMD Millipore Chemicals). LatB-Actin and Chic samples were each diluted in MTB and cleared at 100,000 × g for 20 min at 4°C. Protein concentration in the supernatant was determined by absorbance at 280 nm or 290 nm for LatB-Actin. Proteins were mixed with microtubules (0.5 μM) or buffer in MTB. Samples

were incubated for 15 min and centrifuged at 100,000 × g for 10 min at 25°C. Supernatants were removed, and pellets were washed before resuspending in SDS-PAGE sample buffer.

Proteins were resolved by SDS-PAGE, stained with Sypro-Red (Invitrogen), and quantified using a Pharos FX Plus Molecular Imager with Quantity One software (BioRad). Signals from samples without microtubules were subtracted from the corresponding signals from samples containing microtubules to account for nonspecific protein pelleting. Protein and tubulin concentrations in each pellet sample were quantified using a standard curve for tubulin and the protein in question generated on the same gel. All concentrations reported are dimer concentrations of CapuCT, GST, or tubulin.

Binding data were fit to the McGhee von Hippel model for binding to a polar one-dimensional lattice [85]:

$$C_{total} = MT_{total}v + \frac{K_d v}{1-nv}\left(\frac{1-nv}{1-(n-1)v}\right)^{1-n} \tag{7.1}$$

where

$$K_d = e^{-\Delta_r G/RT} \tag{7.2}$$

The binding density v was measured by dividing the concentration of bound protein by the total concentration of polymerized tubulin dimers in the pellet (MT_{total}). For large C_{total}, the value of v approaches a maximum value of $1/n$ where n represents the number of tubulin dimers per binding site. Because we can arbitrarily use the dissociation constant K_d versus the association constant K_a of the binding reaction, we instead fit the free energy ($\Delta_r G$) of the binding reaction, as this is unbiased by the direction of the reaction. We then converted $\Delta_r G$ to the K_d values reported in Tables 2.1 and 4.2. The fit parameters $\Delta_r G$ and n were determined using the Levenberg-Marquardt algorithm implemented in Python using SciPy [120].

7.4 Pyrene-actin polymerization assays

Pyrene-actin assembly assays were carried out as described [20]. For the experiments in Fig. 2.2, buffers were supplemented with 20 μM taxol from a 10 mM stock in DMSO. Unless stated otherwise, microtubules were added to the polymerization buffer before addition to Mg-G-actin. For experiments with profilin, *S. pombe* profilin was briefly pre-incubated with Mg-G-actin and used at a final concentration of 8 μM. Fluorescence was monitored in a spectrofluorometer (Photon Technology) or a TECAN F200 with $\lambda_{excitation} = 365$ nm and $\lambda_{emission} = 407$ nm.

7.5 Actin elongation TIRF microscopy assays

Cover glass was silanized and functionalized with biotin-PEG as described [20, 121]. Actin was labeled at Cys-374 with OregonGreen488 iodoacetamide (Life Technologies) or EZ-link maleimide-PEG2-biotin (Thermo Scientific) essentially as described [20]. Because labeling with biotin at Cys-374 caused F-actin to depolymerize, the actin was subsequently centrifuged at 195,000 $\times$ g and the supernatant was further purified by size exclusion chromatography on a Superdex 200 10/300 GL (GE Healthcare) in G-buffer (2 mM Tris-Cl, pH 8.0, 0.1 mM $CaCl_2$, 0.2 mM ATP, 0.5 mM TCEP, 0.04% sodium azide). Biotin-actin could incorporate into actin filaments at low labeling fractions ($< 2\%$).

Microtubules were prepared as described above, with the exception that frozen tubulin aliquots contained 20% HiLyte647 tubulin (Cat. # TL670M Lot: 013, $\sim$0.2 dyes per tubulin dimer, Cytoskeleton, Inc.) and 10% biotin tubulin (Cat. # T333P Lot: 013, $\sim$1–2 biotins per tubulin dimer, Cytoskeleton, Inc.). F-actin seeds were polymerized from 99.4% unlabeled actin, 0.6% biotinylated actin, and equimolar AlexaFluor488 phalloidin (Life Technologies). Prior to imaging, approximately 15-μL flow cells were built using double-stick tape. Each flow cell was prepared with the following series of washes: 25 μL 1% Pluronic-F127 (Sigma-Aldrich), 100 μg/mL κ-casein (Sigma-Aldrich) in phosphate buffered saline for 2 min; 25 μL TIRF Buffer (KMEH (50 mM KCl, 10 mM Na-HEPES, pH 7.0, 1 mM EGTA, 1 mM $MgCl_2$),

50 mM DTT, 20 mM Glucose, 0.2 mM ATP, 0.2% methylcellulose (400 cP, Sigma-Aldrich)); 25 μL 40 nM streptavidin (VWR) in KMEH for 1 min; 25 μL TIRF Buffer supplemented with 20 μM taxol, 25 μL 550 nM F-actin seeds and approximately 0.5 μM taxol-stabilized microtubules in KMEH with 40 μM taxol for 2 min; and 25 μL TIRF Buffer supplemented with 20 μM taxol. The Mg-G-actin mix (0.6 μM actin 30% OregonGreen488-labeled, 3 μM Chic, $\pm$ 4 nM CapuCT, TIRF Buffer, 20 μM taxol, 500 μg/mL glucose oxidase, 100 μg/mL catalase, 500 μg/mL κ-casein) was flowed into the cell and imaged after 3–4 min of lag time. Images were collected every 10 seconds on a DMI6000 TIRF microscope (Leica), using a z penetration depth of 110 nm.

7.6 Fluorescence imaging of S2 cells

Wildtype S2 cells were kindly provided by Dr. Al Courey. A stable pMT-GFP-tubulin cell line was a gift of Dr. Steve Rogers. Cells were cultured in Gibco Schneider's Medium (Life Technologies) supplemented with 10% FBS. GFP-tubulin expression was induced by adding 500 μM copper sulfate from a 100 mM DMSO stock the evening prior to imaging.

Cells were transfected using the Effectene Transfection Reagent kit (Qiagen) according to the manufacturer's instructions. The red fluorescent protein tdTomato was sub-cloned into the HindIII and KpnI sites of the pIZ/V5-His vector (Life Technologies). Capu (1–1059), CapuCT (467–1059), and mDia2 (512–1060) were sub-cloned downstream of tdTomato at the BamHI and NotI restriction sites. All constructs contained stop codons to prevent inclusion of the vector's C-terminal V5 and His_6 tags.

To prepare samples for imaging, 35 mm slide dishes were coated in Concanavalin A as previously described [122]. Approximately 100–200 μL of confluent cells were added to prepared slide dishes and allowed to attach for about 1 hour. Where indicated, plated cells were treated with 5 μM Cytochalasin D (MP Biomedicals) and incubated for 1 hour prior to imaging. To arrest cells in metaphase for spindle imaging, 20 μM MG132 (Z-Leu-Leu-Leu-al; Sigma-Aldrich) was added to cells 2 hours prior to plating. Images were collected on a Leica SPE I inverted scanning confocal microsocpe using a 63x oil immersion objective.

7.7 Identification and confirmation of *capu* lesions

To identify *capu* mutations, ovaries were dissected from fattened female flies in cold ionically matched adult *Drosophila* saline buffer [123]. RNA was isolated from the ovaries using the RNeasy Mini Kit (Qiagen) according to the manufacturers instructions for animal tissue samples. cDNA was generated using the Maxima Universal First Strand cDNA Synthesis Kit (Fermentas), sub-cloned into the vector pJET1.2 (Fermentas), and sequenced (GENEWIZ).

To confirm previously reported and newly identified lesions, genomic DNA was isolated from single flies as previously described [124]. The DNA region around each reported mutation site was PCR amplified using intronic primers. Amplified PCR products from at least two flies from each fly line were sequenced (GENEWIZ) to confirm the mutations.

$capu^{1}$, $capu^{2}$, $capu^{EE}$, $capu^{HK}$, $capu^{38}$, and $capu^{2F}$ flies were kindly provided by Dr. Trudi Schüpbach [62]. $capu^{L201}$, $capu^{L219}$, $capu^{L250}$, and $capu^{L277}$ flies were provided by Dr. Stefan Luschnig and the Tübingen *Drosophila* Stock Collection [86]. $capu^{A354}$ flies were provided by Dr. Akira Nakamura [70].

7.8 *Drosophila* oocyte imaging and analysis

Each *capu* fly line was crossed to a Df(2L)ed-dp/SM1 deficiency line obtained from the Bloomington stock center. w^{1118} was used as wildtype. Flies were kept at 25°C and were fed yeast paste approximately 24 hours before being dissected for analysis.

The actin mesh was visualized as previously described [32]. Briefly, ovaries were dissected and fixed in 10% paraformaldehyde and stained with 1 μM AlexaFluor647-phalloidin (Invitrogen). Images of mounted samples were acquired within 24 hours of staining using a Leica SPE I inverted scanning confocal microscope.

To analyze fluid flow within oocytes, live oocytes were dissected under halocarbon 700 oil. Autofluorescent yolk granules were excited at 405 nm, and images were acquired every 10 seconds for 3 min or 5 min using a Leica SPE I inverted scanning confocal microscope. Standard deviation z-projections of 3 min movies were created in Fiji for demonstration of

relative motion [125].

Cytoplasmic streaming velocities were determined as previously described [32] with minor changes. Briefly, confocal images were analyzed using custom-built particle image velocimetry [126] developed by Dr. Justin Bois and implemented in Python using NumPy/SciPy [120]. Movie were analyzed for either 18 or 30 frames with a time gap of 10 seconds between frames. Streaming velocities are reported as the 95th percentile speed for all speeds measured in a given movie.

7.9 Tandem affinity purification

The TAP-Capu (mEGFP-PP-S-peptide-Capu) construct was generated by inserting the coding region of Capu between the BamHI and XbaI sites of pTIGER [127] with mEGFP inserted between the KpnI and SpeI sites and a PreScission Protease cleavage site and S-peptide inserted between SpeI and BamHI. A control construct was created by sub-cloning mEGFP into the KpnI and SpeI sites of pTIGER. Transgenic flies with these plasmids inserted into the attP2 site were made by Genetic Services [128]. TAP-Capu flies were crossed with *nos*-GAL4-vp16 [129] (Bloomington stock center) to drive expression in the germline.

All flies were kept at 25°C. 1–2 day old females were fed yeast paste for approximately 24 hours before being dissected. Ovaries were dissected in cold ionically matched adult *Drosophila* saline [123] and kept on ice for up to 2 hours. Whole ovary samples were snap frozen in liquid nitrogen and stored at -80°C until needed for experiments. Approximately 200 pairs of ovaries were used for each small-scale pulldown experiment (silver stain gel only). At least 2000 pairs of ovaries were used for large-scale pulldown experiments for mass spectrometry.

All tandem affinity purification steps were performed on ice and/or at 4°C. Ovaries were removed from the freezer, ground with a pestle, and passed several times through an 18 G needle before being incubated 20 min in TAP300 Buffer (50 mM HEPES pH 7.4, 300 mM KCl, 1 mM EGTA, 1 mM $MgCl_2$, 10% glycerol, 0.5 mM DTT, 0.5% NP-40) supplemented with 1 tablet per 5 mL cOmplete Protease Inhibitor (Roche). The lysate was centrifuged

15 min at 16,000 × g. The low-speed supernatant was then centrifuged again for 1 hour at 120,000 × g. The high-speed supernatant was added to approximately one-tenth volume Protein A beads conjugated to rabbit anti-GFP antibody (generous gift of Dr. Jorge Torres) and incubated with rocking for 1.5 hours. The sample was then washed 5 times for 5 min each with TAP200 Buffer (50 mM HEPES pH 7.4, 200 mM KCl, 1 mM EGTA, 1 mM $MgCl_2$, 10% glycerol, 0.5 mM DTT, 0.5% NP-40). Recombinant GST-tagged PreScission Protease was added to an approximate final concentration of 4 mg/mL and incubated with rocking overnight. The post-PreScission Protease supernatant was added to approximately one-fifth volume S-protein agarose and incubated with rocking for 4 hours. The sample was then washed 3 times with TAP200 Buffer followed by 2 washes with TAP100 Buffer (50 mM HEPES pH 7.4, 100 mM KCl, 1 mM EGTA, 1 mM $MgCl_2$, 10% glycerol, 0.5 mM DTT). The supernatant was removed and the S-protein agarose beads were boiled in Sample Buffer (100 mM Tris pH 7.6, 100 mM DTT, 4% SDS). The final elution sample was either run on a 7.5% SDS-PAGE gel and silver stained (small-scale) or submitted directly for mass spectrometry (large-scale).

Mass spectrometry analysis was kindly performed by Joe Capri in the laboratory of Dr. Julian Whitelegge at UCLA. Briefly, protein samples were digested with trypsin. Nano-liquid chromatography with tandem mass spectrometry and collision induced dissociation was performed in an Orbitrap (Thermo Fisher) integrated with an Eksigent nano-liquid chromatographer. Spectra were searched using Mascot software (Matrix Science) against two databases: NCBInr 20131226 (all *Drosophila* species) and Drosophila_melanog 020314 (*D. melanogaster only*). Results with $p < 0.05$ (95% confidence interval) were considered significant and indicating identity.

APPENDIX A

Full list of mass spectrometry results

Mass spectrometry results (10,141 peptide queries) were searched against two separate databases: NCBInr 20131226 (Table A.1) and Drosophila_melanog 020314 (Table A.2). Search parameters allowed for up to 2 missed trypsin cleavages. With the *Drosophila* taxonomy filter, the NCBInr database searched 228,960 sequences with an approximate false discovery rate of 4%. The much smaller Drosophila_melanog database searched only 5,129 sequences with an approximate false discovery rate of 10%.

Protein hits are grouped into families based on shared peptide matches. The score given for each protein is derived from the individual ion scores. Ion scores are calculated as $-10log(P)$ where P is the probability that the observed match between the experimental data and the database sequence is a random event. The total number of peptide matches and unique sequence matches are shown for each protein, with the number of significant ($p < 0.05$) peptide matches and unique sequences reported in parentheses. The exponentially modified protein abundance index (emPAI) provides an approximate quantification of the relative abundance of proteins based on protein coverage by the peptide matches in the database search result [130].

Table A.1 – NCBInr 20131226 database search results. Only hits for *D. melanogaster* are shown.

Family	Accession	Score	Mass	Matches	Sequences	emPAI	Description
1	gi|220901934	17795	138486	1047(744)	59 (45)	6.96	cappuccino, isoform E
2	gi|383293219	1894	10481	73 (53)	8 (6)	22.36	cut up, isoform E
3	gi|440217444	1227	71372	75 (55)	32 (26)	3.61	heat shock protein cognate 4, isoform G
3	gi|157658	825	72304	58 (33)	26 (18)	1.54	heat shock protein cognate 72
4	gi|22832221	1127	46301	77 (56)	19 (17)	3.25	yolk protein 3
4	gi|161077703	651	49744	57 (35)	19 (14)	2.18	yolk protein 2
4	gi|7291113	569	48739	49 (36)	17 (15)	2.96	yolk protein 1
5	gi|18079273	615	33116	51 (34)	22 (17)	4.08	stress-sensitive B, isoform A
6	gi|21428756	355	78440	22 (15)	14 (9)	0.51	AT03044p
7	gi|17647519	337	23208	32 (20)	10 (8)	2.85	heat shock protein 26
8	gi|17647521	305	23659	17 (13)	7 (5)	1.53	heat shock protein 27
9	gi|220901630	303	184570	24 (11)	16 (9)	0.17	eukaryotic translation initiation factor 4G, isoform C
10	gi|287945	215	53544	13 (6)	11 (5)	0.35	ATP synthase beta subunit
11	gi|255958336	214	50561	16 (10)	9 (5)	0.46	RH01053p
12	gi|24665395	206	45559	12 (8)	10 (6)	0.63	CG4169, isoform A
13	gi|418207538	134	46818	15 (8)	10 (6)	0.5	alpha tubulin 84B, partial
14	gi|16197889	167	112523	10 (4)	8 (4)	0.12	GH26644p
15	gi|440217445	158	52080	11 (7)	10 (6)	0.45	eukaryotic initiation factor 2gamma, isoform D
16	gi|6048198	147	99800	7 (5)	7 (5)	0.18	importin beta
17	gi|440213525	145	36109	18 (9)	15 (9)	1.21	receptor of activated protein kinase C 1, isoform C
18	gi|21711679	129	84428	9 (6)	9 (6)	0.26	LD09306p
19	gi|383293484	122	38902	10 (7)	9 (6)	0.77	lethal (1) G0156, isoform C

Continued on next page

Table A.1 – Continued from previous page

Family	Accession	Score	Mass	Matches	Sequences	emPAI	Description
20	gi|19921464	119	62414	5 (3)	5 (3)	0.17	CG6453, isoform A
21	gi|7299061	119	85371	12 (6)	8 (4)	0.21	belle, isoform A
22	gi|17946569	117	14271	2 (2)	1 (1)	0.24	RH14088p
23	gi|4580727	116	39366	12 (6)	6 (5)	0.5	phosphate transporter precursor
24	gi|10727173	114	65866	7 (5)	6 (4)	0.22	ripped pocket, isoform A
25	gi|17945411	112	25985	6 (4)	3 (1)	0.27	RE17836p
26	gi|440215241	112	82099	12 (5)	10 (5)	0.22	heat shock protein 83, isoform B
27	gi|24661815	101	51946	10 (6)	8 (6)	0.45	alpha-Tubulin at 67C
28	gi|4164077	96	243432	5 (3)	5 (3)	0.04	rough deal protein
29	gi|157594	90	52663	5 (3)	5 (3)	0.2	RNA helicase
30	gi|20177117	85	122068	6 (4)	6 (4)	0.11	RE37107p
31	gi|1199816	77	60043	6 (2)	5 (2)	0.11	CCT-gamma protein
32	gi|555821	80	58055	5 (1)	5 (1)	0.06	pendulin (NLS-receptor)
33	gi|7295067	77	19219	3 (1)	3 (1)	0.18	ribosomal protein L14
34	gi|272406917	77	31309	2 (1)	2 (1)	0.11	kruppel homolog 2, isoform B
35	gi|21711713	73	115304	8 (1)	7 (1)	0.03	LP08082p
36	gi|440213651	69	140806	12 (6)	10 (5)	0.15	Cullin-associated and neddylation-dissociated 1, isoform B
37	gi|383292947	68	9700	11 (5)	3 (3)	3.65	ribosomal protein S27, isoform B
38	gi|383293491	68	17867	14 (3)	4 (3)	0.68	ribosomal protein S10b, isoform D
39	gi|7293233	67	38850	4 (3)	4 (3)	0.28	eukaryotic translation initiation factor 2alpha
40	gi|156723	65	66081	4 (2)	3 (1)	0.05	protein phosphatase 2A 65 kDa regulatory subunit
41	gi|225321	65	8540	8 (3)	6 (2)	0.99	ubiquitin S6(1)

Continued on next page

Table A.1 – Continued from previous page

Family	Accession	Score	Mass	Matches	Sequences	emPAI	Description
42	gi|157186	65	180078	8 (1)	6 (1)	0.02	defective chorion-1 fc177 protein precursor
43	gi|20129971	63	31961	3 (2)	3 (2)	0.22	CG6543, isoform A
44	gi|7726	62	30061	3 (2)	3 (2)	0.23	chorion protein S36
45	gi|440216810	62	35518	6 (1)	5 (1)	0.09	glyceraldehyde 3 phosphate dehydrogenase 2, isoform C
46	gi|6960212	57	63223	6 (2)	5 (2)	0.11	cytoplasmic protein 89BC
47	gi|23170738	56	59976	2 (1)	2 (1)	0.05	Tcp-1eta
48	gi|7297626	51	28974	1 (1)	1 (1)	0.11	eEF1delta, isoform B
49	gi|383293071	47	30549	5 (3)	4 (2)	0.23	ribosomal protein S3A, isoform F
50	gi|19528367	47	123100	5 (3)	5 (3)	0.08	LP04725p
51	gi|218505921	46	15041	2 (2)	2 (2)	0.5	GM15762p
52	gi|22832717	46	222297	12 (2)	11 (2)	0.03	yolkless, isoform A
53	gi|7292402	45	34562	3 (2)	2 (2)	0.2	Sc2
54	gi|5911472	43	228045	5 (1)	5 (1)	0.01	microtubule associated protein
55	gi|21357161	42	29775	3 (1)	2 (1)	0.11	ribosomal protein L6, isoform B
56	gi|20151897	42	201061	7 (1)	6 (1)	0.02	SD01201p
57	gi|288084	38	29218	1 (1)	1 (1)	0.11	ribosoaml protein S2
58	gi|440216251	37	53974	3 (1)	2 (1)	0.06	dead box protein 80, isoform H
59	gi|228430	33	67588	4 (2)	4 (2)	0.1	protein kinase
60	gi|17946667	29	13593	5 (1)	3 (1)	0.25	RH47995p
61	gi|328751757	27	35481	2 (1)	2 (1)	0.09	LD35750p
62	gi|209945210	27	36039	9 (1)	6 (1)	0.09	abnormal spindle
63	gi|24645515	27	6871	1 (1)	1 (1)	0.58	ribosomal protein S29, isoform A

Continued on next page

Table A.1 – Continued from previous page

Family	Accession	Score	Mass	Matches	Sequences	emPAI	Description
64	gi|158030159	25	59210	7 (1)	6 (1)	0.06	lost, isoform B, partial
65	gi|21626992	24	36054	2 (1)	1 (1)	0.09	CG42351, isoform B
66	gi|19922518	23	51745	1 (1)	1 (1)	0.06	CG5721
67	gi|295317432	18	30135	2 (1)	1 (1)	0.11	RT07780p
68	gi|545746500	13	102484	5 (1)	5 (1)	0.03	FI23918p1

Table A.2 – Drosophila_melanog 020314 database search results.

Family	Accession	Score	Mass	Matches	Sequences	emPAI	Description
1	gi|221330682	29847	138486	1105 (923)	72 (54)	11.12	cappuccino, isoform E
2	gi|17137630	2946	10465	65 (56)	4 (4)	12.17	cytoplasmic dynein light chain 2, isoform A
3	gi|24580785	543	78449	32 (18)	19 (11)	0.63	CG4552
4	gi|17137396	273	36109	21 (15)	17 (14)	2.42	receptor of activated protein kinase C 1, isoform A
5	gi|17137782	215	99886	15 (5)	9 (5)	0.17	female sterile (2) ketel, isoform A
6	gi|19921068	172	140806	29 (12)	18 (10)	0.29	Cullin-associated and neddylation-dissociated 1, isoform A
7	gi|19921464	170	62414	12 (4)	10 (4)	0.23	CG6453, isoform A
8	gi|24581168	159	83085	22 (5)	16 (5)	0.21	dynamin related protein 1, isoform A
9	gi|17136570	135	15005	9 (6)	7 (5)	1.78	ribosomal protein L40, isoform A
10	gi|19921254	132	17623	5 (2)	3 (1)	0.19	ribosomal protein L24
11	gi|24583279	128	52539	14 (4)	11 (4)	0.28	maternal expression at 31B, isoform A
12	gi|24583248	108	29591	11 (4)	7 (4)	0.53	ribosomal protein L7
13	gi|386769341	105	72542	17 (4)	9 (3)	0.14	protein phosphatase 2A at 29B, isoform D
14	gi|17136998	82	58071	23 (1)	11 (1)	0.06	pendulin
15	gi|17737397	76	31309	6 (1)	4 (1)	0.11	kruppel homolog 2, isoform A
16	gi|19921046	60	28974	5 (1)	2 (1)	0.11	eEF1delta, isoform B
17	gi|17136734	47	29110	7 (1)	7 (1)	0.11	ribosomal protein S2, isoform A
18	gi|17647761	43	47407	8 (4)	4 (1)	0.07	odorant receptor 22a
19	gi|19920710	41	28442	18 (1)	9 (1)	0.12	synthesis of cytochrome c oxidase
20	gi|24581274	38	47583	4 (4)	1 (1)	0.14	CG31694
21	gi|19920554	35	35133	13 (3)	7 (1)	0.09	CG10874, isoform A
22	gi|320545030	34	12463	13 (2)	5 (1)	0.28	CG42810

Continued on next page

Table A.2 – Continued from previous page

Family	Accession	Score	Mass	Matches	Sequences	emPAI	Description
23	gi|24580770	31	99340	19 (1)	13 (1)	0.03	asteroid
24	gi|24581314	31	67732	4 (1)	4 (1)	0.05	CG17265
25	gi|24582874	31	74604	23 (1)	17 (1)	0.04	CG13096
26	gi|161076819	31	77566	16 (1)	10 (1)	0.04	hepatocyte nuclear factor 4, isoform D
27	gi|45551003	30	39805	12 (2)	7 (1)	0.08	CG9331, isoform A
28	gi|20129331	29	31750	37 (2)	9 (1)	0.1	CG7164
29	gi|386769246	29	205480	82 (1)	46 (1)	0.02	CG18304, isoform B
30	gi|24581972	29	104833	13 (2)	8 (1)	0.03	glutamate receptor IIA
31	gi|24582653	28	59483	20 (2)	5 (2)	0.11	serpin 28Dc
32	gi|19920826	28	52607	4 (1)	4 (1)	0.06	Sec61alpha
33	gi|24583210	27	85259	21 (1)	18 (1)	0.04	CG13127
34	gi|24581463	27	54405	19 (1)	10 (1)	0.06	CG17593, isoform A
35	gi|24585081	26	50552	21 (2)	10 (1)	0.07	CG10639
36	gi|161076607	25	31028	15 (1)	2 (1)	0.11	CG15880
37	gi|17352461	25	597852	62 (1)	39 (1)	0.01	purity of essence, isoform A
38	gi|320544651	25	18912	2 (1)	2 (1)	0.18	CG42762
39	gi|20129385	25	40397	3 (1)	1 (1)	0.08	beta-site APP-cleaving enzyme
40	gi|17136452	25	66599	14 (2)	11 (2)	0.1	Ran GTPase activating protein, isoform A
41	gi|85726404	25	90899	13 (1)	11 (1)	0.04	Cep97, isoform B
42	gi|19920954	25	76056	8 (1)	6 (1)	0.04	CG13097
43	gi|17136436	24	152558	13 (1)	9 (1)	0.02	rickets, isoform A
44	gi|28574275	23	50379	6 (1)	1 (1)	0.07	CG33116

Continued on next page

Table A.2 – Continued from previous page

Family	Accession	Score	Mass	Matches	Sequences	emPAI	Description
45	gi|24583318	23	305153	41 (1)	28 (1)	0.01	CG5604
46	gi|24582657	23	87800	15 (1)	8 (1)	0.04	transglutaminase, isoform A
47	gi|320545067	23	292549	28 (1)	24 (1)	0.01	wing blister, isoform C
48	gi|19920510	23	48404	9 (1)	6 (1)	0.07	tRNA-guanine transglycosylase
49	gi|17136910	22	123948	46 (1)	20 (1)	0.03	diaphanous, isoform A
50	gi|24581477	22	47372	7 (1)	4 (1)	0.07	hippi
51	gi|62484232	22	67816	19 (3)	3 (1)	0.05	pickpocket 7
52	gi|221473199	22	126050	19 (1)	14 (1)	0.03	cup
53	gi|24583807	21	54876	3 (1)	3 (1)	0.06	CG14945, isoform A
54	gi|24581582	21	41010	8 (1)	4 (1)	0.08	CG31961, isoform A
55	gi|24585112	21	21003	2 (1)	2 (1)	0.16	CG10470
56	gi|19921316	19	75788	9 (1)	7 (1)	0.04	CG4500
57	gi|161076668	19	54668	5 (1)	5 (1)	0.06	CG15412, isoform B
58	gi|221330583	19	595187	79 (1)	55 (1)	0.01	kismet, isoform C
59	gi|386769058	18	146499	11 (1)	8 (1)	0.02	friend of echinoid, isoform F
60	gi|24582487	18	74502	11 (1)	9 (1)	0.04	CG5155
61	gi|386769842	18	110869	19 (1)	13 (1)	0.03	hamlet, isoform B
62	gi|17137542	18	41654	10 (2)	5 (1)	0.08	E2F transcription factor 2
63	gi|17137594	18	50785	23 (1)	7 (1)	0.06	Gonadotropin-releasing hormone receptor, isoform A
64	gi|17647699	17	25296	5 (1)	4 (1)	0.13	mitochondrial ribosomal protein S7, isoform A
65	gi|24585440	17	78143	15 (1)	13 (1)	0.04	cdc23, isoform A
66	gi|17136538	17	165034	32 (1)	28 (1)	0.02	topoisomerase 2, isoform A

Continued on next page

Table A.2 – Continued from previous page

Family	Accession	Score	Mass	Matches	Sequences	emPAI	Description
67	gi|24581010	17	97334	22 (1)	12 (1)	0.03	glycogen phosphorylase, isoform A
68	gi|24581248	17	44907	8 (1)	5 (1)	0.07	CG2975
69	gi|442627075	16	64473	4 (1)	2 (1)	0.05	CG44152
70	gi|281360456	16	47764	5 (1)	4 (1)	0.07	CG31975, isoform B
71	gi|24584302	16	183147	25 (1)	20 (1)	0.02	male sterile (2) 34Fe
72	gi|24580870	16	44288	5 (1)	3 (1)	0.07	CG31661
73	gi|24585143	16	54222	4 (1)	3 (1)	0.06	dopa decarboxylase, isoform B
74	gi|24581089	16	21813	6 (1)	5 (1)	0.15	CG17237
75	gi|17316358	16	51663	8 (1)	8 (1)	0.06	gamma-Tubulin at 37C, isoform A
76	gi|24583268	16	72841	4 (1)	3 (1)	0.05	CG5694, isoform A
77	gi|24580809	15	86666	12 (1)	7 (1)	0.04	phospholipase A2 activator protein, isoform A
78	gi|442628745	15	294039	48 (1)	34 (1)	0.01	CG8677
79	gi|24584117	14	22603	2 (1)	2 (1)	0.15	CG16957
80	gi|24583793	14	67006	18 (1)	7 (1)	0.05	translocase of outer membrane 70, isoform A
81	gi|161076868	13	57706	8 (1)	6 (1)	0.06	CG14913
82	gi|17136914	13	44525	9 (1)	7 (1)	0.07	pelota
83	gi|442625663	13	279594	28 (1)	19 (1)	0.01	CG3523, isoform C
84	gi|24585008	13	47683	9 (1)	7 (1)	0.07	CG31751, isoform A
85	gi|19921534	13	28848	6 (1)	4 (1)	0.12	Rab9
86	gi|45552379	13	56340	7 (1)	6 (1)	0.06	elbow B

References

[1] A. Schirenbeck, T. Bretschneider, R. Arasada, M. Schleicher, and J. Faix, "The diaphanous-related formin dDia2 is required for the formation and maintenance of filopodia," *Nature Cell Biology*, vol. 7, pp. 619–625, June 2005.

[2] E. S. Harris, T. J. Gauvin, E. G. Heimsath, and H. N. Higgs, "Assembly of filopodia by the formin FRL2 (FMNL3)," *Cytoskeleton*, vol. 67, pp. 755–772, Dec. 2010.

[3] A. F. Severson, D. L. Baillie, and B. Bowerman, "A formin homology protein and a profilin are required for cytokinesis and arp2/3-independent assembly of cortical microfilaments in c. elegans," *Current Biology*, vol. 12, pp. 2066–2075, Dec. 2002.

[4] S. Watanabe, Y. Ando, S. Yasuda, H. Hosoya, N. Watanabe, T. Ishizaki, and S. Narumiya, "mDia2 induces the actin scaffold for the contractile ring and stabilizes its position during cytokinesis in NIH 3T3 cells," *Molecular Biology of the Cell*, vol. 19, pp. 2328–2338, May 2008.

[5] T. Ishizaki, Y. Morishima, M. Okamoto, T. Furuyashiki, T. Kato, and S. Narumiya, "Coordination of microtubules and the actin cytoskeleton by the rho effector mDia1," *Nat. Cell Biol*, vol. 3, pp. 8–14, Jan. 2001.

[6] J. E. Gasteier, S. Schroeder, W. Muranyi, R. Madrid, S. Benichou, and O. T. Fackler, "FHOD1 coordinates actin filament and microtubule alignment to mediate cell elongation," *Experimental Cell Research*, vol. 306, pp. 192–202, May 2005.

[7] R. Takeya, K. Taniguchi, S. Narumiya, and H. Sumimoto, "The mammalian formin FHOD1 is activated through phosphorylation by ROCK and mediates thrombin-induced stress fibre formation in endothelial cells," *The EMBO Journal*, vol. 27, pp. 618–628, Feb. 2008.

[8] H. N. Higgs and J. Peterson, "Phylogenetic analysis of the formin homology 2 domain," *Molecular Biology of the Cell*, vol. 16, pp. 1–13, Oct. 2004.

[9] D. Breitsprecher and B. L. Goode, "Formins at a glance," *Journal of Cell Science*, vol. 126, pp. 1–7, Jan. 2013.

[10] M. A. Chesarone, A. G. DuPage, and B. L. Goode, "Unleashing formins to remodel the actin and microtubule cytoskeletons," *Nature Reviews Molecular Cell Biology*, vol. 11, pp. 62–74, Jan. 2010.

[11] A. Paul and T. Pollard, "The role of the FH1 domain and profilin in formin-mediated actin-filament elongation and nucleation," *Current Biology*, vol. 18, pp. 9–19, Jan. 2008.

[12] Y. Xu, J. B. Moseley, I. Sagot, F. Poy, D. Pellman, B. L. Goode, and M. J. Eck, "Crystal structures of a formin homology-2 domain reveal a tethered dimer architecture," *Cell*, vol. 116, pp. 711–723, Mar. 2004.

[13] T. Otomo, D. R. Tomchick, C. Otomo, S. C. Panchal, M. Machius, and M. K. Rosen, "Structural basis of actin filament nucleation and processive capping by a formin homology 2 domain," *Nature*, vol. 433, pp. 488–494, Feb. 2005.

[14] D. Pruyne, "Role of formins in actin assembly: Nucleation and barbed-end association," *Science*, vol. 297, pp. 612–615, July 2002.

[15] C. Higashida, "Actin polymerization-driven molecular movement of mDia1 in living cells," *Science*, vol. 303, pp. 2007–2010, Mar. 2004.

[16] S. H. Zigmond, M. Evangelista, C. Boone, C. Yang, A. C. Dar, F. Sicheri, J. Forkey, and M. Pring, "Formin leaky cap allows elongation in the presence of tight capping proteins," *Current Biology*, vol. 13, pp. 1820–1823, Oct. 2003.

[17] D. R. Kovar, "Profilin-mediated competition between capping protein and formin cdc12p during cytokinesis in fission yeast," *Molecular Biology of the Cell*, vol. 16, pp. 2313–2324, Feb. 2005.

[18] D. R. Kovar, "The fission yeast cytokinesis formin cdc12p is a barbed end actin filament capping protein gated by profilin," *The Journal of Cell Biology*, vol. 161, pp. 875–887, June 2003.

[19] D. R. Kovar, E. S. Harris, R. Mahaffy, H. N. Higgs, and T. D. Pollard, "Control of the assembly of ATP- and ADP-Actin by formins and profilin," *Cell*, vol. 124, pp. 423–435, Jan. 2006.

[20] B. Bor, C. L. Vizcarra, M. L. Phillips, and M. E. Quinlan, "Autoinhibition of the formin cappuccino in the absence of canonical autoinhibitory domains," *Molecular Biology of the Cell*, vol. 23, pp. 3801–3813, Aug. 2012.

[21] A. S. Alberts, "Identification of a carboxyl-terminal diaphanous-related formin homology protein autoregulatory domain," *Journal of Biological Chemistry*, vol. 276, pp. 2824–2830, Jan. 2001.

[22] F. Li and H. N. Higgs, "The mouse formin mDia1 is a potent actin nucleation factor regulated by autoinhibition," *Current Biology*, vol. 13, pp. 1335–1340, Aug. 2003.

[23] F. Li and H. N. Higgs, "Dissecting requirements for auto-inhibition of actin nucleation by the formin, mDia1," *Journal of Biological Chemistry*, vol. 280, pp. 6986–6992, Feb. 2005.

[24] S. Maiti, A. Michelot, C. Gould, L. Blanchoin, O. Sokolova, and B. L. Goode, "Structure and activity of full-length formin mDia1," *Cytoskeleton*, vol. 69, pp. 393–405, June 2012.

[25] R. Gorelik, C. Yang, V. Kameswaran, R. Dominguez, and T. Svitkina, "Mechanisms of plasma membrane targeting of formin mDia2 through its amino terminal domains," *Molecular Biology of the Cell*, vol. 22, pp. 189–201, Jan. 2011.

[26] A. Seth, C. Otomo, and M. K. Rosen, "Autoinhibition regulates cellular localization and actin assembly activity of the diaphanous-related formins FRL and mDia1," *The Journal of Cell Biology*, vol. 174, pp. 701–713, Aug. 2006.

[27] E. Gasteiger, C. Hoogland, A. Gattiker, S. Duvaud, M. R. Wilkins, R. D. Appel, and A. Bairoch, "Protein identification and analysis tools on the ExPASy server," in *The Proteomics Protocols Handbook* (J. M. Walker, ed.), pp. 571–607, Totowa, NJ: Humana Press, 2005.

[28] J. Gaillard, V. Ramabhadran, E. Neumanne, P. Gurel, L. Blanchoin, M. Vantard, and H. N. Higgs, "Differential interactions of the formins INF2, mDia1, and mDia2 with microtubules," *Molecular Biology of the Cell*, vol. 22, pp. 4575–4587, Oct. 2011.

[29] C. J. Gould, S. Maiti, A. Michelot, B. R. Graziano, L. Blanchoin, and B. L. Goode, "The formin DAD domain plays dual roles in autoinhibition and actin nucleation," *Current Biology*, vol. 21, pp. 384–390, Mar. 2011.

[30] C. L. Vizcarra, B. Kreutz, A. A. Rodal, A. V. Toms, J. Lu, W. Zheng, M. E. Quinlan, and M. J. Eck, "Structure and function of the interacting domains of spire and fmn-family formins," *Proceedings of the National Academy of Sciences*, vol. 108, pp. 11884–11889, July 2011.

[31] E. G. Heimsath and H. N. Higgs, "The c terminus of formin FMNL3 accelerates actin polymerization and contains a WH2 domain-like sequence that binds both monomers and filament barbed ends," *Journal of Biological Chemistry*, vol. 287, pp. 3087–3098, Jan. 2012.

[32] M. E. Quinlan, "Direct interaction between two actin nucleators is required in drosophila oogenesis," *Development*, vol. 140, pp. 4417–4425, Oct. 2013.

[33] E. S. Chhabra, "INF2 is a WASP homology 2 motif-containing formin that severs actin filaments and accelerates both polymerization and depolymerization," *Journal of Biological Chemistry*, vol. 281, pp. 26754–26767, June 2006.

[34] M. Kikyo, K. Tanaka, T. Kamei, K. Ozaki, T. Fujiwara, E. Inoue, Y. Takita, Y. Ohya, and Y. Takai, "An FH domain-containing bnr1p is a multifunctional protein interacting with a variety of cytoskeletal proteins in saccharomyces cerevisiae.," *Oncogene*, vol. 18, p. 7046, Nov. 1999.

[35] L. Lee, S. K. Klee, M. Evangelista, C. Boone, and D. Pellman, "Control of mitotic spindle position by the saccharomyces cerevisiae formin bni1p," *The Journal of Cell Biology*, vol. 144, pp. 947–961, Mar. 1999.

[36] F. Chang, "Microtubule and actin-dependent movement of the formin cdc12p in fission yeast," *Microscopy Research and Technique*, vol. 49, pp. 161–167, Apr. 2000.

[37] T. Kato, N. Watanabe, Y. Morishima, A. Fujita, T. Ishizaki, and S. Narumiya, "Localization of a mammalian homolog of diaphanous, mDia1, to the mitotic spindle in HeLa cells," *J. Cell. Sci*, vol. 114, pp. 775–784, Feb. 2001.

[38] B. Leader, H. Lim, M. J. Carabatsos, A. Harrington, J. Ecsedy, D. Pellman, R. Maas, and P. Leder, "Formin-2, polyploidy, hypofertility and positioning of the meiotic spindle in mouse oocytes," *Nature Cell Biology*, vol. 4, pp. 921–928, Dec. 2002.

[39] J. Dumont, K. Million, K. Sunderland, P. Rassinier, H. Lim, B. Leader, and M.-H. Verlhac, "Formin-2 is required for spindle migration and for the late steps of cytokinesis in mouse oocytes," *Developmental Biology*, vol. 301, pp. 254–265, Jan. 2007.

[40] A. F. Palazzo, T. A. Cook, A. S. Alberts, and G. G. Gundersen, "mDia mediates rho-regulated formation and orientation of stable microtubules," *Nat. Cell Biol*, vol. 3, pp. 723–729, Aug. 2001.

[41] Y. Wen, C. H. Eng, J. Schmoranzer, N. Cabrera-Poch, E. J. S. Morris, M. Chen, B. J. Wallar, A. S. Alberts, and G. G. Gundersen, "EB1 and APC bind to mDia to stabilize microtubules downstream of rho and promote cell migration," *Nature Cell Biology*, vol. 6, pp. 820–830, Aug. 2004.

[42] C. H. Eng, T. M. Huckaba, and G. G. Gundersen, "The formin mDia regulates GSK3beta through novel PKCs to promote microtubule stabilization but not MTOC reorientation in migrating fibroblasts," *Molecular Biology of the Cell*, vol. 17, pp. 5004–5016, Sept. 2006.

[43] F. Bartolini, J. B. Moseley, J. Schmoranzer, L. Cassimeris, B. L. Goode, and G. G. Gundersen, "The formin mDia2 stabilizes microtubules independently of its actin nucleation activity," *The Journal of Cell Biology*, vol. 181, pp. 523–536, Oct. 2008.

[44] K. G. Young, S. F. Thurston, S. Copeland, C. Smallwood, and J. W. Copeland, "INF1 is a novel microtubule-associated formin," *Molecular Biology of the Cell*, vol. 19, pp. 5168–5180, Dec. 2008.

[45] L. Andres-Delgado, O. M. Anton, R. Madrid, J. A. Byrne, and M. A. Alonso, "Formin INF2 regulates MAL-mediated transport of lck to the plasma membrane of human t lymphocytes," *Blood*, vol. 116, pp. 5919–5929, Sept. 2010.

[46] S. F. Thurston, W. A. Kulacz, S. Shaikh, J. M. Lee, and J. W. Copeland, "The ability to induce microtubule acetylation is a general feature of formin proteins," *PLoS ONE*, vol. 7, p. e48041, Oct. 2012.

[47] M. E. Quinlan, S. Hilgert, A. Bedrossian, R. D. Mullins, and E. Kerkhoff, "Regulatory interactions between two actin nucleators, spire and cappuccino," *The Journal of Cell Biology*, vol. 179, pp. 117–128, Oct. 2007.

[48] A. E. Rosales-Nieves, J. E. Johndrow, L. C. Keller, C. R. Magie, D. M. Pinto-Santini, and S. M. Parkhurst, "Coordination of microtubule and microfilament dynamics by drosophila rho1, spire and cappuccino," *Nature Cell Biology*, vol. 8, pp. 367–376, Mar. 2006.

[49] E. Lewkowicz, F. Herit, C. Le Clainche, P. Bourdoncle, F. Perez, and F. Niedergang, "The microtubule-binding protein CLIP-170 coordinates mDia1 and actin reorganization during CR3-mediated phagocytosis," *The Journal of Cell Biology*, vol. 183, pp. 1287–1298, Dec. 2008.

[50] A. Akhmanova and M. O. Steinmetz, "Tracking the ends: a dynamic protein network controls the fate of microtubule tips," *Nature Reviews Molecular Cell Biology*, vol. 9, pp. 309–322, Mar. 2008.

[51] K. Okada, F. Bartolini, A. M. Deaconescu, J. B. Moseley, Z. Dogic, N. Grigorieff, G. G. Gundersen, and B. L. Goode, "Adenomatous polyposis coli protein nucleates actin assembly and synergizes with the formin mDia1," *The Journal of Cell Biology*, vol. 189, pp. 1087–1096, June 2010.

[52] D. Breitsprecher, R. Jaiswal, J. P. Bombardier, C. J. Gould, J. Gelles, and B. L. Goode, "Rocket launcher mechanism of collaborative actin assembly defined by single-molecule imaging," *Science*, vol. 336, pp. 1164–1168, June 2012.

[53] K. Zaoui, K. Benseddik, P. Daou, D. Salaun, and A. Badache, "ErbB2 receptor controls microtubule capture by recruiting ACF7 to the plasma membrane of migrating cells," *Proceedings of the National Academy of Sciences*, vol. 107, pp. 18517–18522, Oct. 2010.

[54] N. Yamana, Y. Arakawa, T. Nishino, K. Kurokawa, M. Tanji, R. E. Itoh, J. Monypenny, T. Ishizaki, H. Bito, K. Nozaki, N. Hashimoto, M. Matsuda, and S. Narumiya, "The rho-mDia1 pathway regulates cell polarity and focal adhesion turnover in migrating cells through mobilizing apc and c-src," *Molecular and Cellular Biology*, vol. 26, pp. 6844–6858, Sept. 2006.

[55] P. Goulimari, H. Knieling, U. Engel, and R. Grosse, "LARG and mDia1 link g12/13 to cell polarity and microtubule dynamics," *Molecular Biology of the Cell*, vol. 19, pp. 30–40, Oct. 2007.

[56] B. Butler and J. A. Cooper, "Distinct roles for the actin nucleators arp2/3 and hDia1 during NK-Mediated cytotoxicity," *Current Biology*, vol. 19, pp. 1886–1896, Dec. 2009.

[57] T. S. Gomez, K. Kumar, R. B. Medeiros, Y. Shimizu, P. J. Leibson, and D. Billadeau, "Formins regulate the actin-related protein 2/3 complex-independent polarization of the centrosome to the immunological synapse," *Immunity*, vol. 26, pp. 177–190, Feb. 2007.

[58] M. Dettenhofer, F. Zhou, and P. Leder, "Formin 1-isoform IV deficient cells exhibit defects in cell spreading and focal adhesion formation," *PLoS ONE*, vol. 3, p. e2497, June 2008.

[59] P. Daou, S. Hasan, D. Breitsprecher, E. Baudelet, L. Camoin, S. Audebert, B. L. Goode, and A. Badache, "Essential and nonredundant roles for diaphanous formins in cortical microtubule capture and directed cell migration," *Molecular Biology of the Cell*, vol. 25, pp. 658–668, Jan. 2014.

[60] L. Cheng, J. Zhang, S. Ahmad, L. Rozier, H. Yu, H. Deng, and Y. Mao, "Aurora b regulates formin mDia3 in achieving metaphase chromosome alignment," *Developmental Cell*, vol. 20, pp. 342–352, Mar. 2011.

[61] F. Zhou, P. Leder, and S. S. Martin, "Formin-1 protein associates with microtubules through a peptide domain encoded by exon-2," *Experimental Cell Research*, vol. 312, pp. 1119–1126, Apr. 2006.

[62] L. J. Manseau and T. Schüpbach, "cappuccino and spire: two unique maternal-effect loci required for both the anteroposterior and dorsoventral patterns of the drosophila embryo.," *Genes & Development*, vol. 3, pp. 1437–1452, Sept. 1989.

[63] S. Emmons, H. Phan, J. Calley, W. Chen, B. James, and L. Manseau, "Cappuccino, a drosophila maternal effect gene required for polarity of the egg and embryo, is related to the vertebrate limb deformity locus.," *Genes & Development*, vol. 9, pp. 2482–2494, Oct. 1995.

[64] J.-M. Kugler and P. Lasko, "Localization, anchoring and translational control of *oskar* , *gurken* , *bicoid* and *nanos* mRNA during drosophila oogenesis," *Fly*, vol. 3, pp. 15–28, Jan. 2009.

[65] L. Manseau, J. Calley, and H. Phan, "Profilin is required for posterior patterning of the drosophila oocyte," *Development*, vol. 122, pp. 2109–2116, July 1996.

[66] A. Ephrussi, L. K. Dickinson, and R. Lehmann, "oskar organizes the germ plasm and directs localization of the posterior determinant nanos," *Cell*, vol. 66, pp. 37–50, July 1991.

[67] A. Ephrussi and R. Lehmann, "Induction of germ cell formation by oskar," *Nature*, vol. 358, pp. 387–392, July 1992.

[68] F. S. Neuman-Silberberg and T. Schüpbach, "The drosophila dorsoventral patterning gene gurken produces a dorsally localized RNA and encodes a TGF-like protein," *Cell*, vol. 75, pp. 165–174, Oct. 1993.

[69] K. Dahlgaard, A. A. Raposo, T. Niccoli, and D. St Johnston, "Capu and spire assemble a cytoplasmic actin mesh that maintains microtubule organization in the drosophila oocyte," *Developmental Cell*, vol. 13, pp. 539–553, Oct. 2007.

[70] T. Tanaka, Y. Kato, K. Matsuda, K. Hanyu-Nakamura, and A. Nakamura, "Drosophila mon2 couples oskar-induced endocytosis with actin remodeling for cortical anchorage of the germ plasm," *Development*, vol. 138, pp. 2523–2532, May 2011.

[71] R. M. Parton, R. S. Hamilton, G. Ball, L. Yang, C. F. Cullen, W. Lu, H. Ohkura, and I. Davis, "A PAR-1-dependent orientation gradient of dynamic microtubules directs posterior cargo transport in the drosophila oocyte," *The Journal of Cell Biology*, vol. 194, pp. 121–135, July 2011.

[72] W. E. Theurkauf, "Premature microtubule-dependent cytoplasmic streaming in cappuccino and spire mutant oocytes," *Science*, vol. 265, pp. 2093–2096, Sept. 1994.

[73] I. M. Palacios and D. St Johnston, "Kinesin light chain-independent function of the kinesin heavy chain in cytoplasmic streaming and posterior localisation in the drosophila oocyte," *Development*, vol. 129, pp. 5473–5485, Dec. 2002.

[74] L. R. Serbus, "Dynein and the actin cytoskeleton control kinesin-driven cytoplasmic streaming in drosophila oocytes," *Development*, vol. 132, pp. 3743–3752, July 2005.

[75] N. Vanzo, A. Oprins, D. Xanthakis, A. Ephrussi, and C. Rabouille, "Stimulation of endocytosis and actin dynamics by oskar polarizes the drosophila oocyte," *Developmental Cell*, vol. 12, pp. 543–555, Apr. 2007.

[76] T. Tanaka and A. Nakamura, "The endocytic pathway acts downstream of oskar in drosophila germ plasm assembly," *Development*, vol. 135, pp. 1107–1117, Feb. 2008.

[77] C.-W. Chang, D. Nashchekin, L. Wheatley, U. Irion, K. Dahlgaard, T. G. Montague, J. Hall, and D. St. Johnston, "Anterior-posterior axis specification in drosophila oocytes: Identification of novel bicoid and oskar mRNA localization factors," *Genetics*, vol. 188, pp. 883–896, Aug. 2011.

[78] J. A. Efe, "Yeast mon2p is a highly conserved protein that functions in the cytoplasm-to-vacuole transport pathway and is required for golgi homeostasis," *Journal of Cell Science*, vol. 118, pp. 4751–4764, Oct. 2005.

[79] F. Bartolini, N. Ramalingam, and G. G. Gundersen, "Actin-capping protein promotes microtubule stability by antagonizing the actin activity of mDia1," *Molecular Biology of the Cell*, vol. 23, pp. 4032–4040, Aug. 2012.

[80] B. L. Goode, D. G. Drubin, and G. Barnes, "Functional cooperation between the microtubule and actin cytoskeletons," *Current Opinion in Cell Biology*, vol. 12, pp. 63–71, Feb. 2000.

[81] O. C. Rodriguez, A. W. Schaefer, C. A. Mandato, P. Forscher, W. M. Bement, and C. M. Waterman-Storer, "Conserved microtubuleactin interactions in cell movement and morphogenesis," *Nature Cell Biology*, vol. 5, pp. 599–609, July 2003.

[82] J. Azoury, K. W. Lee, V. Georget, P. Rassinier, B. Leader, and M.-H. Verlhac, "Spindle positioning in mouse oocytes relies on a dynamic meshwork of actin filaments," *Current Biology*, vol. 18, pp. 1514–1519, Oct. 2008.

[83] M. Schuh and J. Ellenberg, "A new model for asymmetric spindle positioning in mouse oocytes," *Current Biology*, vol. 18, pp. 1986–1992, Dec. 2008.

[84] F. Zhou, P. Leder, A. Zuniga, and M. Dettenhofer, "Formin1 disruption confers oligodactylism and alters bmp signaling," *Human Molecular Genetics*, vol. 18, pp. 2472–2482, Apr. 2009.

[85] J. D. McGhee and P. H. von Hippel, "Theoretical aspects of DNA-protein interactions: Co-operative and non-co-operative binding of large ligands to a one-dimensional homogeneous lattice," *Journal of Molecular Biology*, vol. 86, pp. 469–489, June 1974.

[86] S. Luschnig, B. Moussian, J. Krauss, I. Desjeux, J. Perkovic, and C. Nsslein-Volhard, "An f1 genetic screen for maternal-effect mutations affecting embryonic pattern formation in drosophila melanogaster," *Genetics*, vol. 167, pp. 325–342, May 2004.

[87] J. Lu, W. Meng, F. Poy, S. Maiti, B. L. Goode, and M. J. Eck, "Structure of the FH2 domain of daam1: Implications for formin regulation of actin assembly," *Journal of Molecular Biology*, vol. 369, pp. 1258–1269, June 2007.

[88] K. Arnold, L. Bordoli, J. Kopp, and T. Schwede, "The SWISS-MODEL workspace: a web-based environment for protein structure homology modelling," *Bioinformatics*, vol. 22, no. 2, pp. 195–201, 2006.

[89] L. Dehmelt and S. Halpain, "The MAP2/Tau family of microtubule-associated proteins," *Genome Biol*, vol. 6, no. 1, p. 204, 2005.

[90] A. Kobielak, H. A. Pasolli, and E. Fuchs, "Mammalian formin-1 participates in adherens junctions and polymerization of linear actin cables," *Nature Cell Biology*, vol. 6, pp. 21–30, Nov. 2003.

[91] S. Pfender, V. Kuznetsov, S. Pleiser, E. Kerkhoff, and M. Schuh, "Spire-type actin nucleators cooperate with formin-2 to drive asymmetric oocyte division," *Current Biology*, vol. 21, pp. 955–960, June 2011.

[92] J. Steinhauer and D. Kalderon, "Microtubule polarity and axis formation in the-Drosophila oocyte," *Developmental Dynamics*, vol. 235, pp. 1455–1468, June 2006.

[93] C. Kural, "Kinesin and dynein move a peroxisome in vivo: A tug-of-war or coordinated movement?," *Science*, vol. 308, pp. 1469–1472, June 2005.

[94] S. E. St. Pierre, L. Ponting, R. Stefancsik, P. McQuilton, and the FlyBase Consortium, "FlyBase 102advanced approaches to interrogating FlyBase," *Nucleic Acids Research*, vol. 42, pp. D780–D788, Jan. 2014.

[95] D. Staus, J. Taylor, and C. Mack, "Enhancement of mDia2 activity by rho-kinase-dependent phosphorylation of the diaphanous autoregulatory domain," *Biochemical Journal*, vol. 439, pp. 57–65, Oct. 2011.

[96] C. P. Schonbaum, S. Lee, and A. P. Mahowald, "The drosophila yolkless gene encodes a vitellogenin receptor belonging to the low density lipoprotein receptor superfamily.," *Proceedings of the National Academy of Sciences*, vol. 92, pp. 1485–1489, Feb. 1995.

[97] C. Laflamme, G. Assaker, D. Ramel, J. F. Dorn, D. She, P. S. Maddox, and G. Emery, "Evi5 promotes collective cell migration through its rab-GAP activity," *The Journal of Cell Biology*, vol. 198, pp. 57–67, July 2012.

[98] J. Zhang, K. L. Schulze, P. R. Hiesinger, K. Suyama, S. Wang, M. Fish, M. Acar, R. A. Hoskins, H. J. Bellen, and M. P. Scott, "Thirty-one flavors of drosophila rab proteins," *Genetics*, vol. 176, pp. 1307–1322, Dec. 2006.

[99] F. Gnad, J. Gunawardena, and M. Mann, "PHOSIDA 2011: the posttranslational modification database," *Nucleic Acids Research*, vol. 39, pp. D253–D260, Nov. 2010.

[100] N. Blom, T. Sicheritz-Pontn, R. Gupta, S. Gammeltoft, and S. Brunak, "Prediction of post-translational glycosylation and phosphorylation of proteins from the amino acid sequence," *PROTEOMICS*, vol. 4, pp. 1633–1649, June 2004.

[101] J. C. Obenauer, L. C. Cantley, and M. B. Yaffe, "Scansite 2.0: proteome-wide prediction of cell signaling interactions using short sequence motifs," *Nucleic Acids Research*, vol. 31, pp. 3635–3641, July 2003.

[102] H. Nakajima, "Identification of a consensus motif for plk (polo-like kinase) phosphorylation reveals myt1 as a plk1 substrate," *Journal of Biological Chemistry*, vol. 278, pp. 25277–25280, May 2003.

[103] V. Archambault and D. M. Glover, "Polo-like kinases: conservation and divergence in their functions and regulation," *Nature Reviews Molecular Cell Biology*, vol. 10, pp. 265–275, Apr. 2009.

[104] P. Wang, X. Pinson, and V. Archambault, "PP2A-Twins is antagonized by greatwall and collaborates with polo for cell cycle progression and centrosome attachment to nuclei in drosophila embryos," *PLoS Genetics*, vol. 7, p. e1002227, Aug. 2011.

[105] J. L. Kadrmas, M. A. Smith, S. M. Pronovost, and M. C. Beckerle, "Characterization of RACK1 function in drosophila development," *Developmental Dynamics*, vol. 236, pp. 2207–2215, Aug. 2007.

[106] K. Mitra, R. Rikhy, M. Lilly, and J. Lippincott-Schwartz, "DRP1-dependent mitochondrial fission initiates follicle cell differentiation during drosophila oogenesis," *The Journal of Cell Biology*, vol. 197, pp. 487–497, May 2012.

[107] M. Gorjncz, G. dm, I. Trk, B. M. Mechler, T. Szlanka, and I. Kiss, "Importin-2 is critically required for the assembly of ring canals during drosophila oogenesis," *Developmental Biology*, vol. 251, pp. 271–282, Nov. 2002.

[108] T. Soldati and M. Schliwa, "Powering membrane traffic in endocytosis and recycling," *Nature Reviews Molecular Cell Biology*, vol. 7, pp. 897–908, Dec. 2006.

[109] T. Tsuruhara, J. H. Koenig, and K. Ikeda, "Synchronized endocytosis studied in the oocyte of a temperature-sensitive mutant of drosophila melanogaster," *Cell and Tissue Research*, vol. 259, pp. 199–207, Feb. 1990.

[110] E. Ai, D. S. Poole, and A. R. Skop, "RACK-1 directs dynactin-dependent RAB-11 endosomal recycling during mitosis in caenorhabditis elegans," *Molecular Biology of the Cell*, vol. 20, pp. 1629–1638, Jan. 2009.

[111] E. Ai and A. R. Skop, "Endosomal recycling regulation during cytokinesis," *Communicative & Integrative Biology*, vol. 2, pp. 444–447, Sept. 2009.

[112] S. Pfeffer, "A model for rab GTPase localization," *Biochemical Society Transactions*, vol. 33, p. 627, Aug. 2005.

[113] P. Sanghavi, S. Lu, and G. B. Gonsalvez, "A functional link between localized oskar, dynamic microtubules, and endocytosis," *Developmental Biology*, Apr. 2012.

[114] K. Rper and N. H. Brown, "A spectraplakin is enriched on the fusome and organizes microtubules during oocyte specification in drosophila," *Current Biology*, vol. 14, pp. 99–110, Jan. 2004.

[115] A. Subramanian, A. Prokop, M. Yamamoto, K. Sugimura, T. Uemura, J. Betschinger, J. A. Knoblich, and T. Volk, "Shortstop recruits EB1/APC1 and promotes microtubule assembly at the muscle-tendon junction," *Current Biology*, vol. 13, pp. 1086–1095, July 2003.

[116] F. Korobova, V. Ramabhadran, and H. N. Higgs, "An actin-dependent step in mitochondrial fission mediated by the ER-Associated formin INF2," *Science*, vol. 339, pp. 464–467, Jan. 2013.

[117] M. Gorjncz, I. Trk, I. Pomozi, G. Garab, T. Szlanka, I. Kiss, and B. M. Mechler, "Domains of importin-2 required for ring canal assembly during drosophila oogenesis," *Journal of Structural Biology*, vol. 154, pp. 27–41, Apr. 2006.

[118] M. Schuh, "An actin-dependent mechanism for long-range vesicle transport," *Nature Cell Biology*, vol. 13, pp. 1431–1436, Oct. 2011.

[119] S. MacLean-Fletcher and T. D. Pollard, "Identification of a factor in conventional muscle actin preparations which inhibits actin filament self-association," *Biochemical and Biophysical Research Communications*, vol. 96, pp. 18–27, Sept. 1980.

[120] T. E. Oliphant, "Python for scientific computing," *Computing in Science & Engineering*, vol. 9, no. 3, pp. 10–20, 2007.

[121] S. D. Hansen and R. D. Mullins, "VASP is a processive actin polymerase that requires monomeric actin for barbed end association," *The Journal of Cell Biology*, vol. 191, pp. 571–584, Nov. 2010.

[122] S. L. Rogers and G. C. Rogers, "Culture of drosophila s2 cells and their use for RNAi-mediated loss-of-function studies and immunofluorescence microscopy," *Nature Protocols*, vol. 3, pp. 606–611, Mar. 2008.

[123] K. Singleton and R. I. Woodruff, "The osmolarity of adult drosophila hemolymph and its effect on oocyte-nurse cell electrical polarity," *Developmental Biology*, vol. 161, pp. 154–167, Jan. 1994.

[124] G. B. Gloor and W. R. Engels, "Single-fly DNA preps for PCR," *Drosophila Information Service*, vol. 71, pp. 148–149, 1992.

[125] J. Schindelin, I. Arganda-Carreras, E. Frise, V. Kaynig, M. Longair, T. Pietzsch, S. Preibisch, C. Rueden, S. Saalfeld, B. Schmid, J.-Y. Tinevez, D. J. White, V. Hartenstein, K. Eliceiri, P. Tomancak, and A. Cardona, "Fiji: an open-source platform for biological-image analysis," *Nature Methods*, vol. 9, pp. 676–682, June 2012.

[126] M. Raffel, ed., *Particle image velocimetry: a practical guide*. Heidelberg ; New York: Springer, 2nd ed ed., 2007.

[127] S. B. Ferguson, M. A. Blundon, M. S. Klovstad, and T. Schüpbach, "Modulation of gurken translation by insulin and TOR signaling in drosophila," *Journal of Cell Science*, vol. 125, pp. 1407–1419, Feb. 2012.

[128] A. C. Groth, M. Fish, R. Nusse, and M. P. Calos, "Construction of transgenic drosophila by using the site-specific integrase from phage c31," *Genetics*, vol. 166, pp. 1775–1782, Apr. 2004.

[129] M. Van Doren, A. L. Williamson, and R. Lehmann, "Regulation of zygotic gene expression in drosophila primordial germ cells," *Current Biology*, vol. 8, pp. 243–246, Feb. 1998.

[130] Y. Ishihama, Y. Oda, T. Tabata, T. Sato, T. Nagasu, J. Rappsilber, and M. Mann, "Exponentially modified protein abundance index (emPAI) for estimation of absolute protein amount in proteomics by the number of sequenced peptides per protein," *Molecular & Cellular Proteomics*, vol. 4, pp. 1265–1272, June 2005.